Receiver Design for Massive MIMO

A thesis

submitted in partial fulfilment

of the requirements for the Degree

of

Doctor of Philosophy

in

Department of Electrical and Computer Engineering

and Wireless Research Centre

by

Khawla A. Alnajjar

Supervisor: Prof. Peter J. Smith

Co-supervisor: Dr. Graeme K. Woodward

University of Canterbury

2015

To my family.

Abstract

Massive multiple-input-multiple-output (MM) is becoming a promising candidate for wireless communications. The idea behind MM is to use a very large number of antennas to increase throughput and energy efficiency by one or more orders of magnitude. In order to make MM feasible, many challenges remain. In the uplink a fundamental question is whether to deploy single massive arrays or to build a virtual array using cooperative base stations. Also, in such large arrays the signal processing involved in receiver combining is non-trivial. Therefore, low complexity receiver designs and deployment scenarios are essential aspects of MM and the thesis mainly focuses on these two areas.

In the first part, we investigate three deployment scenarios: (i) a massive co-located array at the cell center; (ii) a massive array clustered at B discrete locations; and (iii) a massive distributed array with a uniform distribution of individual antennae. We also study the effect of propagation parameters, system size, correlation and channel estimation error. We demonstrate by analysis and simulation that in the absence of any system imperfections, a massive distributed array is preferable. However, an intermediate deployment such as a massive array clustered at a few discrete locations can be more practical to implement and more robust to imperfect channel state information. We then focus on the performance of the co-located scenario with different types of antenna array, uniform square and linear arrays. With MM, it may be the case that large numbers of antennas are closely packed to fit in some available space. Hence, channel correlations become important and therefore we investigate the space requirements of different array shapes. In particular, we evaluate the system performance of uniform square and linear arrays by using ergodic capacity and capacity outage. For a range of correlation models, we demonstrate that the uniform square array can yield similar performance to a uniform linear array while providing considerable space saving.

In the second part of the thesis we focus on low complexity receiver designs. Due to the

high dimension of MM systems there is a considerable interest in detection schemes with a better complexity-performance trade-off. We focus on linear receivers (zero forcing (ZF) and maximum ratio combining (MRC)) used in conjuction with a Vertical Bell Laboratories Layered Space Time (V-BLAST) structure. Our first results show that the performance of MRC V-BLAST approaches that of ZF V-BLAST under a range of imperfect CSI levels, different channel powers and different types of arrays as long as the channel correlations are not too high. Subsequently, we propose novel low complexity receiver designs which maintain the same performance as ZF or ZF V-BLAST. We show that the performance loss of MRC relative to ZF can be removed in certain situations through the use of V-BLAST. The low complexity ordering scheme based on the channel norm (C-V-BLAST) results in a V-BLAST scheme with MRC that has much less complexity than a single ZF linear combiner. An analysis of the SINR at each stage of the V-BLAST approach is also given to support the findings of the proposed technique. We also show that C-V-BLAST remains similar to ZF for more complex adaptive modulation systems and in the presence of channel estimation error, C-V-BLAST can be superior. These results are analytically justified and we derive an exhaustive search algorithm for power control (PC) to bound the potential gains of PC. Using this bound, we demonstrate that C-V-BLAST performs well without the need for additional PC. The final simplification is based on the idea of ordering users based on large scale fading information rather than instantaneous channel knowledge for a V-BLAST scheme with MRC (P-V-BLAST). An explicit closed form analysis for error probability for both co-located and distributed BSs is provided along with a number of novel performance metrics which are useful in designing MM systems. It is shown that the error performance of the distributed scenario can be well approximated by a modified version of a co-located scenario. Another potential advantage of P-V-BLAST is that the ordering can be obtained as soon as the link gains are available. Hence, it is possible that mean SINR values could be used for scheduling and other link control functions. These mean values

are solely functions of the link gains and hence, scheduling, power adaptation, rate adaptation, etc. can all be performed more rapidly with P-V-BLAST. Hence, the P-V-BLAST structure may have further advantages beyond a lower complexity compared to C-V-BLAST.

Acknowledgments

I Praise God, the Lord Almighty, the most Gracious, the most Merciful of His blessing during my life and giving me health and wealth to complete this study.

I would like to extend my appreciation to the Wireless Research Centre, University of Canterbury, the Ministry of Higher Education & Scientific Research and National Research Foundation in United Arab Emirates for support and research funding. I would like to take this opportunity to extend my appreciation to my supervisor, Prof. Peter Smith. His excellent guidance with the help of invaluable comments, suggestions and directions were very helpful throughout the progression of my research. I also thank my co-supervisor Dr. Graeme Woodward. His advice and encouragement have increased my motivation over the years. My appreciation also extends to my collaborators: Prof. Mansoor Shafi from Spark in New Zealand, Prof. Philip Whiting from Macquarie University in Australia and Dr. Dushyantha Basnayaka from The University of Edinburgh in United Kingdom. Many thanks to my beloved husband and my family for their constant support and love through my life. Finally, I would like to thank my friends and colleagues for their continuous encouragement.

Table of Contents

List of Figures

List of Tables

Glossary

ACF Autocorrelation Function.

AM Adaptive Modulation.

AWGN Additive White Gaussian Noise.

BER Bit Error Rate.

BPSK Binary Phase Shift Keying.

BS Base Station.

CDF Cumulative Distribution Function.

CDMA Code Division Multiple Access.

CF Characteristic Function.

CPU Central Processing Unit.

COL One massive co-located array.

CSI Channel State Information.

CV Coefficient of Variation.

C-V-BLAST MRC V-BLAST with one shot ordering based on channel norms.

dB Decibels.

DIST One massive array with geographically distributed single antenna BSs.

DOF Degrees of Freedom.

eNodeB Long Term Evolution terminology for a basestation, referred to throughout this thesis as BS.

HetNets Heterogeneous Networks.

i.i.d. Independent and Identically Distributed.

LTE Long Term Evolution.

MF Matched Filter.

MIMO Multi-Input Multi-Output.

MISO Multi-Input Single-Output.

MM Massive Multi-Input Multi-Output.

MMSE Minimum Mean-Square Error.

mmWave Millimeter Wave.

MRC Maximum Ratio Combining.

MU-MIMO Multiuser-Multi-Input Multi-Output.

OFDM Orthogonal Frequency-Division Multiplexing.

PC Power Control.

PDF Probability Density Function.

Prob.Dis. Probability of Disagreement.

PSK Phase Shift Keying.

P-V-BLAST MRC V-BLAST with one shot ordering based on link gains.

QAM Quadrature Amplitude Modulation.

QPSK Quadrature Phase Shift Keying.

SER Symbol Error Rate.

SIC Successive Interference Cancellation.

SIMO Single-Input Multiple-Output.

SISO Single-Input Single-Output.

SINR Signal-to-Interference-and-Noise Ratio.

SNR Signal-to-Noise-Ratio.

SQ Uniform Square Array.

S-V-BLAST MRC V-BLAST with one shot ordering based on signal-to-interference-and-noise ratio values.

TDD Time Division Duplexed.

UE User Equipment.

ULA Uniform Linear Array.

V-BLAST Vertical Bell Laboratories Layered Space Time.

ZF Zero Forcing.

2BS Two collaborative base stations with multiple antennas at each.

3G Third Generation (with reference to third generation mobile telephony).

4BS Four collaborative base stations with multiple antennas at each.

5G Fifth Generation.

Notation

a, μ, A	Scalar. Italics characters of standard weight.
$\mathbf{v}$	Vector. Boldface, lower case. alphabeticals. Column vector unless otherwise stated.
$\mathbf{M}$	Matrix. Boldface, upper case alphabeticals.
$\mathbf{v}_i$	Element i of vector $\mathbf{v}$.
a^*	Complex conjugation.
$\mathbf{M}^{\mathrm{T}}, \mathbf{v}^{\mathrm{T}}$	Matrix and vector transpose.
$\mathbf{M}^{\mathrm{H}}, \mathbf{v}^{\mathrm{H}}$	Matrix and vector Hermitian transpose (conjugate transpose).
$\mathbf{M}^{-1}$	Matrix inverse.
$\mathbf{M}^{+}$	Moore-Penrose generalized inverse of $\mathbf{M}$.
$\mathrm{diag}\{\mathbf{M}\}$	Vector containing the diagonal elements of matrix $\mathbf{M}$.
$\mathrm{Tr}(\mathbf{M})$	Trace of matrix $\mathbf{M}$.
$\mathrm{rank}\{\mathbf{M}\}$	Rank of matrix $\mathbf{M}$.
$\|\mathbf{v}\|$	Euclidean norm of vector $\mathbf{v}$. $\|\mathbf{v}\|^2 \triangleq \mathbf{v}^{\mathrm{H}}\mathbf{v}$.
$\{a_i\}$	The set containing elements a_i.
$\max\{\cdot\}$	The maximum value taken by the argument.
$\min\{\cdot\}$	The minimum value taken by the argument.
$\mathrm{E}[x]$	Expectation of random variable x.
$\mathrm{Q}(x)$	Q-function (related to the complementary error function).

$$\begin{aligned} Q(x) &= \frac{1}{\sqrt{2\pi}} \int_x^\infty e^{-\frac{u^2}{2}} du \\ &= \frac{1}{2}\mathrm{erfc}(\frac{x}{\sqrt{2}}). \end{aligned}$$

$\mathbb{R}$	Real field.
$\mathbb{C}$	Complex field.
$\in$	In (an element of a set).
ab	Multiplication of a and b.
$a \times b$	Notation for matrix dimension where a is the number of rows and b is the number of columns.
$\sim$	Is distributed as.
$\mathcal{CN}(0, \sigma^2)$	A complex Gaussian distribution with zero mean and variance σ^2.
$\mathrm{Perm}(.)$	Permanent of a matrix.
$O(f(x))$	The order of the function $f(x)$. Assume that the point x approaches x_0. If there exists an $N > 0$ such that $\|g(x)\| \leq N\|f(x)\|$ in some sufficiently small neighborhood of the point x_0, we write $g(z) = O(f(z))$.
$\mathbf{y}$	A received signal.
$\mathbf{W}$	A combiner matrix.
$\mathbf{H}$	A channel matrix.
N_t	Total number of transmit antennas.
N_r	Number of receive antennas.
$\mathbf{n}$	A noise vector.
$\mathbf{I}$	The identity matrix.
ρ	The ratio of the transmit signal power to the noise power.
σ^2	The noise power.
r_0	The correlation coefficient between the true channel and its estimate.
δ_{ij}	The Kronecker delta function is defined as

$$\delta_{ij} = \begin{cases} 1 & \text{if } i = j \\ 0 & \text{if } i \neq j. \end{cases}$$

$\arg(.)$	The argument of (.).
A	A constant depending on transmit power, etc. which scales the link gains.
γ	The path loss exponent.
σ_{SF}	The shadowing factor standard deviation.
d_a	A cell diameter scaling factor.
b	The fraction of the cell radius fraction of the at which decorrelation occurs.
β	A parameter which controls the rate of decay of the link gains.
$\mathcal{A}$	The link gain of the strongest user.
α_u	The correlation between adjacent antennas in a uniform linear array.
Δ	The distance between adjacent antennas.
$\mathbf{R}_r$	The channel correlation matrix.
b_{ULA}	The length of the uniform linear array.
b_{SQ}	The width of the uniform square array.
R_{target}	The correlation target.
C_{out}	The outage Capacity.
$J_0(.)$	The zero$^{\mathrm{th}}$ order Bessel function.
$\log_n(.)$	The Logarithm operation of base n.
P_G	Group error probability.
$I_q(.)$	An incomplete beta function.
χ^2_n	Chi squared distribution with n degrees of freedom.

Chapter I

Introduction

This chapter is organized as follows. The problem statement and focus is given in Section 1.1 and a statement of originality is provided in Section 1.2. Section 1.3 illustrates the thesis outline and contributions, and Section 1.4 presents the published work, submitted work and papers under preparation.

1.1 Problem Statement and Focus

In the next decade, the demand for higher data rates and quality of service in wireless and mobile communications is expected to continue to grow rapidly. For example, according to the Telecommunication Regulatory Authority, in 2012, the United Arab Emirates' (UAE) mobile usage rose with an increase in active mobile subscribers to 11.72 million. That is a 7.33 percent increase in users from 2010, when there were 10.92 millions subscribers [3] [1] In addition, Commercial and Industrial Security Corporation made a prediction that global mobile traffic growth will increase by a factor of three from 2014 - 2019 [4]. Moreover, the internet of things is also predicted to increase the number of interconnected devices. This will potentially exceed the number of human subscriptions to cellular networks. According to a recent research forecast, the internet of things is predicted to reach 25 billion smart objects by 2020 [5]. Overall, this predicted growth in users, devices and traffic is expected to exceed the improvements in wireless communication technology that are currently possible with today's technology. As a

[1] The population of the UAE in 2012 was 9.2 million, of which 1.4 million were Emirati citizens.

result, telecom operators around the world are attempting to gain more spectrum. However, spectrum is scarce and expensive and industry and academia are already looking ahead to new ideas and new technologies that can help to meet the needs of future wireless services. Massive multi-input multi-output (MIMO), my area of study, is one of the technologies proposed both in university laboratories and in international industrial partnerships as a key enabler in the future. The idea is to have a large number of antennas in the transceivers to enhance the performance of a radio link [1,6–8]. Adding large numbers of antennas (10s-100s) at the base stations can be advantageous even under noisy channels [6].Despite several issues with massive MIMO (MM) [7] including array size [7], pilot contamination [7], mutual coupling [9], latency [10], cost and complexity, MM remains a very promising area. Companies are working in this area to standardize MM. For instance, Zhongxing Telecommunication Equipment Corporation has investigated MM in partnership with China Mobile as Huawei introduced the MM prototype in 2014 [11]. Vendors and operators such as Samsung and South Korea Telecommunication Company (SK Telecom) have experimented with MM prototypes [12].

In the 1990s, the development of multi-antenna communication increased the level of spectral efficiency and reliability that wireless channels could provide. MIMO technology has now been integrated into various developments such as WiFi and the Long Term Evolution (LTE) standard [13]. MM takes the development further, by increasing the scale of the MIMO concept. The degrees of freedom (DOF) in the wireless channel can be increased using MM where a large number of antennas are deployed [14]. Note that, as the number of antennas is increased at the transceivers, the better the performance that can be achieved in terms of data rate and link reliability [15].

In this thesis, we focus on the uplink of a MM system and receiver design in particular. With such a large number of antennas at the BS receiver, questions of deployment become even more relevant for MM than traditional MIMO. For example, should the 100s of antennas be

co-located at one BS or distributed at several BSs in the coverage area which are backhauled together to form a virtual array? (Note that, as antennas are distributed over a large geographical area, backhaul requirements and latency will be increased). In addition, at each BS should the antennas be deployed in a linear array or in a more compact shape such as a square? These issues are also closely related to the presence of channel correlation since the large MM arrays may be constructed in a small physical space. This reduces antenna spacing and increases the likelihood of high channel correlation. For these reasons, deployment issues and channel correlation effects are also considered in the thesis in addition to receiver design.

In terms of uplink receiver design, two important factors for MM are complexity and channel state information (CSI). Typical linear receiver (zero forcing (ZF) and minimum mean-square error (MMSE)) are commonly considered to be low-complexity for traditional MIMO systems. However, with a MM system there might be 100s of antennas serving 10s of users. Here, the processing involved in computing the receiver weights is non-negligible, especially when matrix inverses are required. Hence, there is an increased focus on further complexity reduction for MM. Finally, MM is likely to suffer from less accurate channel estimation than smaller systems due to effects such as latency in distributed arrays [10] and pilot contamination [7]. Hence, in this thesis both perfect and imperfect CSI are considered. In terms of receiver design, the thesis develops and analyzes a novel low-complexity receiver which has lower complexity than a linear ZF reciever while maintaining similar performance in a wide range of conditions.

1.2 Statement of Originality

This thesis represents original work by the author, unless otherwise mentioned. None of the material of this thesis has been previously submitted for examination for any degree. Most of the material in this thesis has been published, submitted for publication, or is under preparation for publication. The thesis outline, author's contribution and publications are listed in Sections

1.3 and 1.4. This work has been undertaken under the support and guidance of my supervisors: Prof. Peter Smith and Dr. Graeme Woodward.

1.3 Thesis Outline and Contributions

This thesis studies MM receiver designs and their performance in a multiuser context. In terms of performance metrics, the output signal-to-interference-and-noise-ratio (SINR), symbol error rate (SER) and ergodic capacity are used for facilitating system comparison. Brief summaries of each chapter are shown below.

- **Chapter 2: Background and Literature Review**

  This chapter gives an overview of MIMO, multiuser MIMO, MM, MM deployment and MM arrays. In addition, channel models, system models, receivers, performance metrics, power control (PC) and adaptive modulation (AM) are introduced.

- **Chapter 3: Distributed vs Co-located Base Station Deployment**

  To evaluate the benefits of distributed arrays in MM systems, we investigate the interaction between linear receivers (maximum ratio combining (MRC) and ZF and three deployments scenarios: (i) a massive co-located array at the cell center; (ii) a massive array clustered at B discrete locations; and (iii) a massive distributed array with a uniform distribution of individual antennas. We also study the effect of propagation parameters, system size, correlation and channel estimation error. We demonstrate by analysis and simulation that in the absence of any system imperfections, a massive distributed array is preferable. An intermediate deployment such as a massive array clustered at a few discrete locations, can be more practical to implement and more robust to imperfect CSI. We show an example with a 128 antenna deployment where four locations achieves one third of the gains due to a fully distributed array.

- **Chapter 4: Array Size and Shape**

  With MM, it may be the case that large numbers of antennas are closely packed to fit in some available space. Here, channel correlations become important and it is of interest to investigate the space requirements of different array shapes. Here, we focus on uniform square and linear arrays and consider a range of correlation models. We show that the benefits of two-dimensional arrays are dependent on the type of correlation. When the correlation decays slowly over small antenna separations then square arrays can be far more compact than linear arrays or they can offer substantial capacity enhancements. When the correlation decays more quickly, then the main benefit is compactness.

- **Chapter 5: Performance of Traditional Vertical Bell Laboratories Layered Space Time (V-BLAST) Based on Optimal Ordering**

  In an uplink MM deployment with distributed single-antenna user equipments (UEs) and a large base-station (BS) array, we consider, in this chapter, the performance of vertical Bell Laboratories Layered Space Time (V-BLAST) with MRC and V-BLAST with ZF. In the performance evaluation, we include the effects of imperfect CSI and channel correlation since these system imperfections are of particular importance in MM. The main contribution is that the performance of MRC V-BLAST is shown to approach that of ZF V-BLAST under a range of imperfect CSI levels, different channel powers and different types of array, as long as the channel correlations are not too high.

- **Chapter 6: Low Complexity MRC V-BLAST Based on Channel Norm Ordering**

  In an uplink MM deployment with distributed single-antenna UEs and a large BS array, we consider, in this chapter, several combinations of receivers using linear combiners (MRC and ZF) in conjunction with V-BLAST. We show that the performance loss of MRC relative to ZF can be removed in certain situations through the use of V-BLAST.

Furthermore, we develop a low complexity ordering scheme based on the channel norm (C-V-BLAST) which results in a V-BLAST scheme with MRC which has much less complexity than a single ZF linear combiner. An analysis of the SINR at each stage of the V-BLAST approach is also given to support the findings of the proposed technique.

- **Chapter 7: Low Complexity MRC V-BLAST Based on Channel Norm Ordering with Adaptive Modulation and Power Control**

  We consider the performance of a low complexity V-BLAST system with an MRC receiver (C-V-BLAST) in an uplink MM deployment with single antenna UEs. We show in Chapter 6 that this receiver gives a similar error rate performance to ZF for simple systems while reducing complexity. In this chapter, we show that C-V-BLAST remains similar to ZF for more complex adaptive modulation systems and in the presence of channel estimation error, C-V-BLAST can be superior. These results are analytically justified and we derive an exhaustive search algorithm for PC to bound the potential gains of PC. Using this bound, we demonstrate that C-V-BLAST performs well without the need for additional PC.

- **Chapter 8: Analysis of Low Complexity MRC V-BLAST based on Link Gain Ordering**

  An uplink MIMO deployment with distributed single-antenna UEs and a large BS array is considered. Due to the high dimension of MM systems there is a considerable interest in detection schemes with a better complexity-performance trade-off. In this chapter, a simplified version of a low complexity ordering scheme based on large scale fading information is developed and analyzed for a V-BLAST scheme with MRC, and compared with other more complex detection schemes such as the linear ZF receiver. Moreover, an explicit closed form analysis for error probability for both co-located and distributed

BSs is provided along with a number of novel performance metrics which are useful in designing MM systems. It is shown that the error performance of the distributed scenario can be well approximated by a modified version of a co-located scenario. The simulation study in the absence of any system imperfections demonstrates the performance of the proposed scheme and confirms the accuracy of analytical results.

- **Chapter 9: Conclusions and Future Work**

  This chapter provides conclusions and details of possible future work.

1.4 Publications

A list of published, submitted papers and presentations produced during my PhD studies is shown below.

1. *Journal Articles*

   - **K. A. Alnajjar**, P. J. Smith and G. K. Woodward, "Co-located and distributed antenna systems: deployment options for massive MIMO", *accepted for publication in IET Microwaves, Antennas & Propagation*, Jun 2015.

2. *Submitted Papers*

   - **K. A. Alnajjar**, P. J. Smith, G. K. Woodward and D. A. Basnayaka, "Analysis of Low complexity MRC V-BLAST based on link gain ordering for massive MIMO", *Submitted to IEEE Transactions on Wireless Communications (TWC)*, 2015.
   - **K. A. Alnajjar**, P. J. Smith, G. K. Woodward and P. Whiting, "An investigation of size and array shape for "Size and array shape for massive MIMO", *Submitted to IEEE Wireless Communications letters*, 2015.

3. *Conference Proceeding Papers*

- **K. A. Alnajjar**, P. J. Smith and G. K. Woodward, "Low complexity V-BLAST for massive MIMO", in *Proc. IEEE Australian Communications Theory Workshop (AusCTW)*, Sydney, Australia, Feb. 2014.
- **K. A. Alnajjar**, P. J. Smith and G. K. Woodward, "Performance of massive MIMO V-BLAST with channel correlation and imperfect CSI", *in Proc. IEEE on Australian Telecommunication Networks and Applications Conference (ATNAC)*, Melbourne, Australia, Nov. 2014.
- **K. A. Alnajjar**, P. J. Smith and G. K. Woodward, "Low complexity V-BLAST for massive MIMO with adaptive modulation and power control", *in Proc. IEEE Conf. on Information and Communication Technology Research (ICTRC)*, Abu Dhabi, UAE, May. 2015 (**Awarded for the Best Oral Paper**).

4. *Additional Presentations*

- **K. A. Alnajjar**, P. J. Smith and G. K. Woodward, "What is the best deployment for massive MIMO ?", *IEEE New Zealand Wireless Workshop*, Wellington, New Zealand, Sep. 2013.
- **K. A. Alnajjar**, P. J. Smith and G. K. Woodward, "Deployment scenarios in massive MIMO", *UC SHOWcase*, Christchurch, New Zealand, Nov. 2013.
- **K. A. Alnajjar**, P. J. Smith and G. K. Woodward, "Receiver design for massive MIMO", *WRC Seminar*, Christchurch, New Zealand, May. 2014.
- **K. A. Alnajjar**, P. J. Smith and G. K. Woodward, "Performance of massive MIMO with channel correlation and imperfect CSI", *IEEE ICTRF2014/GERS2014 symposium*, Abu Dhabi, United Arab Emirates, May. 2014.

- **K. A. Alnajjar**, P. J. Smith and G. K. Woodward, "Low complexity V-BLAST for massive MIMO", *Seminar in University of Sharjah*, Sharjah, United Arab Emirates, May. 2014.
- **K. A. Alnajjar**, P. J. Smith and G. K. Woodward, "Technical work: Receiver design for massive MIMO and personal experience of studying abroad and the challenges", *Seminar in Khalifa University*, Abu Dhabi, United Arab Emirates, May. 2014.
- **K. A. Alnajjar**, P. J. Smith and G. K. Woodward, "Massive MIMO receiver design", *Thesis in 3*, Christchurch, New Zealand, August. 2014.
- **K. A. Alnajjar**, P. J. Smith and G. K. Woodward, "Power control with low complexity V-BLAST for massive MIMO with adaptive modulation", *IEEE New Zealand Wireless Workshop*, Christchurch, New Zealand, Sep. 2014.
- **K. A. Alnajjar**, P. J. Smith and G. K. Woodward, "Recent research outcomes in massive MIMO receiver design", *Seminar in University of Sharjah*, Sharjah, United Arab Emirates, Jan. 2015.
- **K. A. Alnajjar**, P. J. Smith and G. K. Woodward, "Recent research outcomes in massive MIMO receiver design", *Seminar in American University of Sharjah*, Sharjah, United Arab Emirates, Jan. 2015.

Chapter II

Background and Literature Review

2.1 Introduction

This chapter provides the relevant background information. Sections 2.2, 2.3 and 2.4 give an overview of Multiple-Input-Multiple-Output (MIMO), multiuser MIMO and massive MIMO (MM), respectively. In Section 2.5 some issues concerning deployment and array design are presented. Section 2.6 provides channel models and Section 2.7 gives the system model. We present in Section 2.8 the basic receiver designs considered including linear combiners and the Vertical Bell Laboratories Layered Space Time (V-BLAST) technique. We present performance metrics, power control and adaptive modulation in Sections 2.9, 2.10 and 2.11, respectively. We provide parameter values in Section 2.12 and conclude in Section 2.13.

2.2 Multiple-Input-Multiple-Output (MIMO)

The wireless channel changes over time and space because of random movements of obstacles or UEs [16]. Owing to the presence of scattering in the wireless channel, the received signal at the destination experiences a random superposition of multi-path components [16]. Figure 2.1 illustrates an example of possible paths for the received signal. The undesired random channel fluctuations, called fading, severely affect quality and reliability.

MIMO is one of the techniques designed to combat and exploit these problems. MIMO is

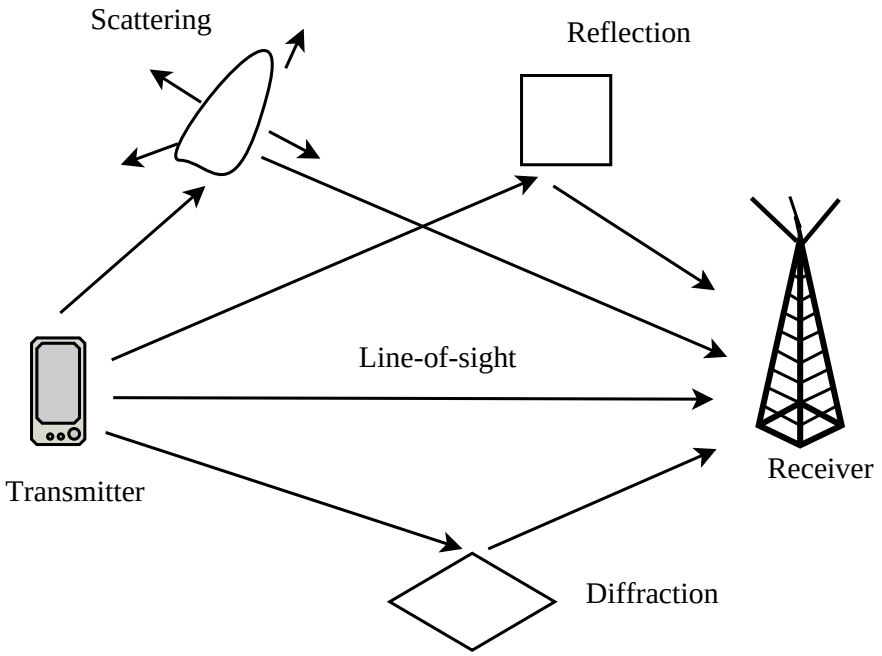

Figure 2.1: An example of possible paths for the received signal in a wireless channel.

a combination of single-input-multiple-output (SIMO) and multiple-input-single-output design (MISO) [17]. MIMO exploits spatial diversity at each end of the link [17, 18]. The MIMO channel is constructed with multiple element arrays at both ends of the wireless link. Multiplexing gain and diversity gain are two major MIMO gains [17, 18]. Multiplexing gain requires multiple receive and transmit antennas where transmitters send multiple streams [17, 18]. However, diversity gain requires multiple transmit and/or receive antennas and deals with one data stream which can be viewed multiple times via different fading channels [17, 18]. Figure 2.2 shows an example of a MIMO system model. It has been shown that large gains in capacity compared with traditional single-input-single-output (SISO), SIMO or MISO channels are feasible in MIMO systems. However, hardware costs and some additional processing are required when using MIMO [19]. There are many factors affecting the performance of MIMO systems. The number of antennas, antenna spacing, channel characteristics (line-of-sight or non-line-of-sight), and choice of codes and signal combining methods [20] are all important factors in

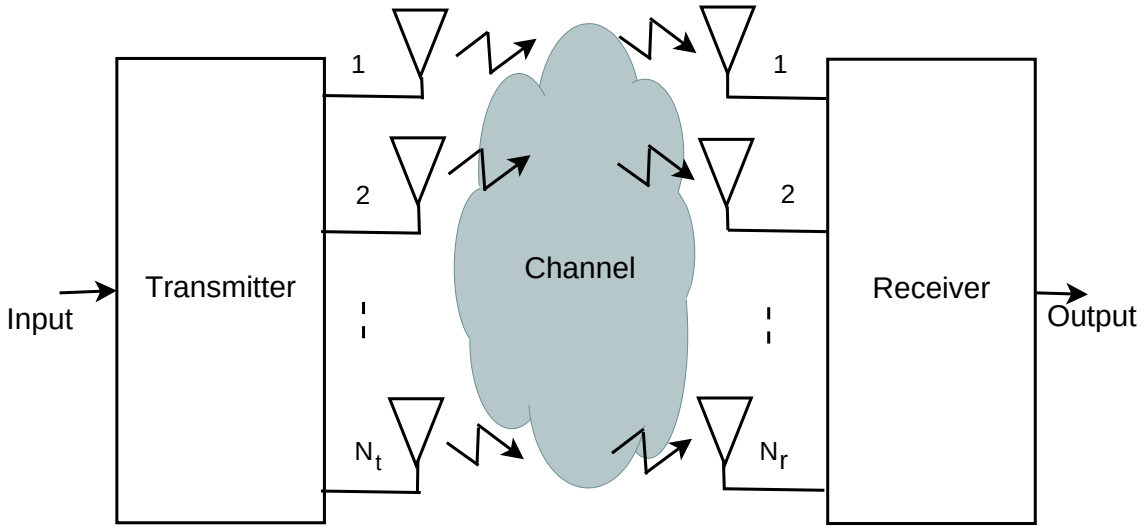

Figure 2.2: A MIMO system model.

MIMO performance.

2.2.1 Detection

In MIMO systems, the joint detection of signals is essential and can be performed optimally by the exhaustive search method, namely maximum likelihood detection [17, 18, 21]. Due to its exponential complexity with the number of transmitters and the constellation size [18], suboptimal methods have been investigated [21] including linear combiners, successive interference cancellation (SIC) detection, list decoding and lattice reduction aided detection [21]. As the number of antennas grows, the simpler methods become more and more attractive due to the computational demands of the near-optimal approaches.

2.3 Multiuser MIMO

Multiuser MIMO systems allow multiple UEs to transmit to the BS [1] which receives separate signals simultaneously in the same time and frequency slot [17, 22]. Multiuser MIMO has been studied in both downlink (broadcast channel) and uplink (multiple access channel) scenarios [17, 22]. A multiuser MIMO base station can be deployed in co-located or distributed configurations. In the co-located scenario, there is only one BS that serves many UEs, but in the distributed scenario, many BSs can collaborate and serve many UEs. Note that these distributed BSs are located in different places and each BS is connected to a central processing unit (CPU) to share information. The motivation for the distributed scenario was to increase coverage areas and reduce outage by using several inexpensive BSs spread across the cell [23]. Figures 2.3 and 2.4 show examples of uplink multiuser MIMO systems. Figure 2.3 shows the co-located scenario example where one BS receives signals from three UEs. Figure 2.4 displays the distributed scenario example where three BSs support four UEs. The downside of using distributed BSs includes cost, latency, environmental issues and complexity. This is due to increased backhaul from each antenna to the central processing location (which has implications on cost, latency and complexity) and getting access to many more antenna sites (cost, regulatory, environmental, complexity).

2.3.1 Detection for MIMO

The maximum likelihood multiuser detector can be used for the uplink scenario for obtaining optimal performance [21]. It has also been shown that an iterative lattice reduction based detection method can achieve the same diversity as that of the maximum likelihood multiuser detection with reduced complexity [21]. However, these receivers lead to a complex system

[1] In the long term evolution (LTE), the BS is usually called E-UTRAN Node B (eNodeB) or Evolved Node B (eNB) [13].

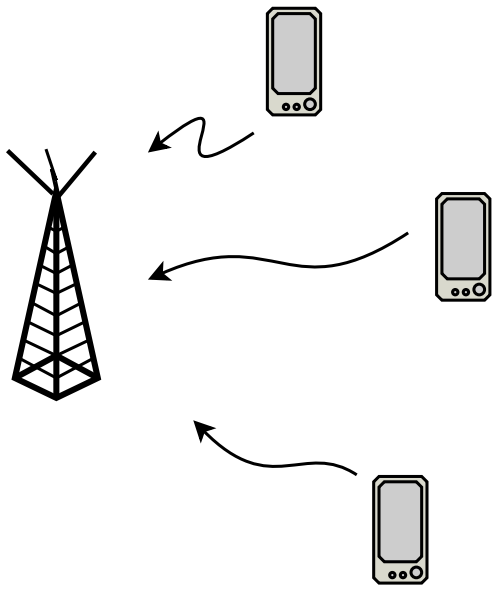

Figure 2.3: An uplink multiuser MIMO system, co-located scenario.

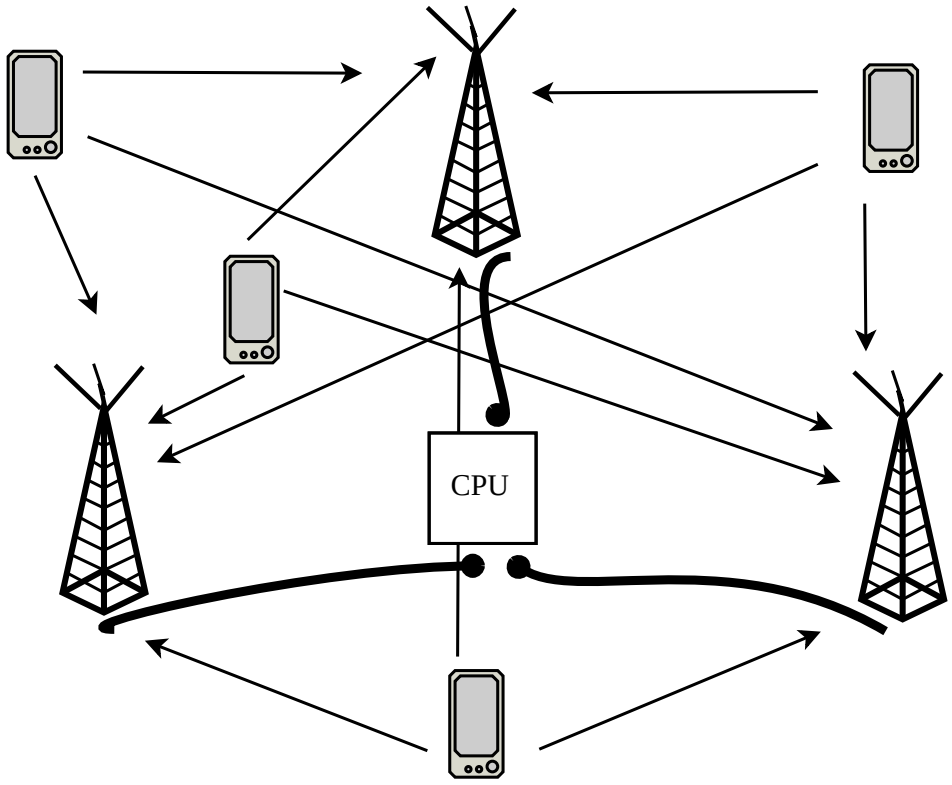

Figure 2.4: An uplink multiuser MIMO system, distributed scenario.

implementation, especially for large systems. Consequently, the linear combiners discussed in Section 2.8.1 are commonly used alternative suboptimal MIMO detection techniques.

2.4 Massive MIMO

Massive MIMO or very large MIMO is becoming a promising candidate for wireless communications [1, 6–8]. In addition, MM is an active area for 5^{th} generation wireless systems (5G) due to its potential to achieve high performance [6] and to reap all the benefits of conventional MIMO but on a larger scale [1]. MM is also known as a large-scale antenna system, very large MIMO, hyper MIMO and full-dimension MIMO. MM systems are a type of cellular communication system where a BS has a large number of antennas (10-100)s either in one location or in different locations [6]. By using large numbers of antennas at the BS, different UEs become orthogonal to each other and the inter-user interference diminishes. Therefore, the data rate will increase and low complexity signal processing techniques can be utilized [6]. However, there are some disadvantages in using MM. More details are given in the following sections.

2.4.1 Massive MIMO Advantages

With MM, the DOF can be increased [15] and the transmitted power can be reduced [24]. In contrast to the expensive high power linear amplifiers used in traditional MIMO systems, inexpensive low power (milliwatts) amplifiers can be used in MM [24]. In addition, MM can average out the effect of small-scale fading and create quasi-orthogonal UEs [24]. As a result, it is powerful against fading and robust against failure of one or a few antennas [1]. Adding large numbers of antennas (10s-100s) at the BSs can be advantageous even under noisy channels [1, 6–8]. Note that large arrays at the BSs can handle large number of UEs because the DOF increases. Large multiplexing gains and an improved radiation efficiency are other advantages of using MM [1]. For example, MM can utilize a very narrow (pencil) radiation beam pattern

or a high directivity gain [25].

MM represents a paradigm shift in theory, systems and implementation [1, 6–8, 15, 26]. For instance, although interference mitigation techniques have been the focus in traditional MIMO, these techniques are less critical for large systems. By using the simplest forms of UE detection and precoding (MRC and matched filtering (MF)), good performance is obtained in MM [7, 15, 26].

2.4.2 Massive MIMO Disadvantages

The performance of MM systems depends heavily on the antenna properties and the propagation environment [7]. The MM performance can be enhanced by using channel state information (CSI) at the BS [7, 25]. For instance, in time division duplex (TDD), CSI is assumed to be available due to channel reciprocity [7, 25]. However, hardware impairments in MM systems can lead to imperfect CSI and decreasing system performance [25, 27, 28]. Additionally, with TDD operation, the performance of MM becomes limited by the interference arising from the re-use of pilots in neighboring cells [7, 25]. The number of orthogonal sequences is limited by the coherence time [7, 25], which itself depends on the mobility of the terminals. Thus, the pilots must be reused and therefore, inter-cell interference remains [29]. Hence, with imperfect channel estimation, the system performance can degrade severely due to pilot contamination.

MM array size, deployment and configuration are some of the crucial issues in MM [7, 25]. Placing the antennas in a two dimensional grid or in three dimensions, and in co-located or distributed configurations are some practical issues that need to be considered for the antenna arrays [1, 25, 30–34]. Mutual coupling [9] can only be ignored when the antennas are separated from each other and this is unlikely in the MM scenario [25]. Furthermore, due to the communication required between BSs in the distributed case, latency [1, 10] and backhaul requirements will increase. Moreover, hardware cost and complexity remain crucial in MM [7, 25].

Propagation models are complicated by the number of antennas, although ongoing research adapts the Rayleigh fading model to analyze MM systems [25]. Some experimental studies have shown that antenna correlations can be significant [25]. Also, for highly correlated channels, channel vectors tend to be less orthogonal than for independent channels [7, 25]. Such effects are important in MM, since if the large arrays are located within a small area, then the channel correlations may be substantial [7].

2.4.3 Massive MIMO Companion Technologies

Millimeter wave (mmWave) is another technology proposed for 5G [8, 25]. It has been standardized for short range usage (IEEE 802.11ad) and deployed for niche applications such as small-cell backhaul [8]. The available mmWave frequency bands include 28-30 GHz, the free band at 60 GHz and the E-band at 71-76 GHz, 81-86 GHz and 92-95 GHz [8]. mmWave offers spectral availability and shorter wavelengths allowing for small dense antenna arrays with, relatively, low correlation at small antenna spacings. The main problem with mmWave is the sensitivity to blockages [8]. The advantages of using mmWave with MM is increased capacity and spectral efficiency for communication systems [35]. For instance, using both technologies can be significant in increasing throughput backhaul in areas where it is expensive to install fiber or wire connections [35]. In fact, MM has been proposed as a method to relay information back and forth between cells or closer network hubs [35]. This has considerable advantages over microwave backhaul links which require dish antenna and physical antenna alignments [35]. Interestingly, MM arrays can alter transmit and receive beams under environmental changes without the demand of physical readjustments and MM arrays can also communicate with many backhaul stations because their beams are steerable [35]. Moreover, compact dimensions, flexibility and adaptivity in small cells can be achieved using both technologies.

Besides the mmWave technology, heterogeneous networks (HetNets) are another technol-

ogy which can link with MM. HetNets involve a mixture of cell types, commonly including macro-cells containing low-cost small cells such as pico-cells or femto-cells [14, 25]. By using HetNets with MM, interference management, energy efficiency and throughput can be improved and this is an important future research direction [25]. For instance, during downlink transmission, the macro-cell BS can estimate the null space of the small cells and project its downlink data into the null space for interference free transmission. By using a MM array at the macro-cell BS, the increased degrees of freedom can be used to handle more small cells and improve system performance [25]. Several studies have proposed some solutions for interference coordination, precoding techniques and backhaul requirements [14, 36, 37] to improve system performance when using both technologies.

2.4.4 Massive MIMO in Practice

There are numerous recent prototypes that provide high spectral efficiency with large arrays. For example, the Ngara testbed uses a 32 element BS to serve 18 UEs [38] and 64×64 MIMO channel sounding measurements at 5GHz in an indoor environment are discussed in [39]. In addition, the Argos testbed also used 64 antennas as described in [40]. Companies are also working to standardize MM. For instance, Zhongxing Telecommunication Equipment Corporation has investigated MM in partnership with China Mobile and Huawei introduced the MM prototype in 2014 [11]. Finally, Samsung and South Korea Telecommunication Company have experimented with MM in a mmWave prototype [12] in 2015.

2.4.5 Detection for Massive MIMO

Many detection methods have been studied in MM to extract the desired signal from the received signal. The complexity of optimal detectors is based on a maximum likelihood or maximum posteriori probability criterion and is exponential in the number of transmit antennas [6]. De-

tectors which approach optimal performance (i.e., the sphere decoder and variants) introduce usually high complexity. In contrast, popular low complexity approaches are usually based on linear receivers such as ZF, MMSE and MRC. However, in MM, linear receivers can approach optimal performance and there are several algorithms proposed to achieve high performance with the same complexity as linear detectors. Examples include detectors based on local search and belief propagation [41].

One of the most popular schemes in traditional MIMO is the V-BLAST approach, which is a multi-layer symbol detection scheme. It uses nonlinear (serial cancellation) and linear combining (interference suppression) and has been studied with imperfect channel estimation [42] and with correlated channels [43]. Most of the work on traditional V-BLAST discusses ZF or MMSE combiners and rarely considers MRC [44, 45]. Also, very little work has appeared on V-BLAST with MM since the prime focus of MM is simplicity whereas V-BLAST requires repeated detection and ordering. However, by replacing ZF or MMSE receivers with MRC and using a one-shot ordering method (see Chapter 6 and Chapter 8) this thesis develops a version of V-BLAST for MM with a lower complexity than linear ZF detection and a similar performance.

2.4.6 Precoding for Massive MIMO

In MM there is a very large array at the BS serving many UEs with small numbers of antennas. Hence, both the computational processing power and the DOF are heavily weighted towards the BS. As a result, most work on MM focuses on uplink combining or downlink precoding. In both cases, the BS uses the large array to separate the signals associated with multiple UEs. In this context, uplink precoding at the UEs is often neglected. This is because the MM array already has the power to separate the UEs and the further enhancement offered by uplink precoding may be small. More importantly, uplink precoding also involves an extra feedback stage from the BS to the UEs so that precoding information can be computed at the BS and sent out to

the UEs. Since only a limited number of feedback bits are usually available, the precoding information actually delivered to the UEs is not perfect. The use of an extra feedback stage to provide imperfect precoding information to the UEs is often considered too expensive for implementation. Hence, following much of the MM literature, we do not assume any precoding at the UEs in the thesis.

Nevertheless, uplink precoding may have its place in some systems. In the LTE system, for example, an uplink precoder has been standardized [46].

2.5 Deployment and Array Design

2.5.1 Deployment

MM can result from a large number of antennas deployed at one location or from an array of distributed antennas linked together to form a massive network MIMO system [7]. Hence, the following scenarios are considered in the thesis:

- one massive co-located array (COL);
- B-collaborative base stations with multiple antennas at each BS (BBS);
- one massive array with geographically distributed single antenna BSs (DIST).

In all deployment scenarios, we assume that the UEs are located uniformly and randomly in the coverage area. For example, suppose the UEs are located randomly in the coverage area (assumed to be square for simplicity) and the number of received antennas is 81. The BSs are located symmetrically in the region as in Figure 2.5. In this example we consider the specific cases given by COL: 81 co-located antennas; 3BS : 27 antennas at 3 BSs; and DIST: 81 single antenna BSs located in a symmetric 9×9 grid.

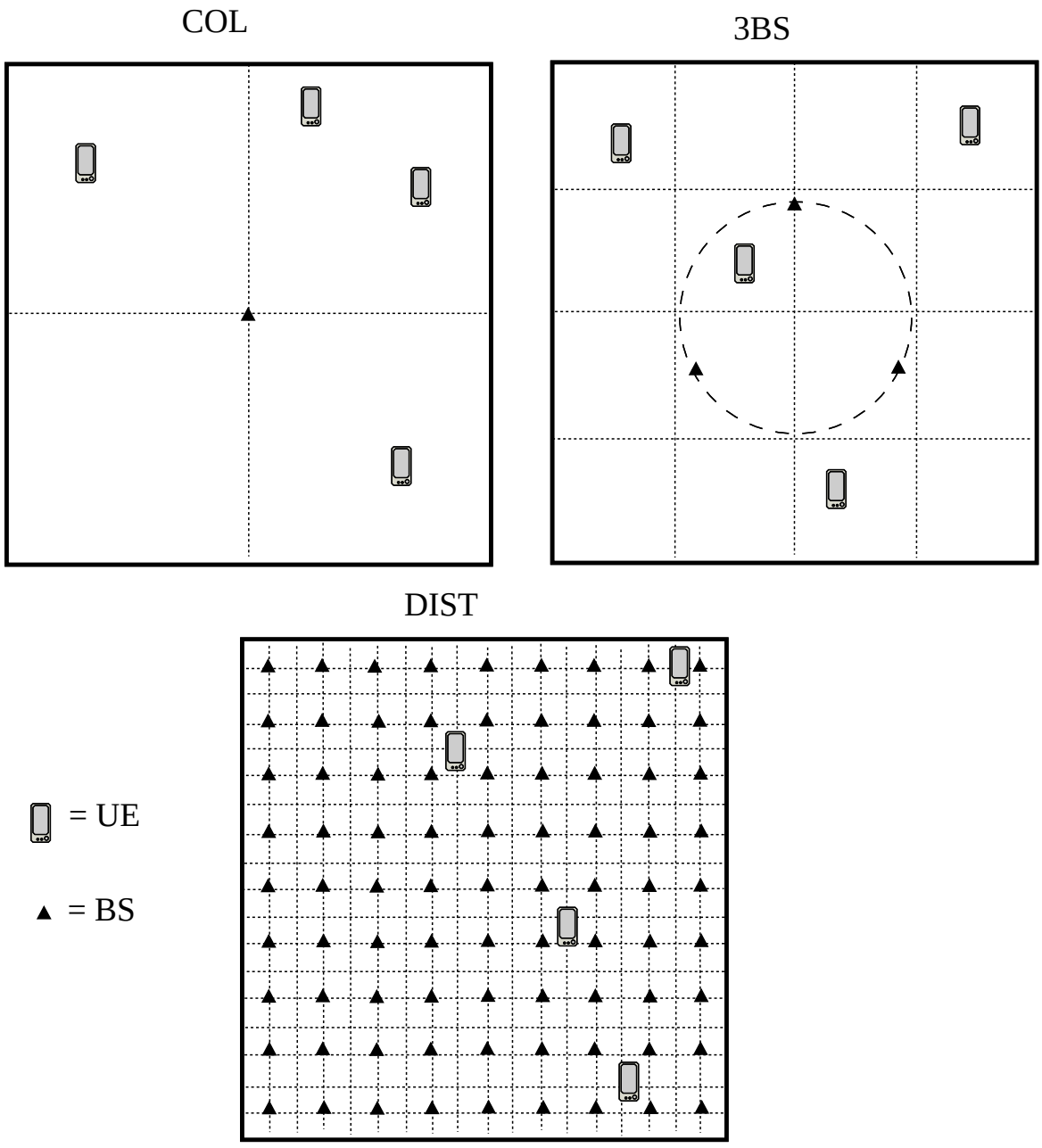

Figure 2.5: Example of deployment scenarios. COL: one massive co-located array. 3BS: 3-collaborative base stations with multiple antennas at each BS. DIST: one massive array with geographically distributed single antenna BSs.

2.5.2 *Arrays*

MM array types can take different shapes such as [7]:

- Linear Array.
- Square Array.
- Circular Array.
- Rectangular Array.
- Cylindrical Array.

Figure 2.6 shows an example of antenna arrays and deployment scenarios for a MM base station [1].

If the large arrays are located within a small area, then the channel correlations may become quite high impacting on system performance [7]. With a limited dimension on the antenna array, the DOF, and thus the sum-capacity, only grows as the square-root of the number of antennas [15]. In this thesis, we consider the uniform linear array (ULA) and the uniform square array (SQ). The difference between the two types of array is dependent on the scenario. For example, a SQ can be more compact than a ULA if space is limited. However, if space is not an issue, SQ can offer increased antenna spacing for the same overall length of array. These situations are described as Case 1 and Case 2 respectively in Figure 2.7. In Case 1, the SQ is very compact compared to the ULA, which can be useful in MM when there is limited space available for the array. However, if the correlation increases, the antennas in the SQ may need to be separated to give the same performance as the ULA. In Case 2, we see that using the same width as the ULA gives increased spacings and reduced correlation with SQ. Hence, the choice of array is governed by two key factors: the available space for deployment and the size of the

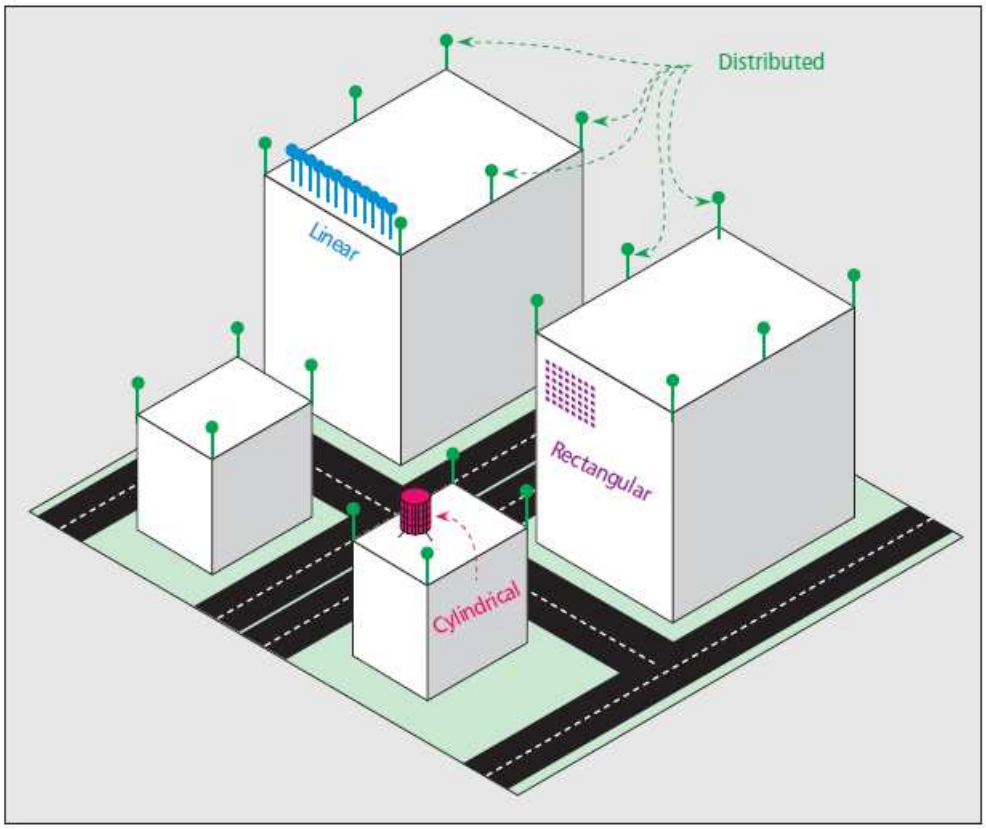

Figure 2.6: An example of antenna arrays and deployment scenarios for a MM base station [1].

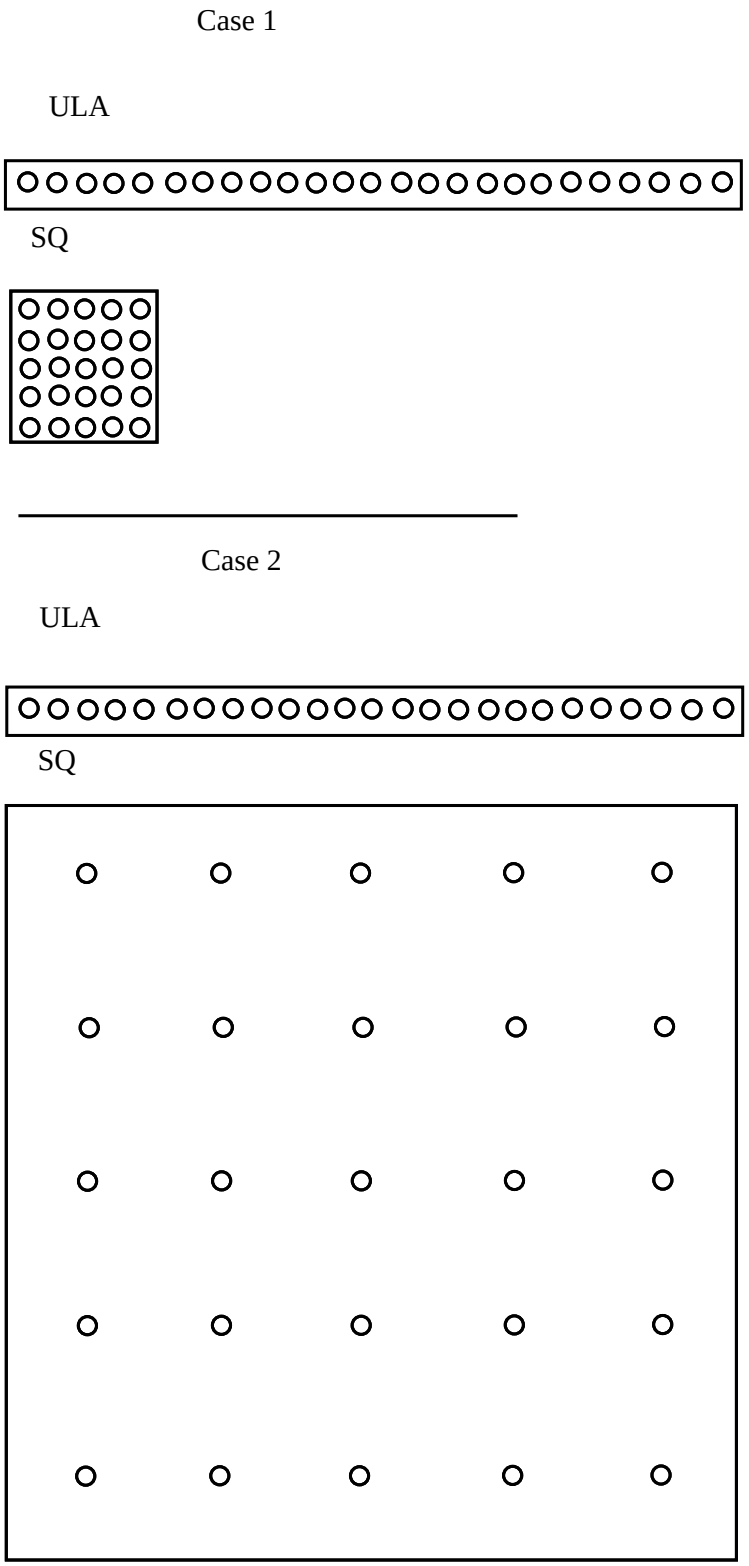

Figure 2.7: Two deployment cases with two types of array (SQ and ULA).

arrays needed to provide a given performance. Hence, there is a trade off between performance and antenna spacing.

2.6 Channel Models

A channel is a medium, wired or wireless, which is used to convey an information signal [6, 17, 47]. The wireless channel is usually considered to be random with the variation of the channel strength, being classified into large scale fading and small scale fading [6,17,47]. The large scale fading, which can be independent of frequency [48], results from signal path loss (a distance function) and shadowing, from large obstacles such as buildings. On the other hand, small-scale fading, which is frequency dependent, is a consequence of multiple signal paths between the transmitter and receiver that lead to both constructive and destructive interference [6, 17, 47].

2.6.1 MIMO Channel Models

Assume the number of receive antennas is N_r and the number of transmit antennas is N_t. The channel matrix of size $N_r \times N_t$ can be written as

$$\mathbf{H} = [\mathbf{h}_1 \cdots \mathbf{h}_{N_t}] = \begin{bmatrix} h_{11} & h_{12} & \dots & h_{1N_t} \\ h_{21} & h_{22} & \dots & h_{2N_t} \\ \vdots & \vdots & \ddots & \vdots \\ h_{N_r1} & h_{N_r2} & \dots & h_{N_rN_t} \end{bmatrix}, \tag{2.1}$$

where $\mathbf{h}_i = [\mathbf{h}_{1i}\ \mathbf{h}_{2i} \cdots \mathbf{h}_{N_ri}]^T$. The channel matrix $\mathbf{H}$ describes the fading characteristics of the entire MIMO link. According to the geographical distribution of the transmit and receive antennas, each link can have a different average link power. Because our focus is on multiuser MIMO, where each UE has a single antenna, each column corresponds to a UE. The channel coefficient, h_{ij}, from UE j to receive antenna i has power $E[|h_{ij}|^2] = P_{ij}$. Therefore the link

gain power matrix can be written as

$$\mathbf{P} = \begin{bmatrix} P_{11} & P_{12} & \dots & P_{1N_t} \\ P_{21} & P_{22} & \dots & P_{2N_t} \\ \vdots & \vdots & \ddots & \vdots \\ P_{N_r1} & P_{N_r2} & \dots & P_{N_rN_t} \end{bmatrix}. \tag{2.2}$$

In the COL scenario shown in Figure 2.8, there is a single massive co-located array. Each link from a user to the co-located BS therefore has the same power. Therefore, $P_{ij} = P_j$ and the $\mathbf{P}$ matrix can be written as

$$\mathbf{P} = \begin{bmatrix} P_1 & P_2 & \dots & P_{N_t} \\ P_1 & P_2 & \dots & P_{N_t} \\ \vdots & \vdots & \ddots & \vdots \\ P_1 & P_2 & \dots & P_{N_t} \end{bmatrix}. \tag{2.3}$$

In the BBS scenario shown in Figure 2.9, there are B-collaborative base stations with multiple antennas at each (BBS). Each link from a user to each group of BS has the same power. Hence,

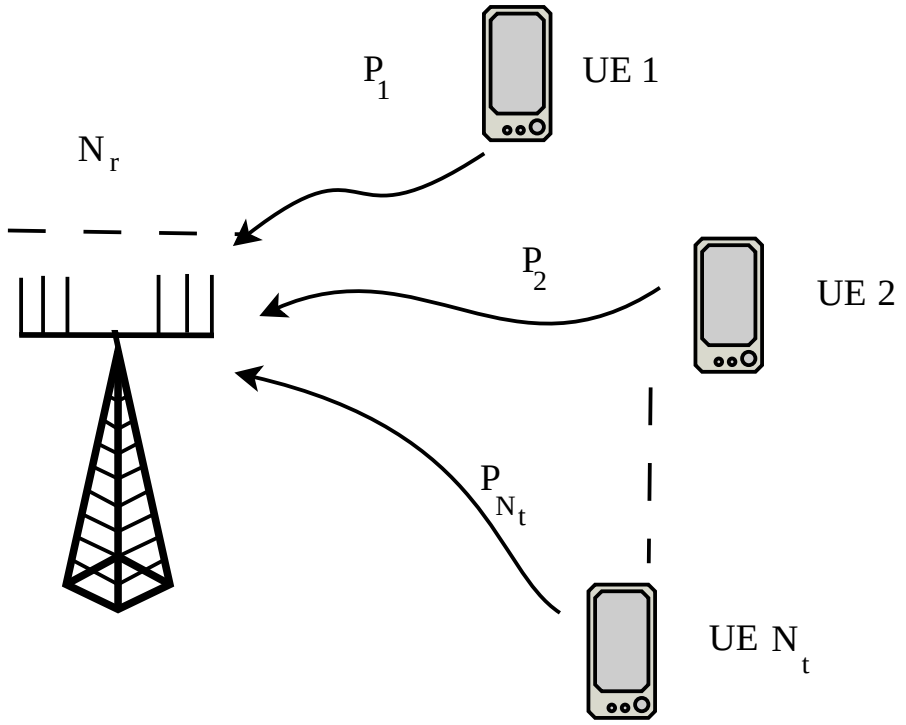

Figure 2.8: An example of a COL scenario with a link gain profile.

$P_{ij} = P_j^{(k)}$ where $k = \{1 \ldots, B\}$ and $\mathbf{P}$ can be written as

$$\mathbf{P} = \begin{bmatrix} P_1^{(1)} & P_2^{(1)} & \ldots & P_{N_t}^{(1)} \\ P_1^{(1)} & P_2^{(1)} & \ldots & P_{N_t}^{(1)} \\ \vdots & \vdots & \ddots & \vdots \\ P_1^{(2)} & P_2^{(2)} & \ldots & P_{N_t}^{(2)} \\ P_1^{(2)} & P_2^{(2)} & \ldots & P_{N_t}^{(2)} \\ \vdots & \vdots & \ddots & \vdots \\ P_1^{(B)} & P_2^{(B)} & \ldots & P_{N_t}^{(B)} \\ P_1^{(B)} & P_2^{(B)} & \ldots & P_{N_t}^{(B)} \end{bmatrix}. \tag{2.4}$$

In the DIST scenario, there is one massive array with geographically distributed single antenna

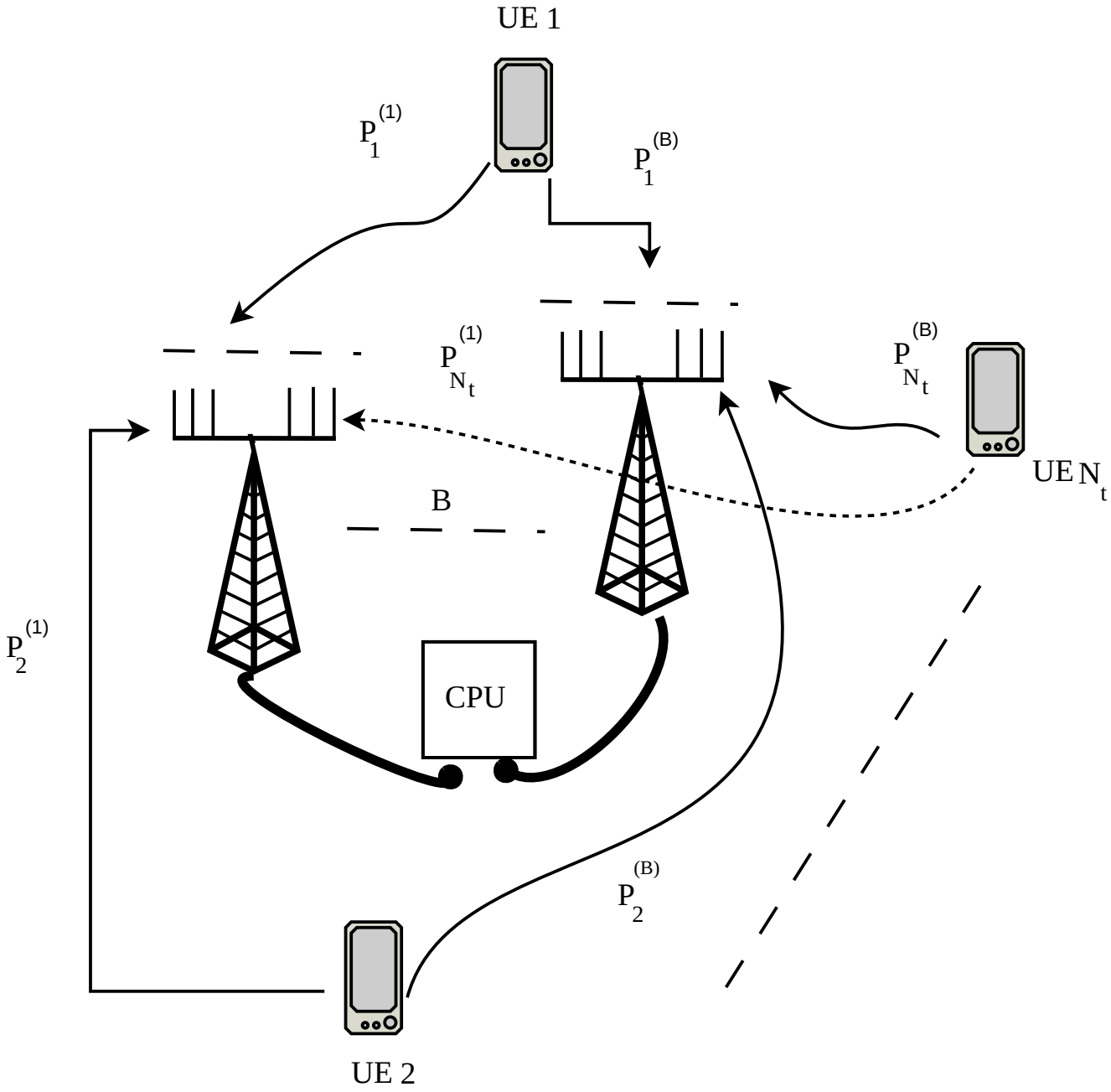

Figure 2.9: An example of a BBS scenario with a link gain profile.

BSs. Each link from a user to a BS has different power. Therefore $\mathbf{P}$ can be written as in (2.2).

In the following subsections, the specific types of channel models and link gain structures are described.

2.6.2 Rayleigh Fading Channel Model

A Rayleigh fading model describes the received power in a situation where there is no line of sight between transmitter and receiver due to a dense urban environment containing a large number of scatterers [47]. In Rayleigh fading, the channel coefficient, h_{ij}, from UE j to receive antenna i can be written as [49]

$$h_{ij} = U_{ij}, \tag{2.5}$$

where $U_{ij} \sim \mathcal{CN}(0, \sigma_x^2)$. The variable $X = |h_{ij}|$ has a Rayleigh distribution. The probability density function (PDF) of the Rayleigh distribution is given by [50, equation (2.5), page 9]

$$f_X(x) = \left\{ \frac{x}{\sigma_x^2} \exp\left(\frac{-x^2}{2\sigma_x^2}\right) \quad x \geq 0. \right.$$

2.6.3 Kronecker Channel Model

This model assumes that the transmitter and receiver correlations are separable. In fact, the covariance matrix can be written as [51]

$$\mathbf{R} = \mathrm{E}[\mathrm{vec}\,(\mathbf{H})\,\mathrm{vec}\,(\mathbf{H})^H] = \mathbf{R}_t \otimes \mathbf{R}_r, \tag{2.6}$$

where $\mathrm{vec}(.)$ is a vector operation which stacks a matrix into a vector, $\otimes$ is the Kronecker product, and $\mathbf{R}_r$ and $\mathbf{R}_t$ are the correlation matrices at the receiver and transmitter, respectively.

Therefore, the correlated channel matrix can be written as [52]

$$\mathbf{H} = \mathbf{R}_r^{1/2}\mathbf{U}\mathbf{R}_t^{1/2}, \tag{2.7}$$

where the elements of $\mathbf{U}$ are i.i.d $\mathcal{CN}(0, 1)$.

The Kronecker model is valid if and only if two conditions are jointly satisfied [51]. The transmitter correlation coefficients are independent from the receiver antenna and vice versa. In addition, the correlation matrix must be equal to the Kronecker product of the transmitter and receiver correlation matrices [51].

2.6.4 One Sided Correlation Model

In the special case where correlation is present only at one end of the link, the model is called the one-sided Kronecker model [53]. Here, (2.7) simplifies to

$$\mathbf{H} = \mathbf{R}_r^{1/2}\mathbf{U} \quad \text{or} \quad \mathbf{H} = \mathbf{U}\mathbf{R}_t^{1/2}. \tag{2.8}$$

This model is used when sufficiently large antenna spacings at one side allows decorrelation across the antennas at that side.

2.6.5 Large Scale Fading Model

The channel coefficient, h_{ij}, from UE j to receive antenna i can be written as

$$h_{ij} = \sqrt{P_{ij}}U_{ij}, \tag{2.9}$$

where $U_{ij} \sim \mathcal{CN}(0,1)$. The link gain, P_{ij} including path loss and shadowing [47, page 104], is defined by

$$P_{ij} = AL_{ij}d_{ij}^{-\gamma}. \tag{2.10}$$

In (2.10), $j \in \{1, 2, \ldots, N_t\}$ identifies the UEs, A is a constant depending on transmit power, antenna height, etc., L_{ij} is a lognormal shadow fading variable defined by $L_{ij} = 10^{\frac{\mathcal{L}_{ij}}{10}}$, where $\mathcal{L}_{ij}$ is an independent and identically distributed (i.i.d.) complex Gaussian variable with zero mean and constant shadow fading variance σ_{SF}^2, $\mathcal{L}_{ij} \sim \mathcal{CN}(0, \sigma_{SF}^2)$, d_{ij} is the link distance and γ is the path loss exponent. For simplicity, we assume A, σ_{SF} and γ are constant for all UEs. This model is a classical statistical model which is widely used for evaluating system performance. This model is used in most of the chapters in this thesis.

Link Gain Calculation

The difference between the channel coefficients for the scenarios lies solely in the structure of the link gains (see (2.10)). Referring to Figure 2.8 and (2.3), for COL, where one massive co-located array at BS is considered,

$$P_{ij} = P_j = AL_j d_j^{-\gamma}, \tag{2.11}$$

as all N_r paths from UE j to the BS have the same power defined by a single shadow fading variable, L_j and a single distance, d_j. In the BBS scnario, referring to Figure 2.9 and (2.4), there are B-collaborative base stations with multiple antennas at each BS. The BS powers are defined by

$$P_{ij} = P_j^{(k)} = AL_j^{(k)}(d_j^{(k)})^{-\gamma}, \tag{2.12}$$

where $k = \{1 \ldots, B\}$, the B lognormals $L_1 \ldots L_B$ are independent, distances are distinct and k is the index of the BS. Referring to Figure 2.5 and (2.2), for DIST, where there is one massive

array with geographically distributed single antenna BSs, the link gains are defined by

$$P_{ij} = AL_{ij}d_{ij}^{-\gamma}. \tag{2.13}$$

2.6.6 Correlated Channels with Random Large Scale Fading

The channel model including fast fading, correlation and random large scale fading is defined as

$$\mathbf{H} = \mathbf{R}_r^{1/2}\mathbf{G}, \tag{2.14}$$

where $G_{ij} = \sqrt{P_{ij}}U_{ij}$, the $U_{ij} \sim \mathcal{CN}(0,1)$ are i.i.d. fast fading terms, $\mathbf{R}_r^{1/2}$ is the spatial correlation matrix at the receive array and P_{ij} is defined in (2.10), where $P_{ij} = AL_{ij}d_{ij}^{-\gamma}$.

In (2.14), the channel correlation matrix at the receiver has the block diagonal form

$$\mathbf{R}_r = \begin{bmatrix} \mathbf{R}_b & 0 & \dots & 0 \\ 0 & \mathbf{R}_b & \dots & 0 \\ \vdots & \vdots & \ddots & \vdots \\ 0 & 0 & \dots & \mathbf{R}_b \end{bmatrix}. \tag{2.15}$$

where $\mathbf{R}_b$ is the correlation matrix at each of the B arrays. The result in (2.15) is valid only if all BSs are identical, i.e., when each BS has the same number of antennas, the same shape, etc. In practice different users have different correlation but we employed a simplified model where the correlations are the same.

Figure 2.10 demonstrates an example of correlated channels in the 2BS scenario. Suppose there are three UEs (UE 1, UE 2 and UE 3) and each of them has correlated links with BS1 and BS2. For example, UE 2 has correlated links to BS1 and another set of correlated links with BS2 (see Figure 2.10). However, the links from UE 2 to BS 1 are not correlated with the links from UE 2 to BS 2. Moreover, due to spatial separations, all links from UE 2 to BS 1 and BS

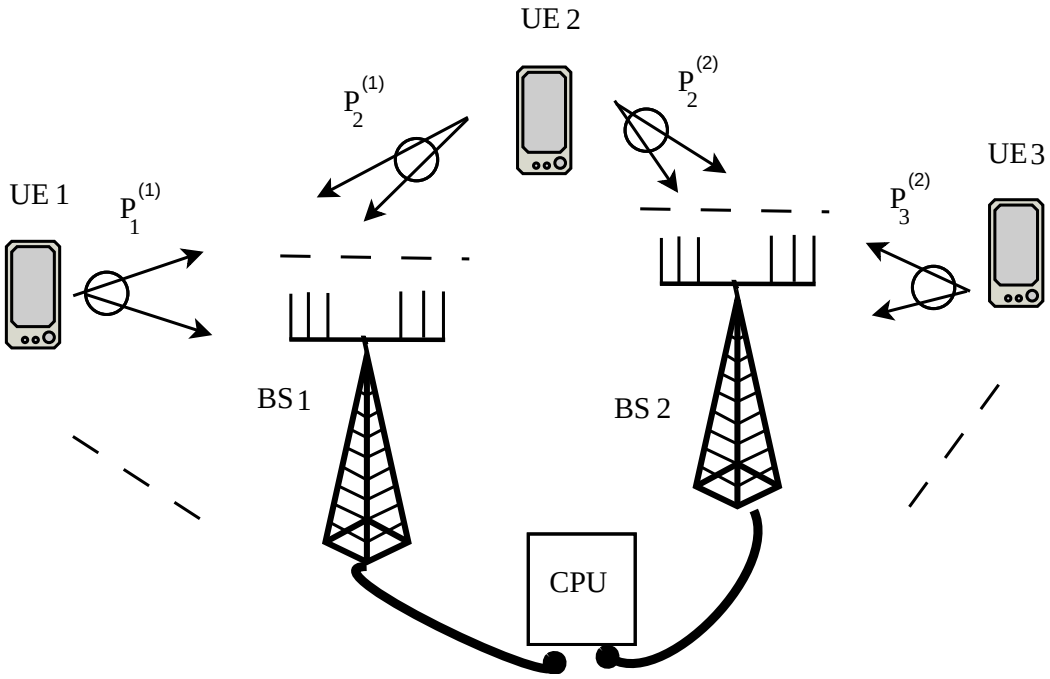

Figure 2.10: An example of correlated channels in the 2BS scenario.

2 are also not correlated to those from UE 1 or UE 3. Subsequently, the correlation matrix for each UE can be separated into a block-diagonal structure with blocks of $\mathbf{R}_b$ in the diagonal as in (2.15). Note that $\mathbf{R}_b$ is the common correlation matrix at each BS.

2.6.7 Correlated Channel for the Co-located Scenario Based on a Simple Exponential Decay for the Link Gains

The channel model in Section 2.6.6 can cover several BS deployment scenarios: COL, BBS and DIST. Here, we consider only the COL scenario. Thus, the channel matrix is a special case of (2.14) and can be defined as

$$\mathbf{H} = \mathbf{R}_r^{\frac{1}{2}} \mathbf{U} \mathbf{P}^{\frac{1}{2}}, \tag{2.16}$$

where the elements of $\mathbf{U}$ are i.i.d. $\mathcal{CN}(0,1)$, $\mathbf{P} = \mathrm{diag}(P_1, P_2, \ldots, P_{N_t})$ and P_j is the link gain of user j. Note that for this simplified model, the matrix P is constructed differently to

(2.3), however the interpretation of the individual components as the expectations of the link gain powers (Section 2.6.1) remains. Traditionally, P_j is modeled as in (2.11) which includes path loss, shadowing, etc. In contrast, we employ in this section a simple model [54] so that P_j is defined as $P_j = \mathcal{A}\beta^{j-1}$, $j = \{1, 2, \ldots, N_t\}$, where $\mathcal{A}$ is the link gain of the strongest UE and β is a parameter which controls the rate of decay of the link gains and $0 < \beta \leq 1$. This model is simple as the power can be changed by a single parameter, β. This model gives $P_1 > P_2 > \cdots > P_{N_t}$ so that the link gains of the UEs are ordered. This has no effect on the generality of the results since the user order is arbitrary. As $\beta \to 1$ the link gains become equal and as $\beta \to 0$ the link gains are dominated by one strong UE.

2.6.8 Correlation Models

Here, we list a few candidate models for the correlations. Let $\mathbf{R}_r = (R_{ij})$, then the element R_{ij} could be defined by a wide variety of different models. We consider four common models from the literature [55]. These models depend upon a single parameter μ. We chose these models due to their simplicity and the wide range of behavior covered by these correlations.

- The Jakes model (Jakes): $R_{ij} = J_0(2\pi\mu d_{ij})$, where $J_0(.)$ is the zero$^{\text{th}}$ order Bessel function and d_{ij} is the physical distance between two antennas measured in terms of the wavelength [56].

- A Gaussian decay model (Gauss): $R_{ij} = \mu^{d_{ij}^2}$ [57].

- A square root model (Sqrt): $R_{ij} = \mu^{\sqrt{d_{ij}}}$ [55].

- The exponential correlation model (Exp): $R_{ij} = \mu^{d_{ij}}$, where $0 < \mu < 1$ [58].

2.6.9 A Statistical Model for Imperfect Channel Estimation

If at the receiver, only an estimate, $\hat{\mathbf{H}}$, of the true channel, $\mathbf{H}$, is available, we consider the equivalent imperfect channel estimation model in [59],

$$\mathbf{H} = r_0\hat{\mathbf{H}} + \sqrt{1 - r_0^2}\mathbf{E}, \tag{2.17}$$

where r_0 is the correlation coefficient between the true channel, $\mathbf{H}$, and the estimated channel, $\hat{\mathbf{H}}$, and $\mathbf{E}$ has the same statistics as $\mathbf{H}$ and is independent of $\hat{\mathbf{H}}$.

2.7 System Model

Consider a BS with N_r receive antennas serving N_t single antenna UEs. For this uplink model the received signal, $\mathbf{y} \in \mathbb{C}^{N_r}$, is given by

$$\mathbf{y} = \mathbf{H}\mathbf{x} + \mathbf{n} = \sum_{m=1}^{N_t} \mathbf{h}_m x_m + \mathbf{n}, \tag{2.18}$$

where $\mathbf{H} = [\mathbf{h}_1 \cdots \mathbf{h}_{N_t}]$ is the $N_r \times N_t$ channel matrix, $\mathbf{x}$ is the $N_t \times 1$ vector of transmitted symbols, $\mathbf{x} = [x_1, x_2, \ldots x_{N_t}]^T$, and $\mathbf{n} = [n_1 \cdots n_{N_r}]^T$ is the $N_r \times 1$ noise vector with i.i.d. uncorrelated complex Gaussian components, $n_i \sim \mathcal{CN}(0, \sigma^2)$. Without loss of generality we assume the transmit symbols are normalized so that $E[|x_j|^2] = E_s = 1$ and the noise power is $E[|n_i|^2] = \sigma^2$. ρ is the ratio of the signal power to the noise power so that $\rho = E[|x_j|^2]/\sigma^2$. The channel coefficient, h_{ij}, from UE j to receive antenna i has power $E[|h_{ij}|^2] = P_{ij}$.

2.8 Receivers

2.8.1 Linear Combiners

Linear combiners have been extensively studied in the literature [21, 60]. They are an attractive low complexity alternative to optimal processing for MIMO communications [21, 60]. The role of linear combiners is to extract the desired signal from the received signal and suppress or reduce the effect of interference [21, 60]. To compute the coefficients of a linear combiner typically requires matrix inversion [21, 60]. The sizes of the matrices to invert grows with the number of antennas which can become challenging in a practical implementation of MM [21, 60]. Some techniques based on Neumann series expansions have been studied in [61, 62] to simplify the inverse computation.

The traditional types of linear combiner are ZF, MMSE and MRC [21, 60]. Under the assumption of availability of perfect channel state information, we consider linear detectors where the estimated symbol, $\hat{\mathbf{x}}$, is found by a transformation of the received vector, $\mathbf{y}$, of the form

$$\hat{\mathbf{x}} \quad = \quad \hat{Q}(\mathbf{W}^H \mathbf{y}). \tag{2.19}$$

In (2.19), $\mathbf{W}$ is the linear combiner in matrix form, $\mathbf{W}^H$ represents the complex conjugate transpose of $\mathbf{W}$ and $\hat{Q}$ is a quantizer that maps its argument to the closest signal point using Euclidean distance.

Zero Forcing Combiner

The ZF combiner converts the joint decoding problem into N_t single stream decoding problems [21, 60]. The ZF combiner requires that the number of transmitters is fewer than or equal to the

number of receivers [21]. The ZF combiner is calculated by

$$\mathbf{W} = \mathbf{H}(\mathbf{H}^H\mathbf{H})^{-1}. \tag{2.20}$$

This combiner neglects the effect of noise and suppresses completely the effect of interference without regarding the loss in energy of the desired stream and satisfies the following condition [63]:

$$\mathbf{w}_i^H\mathbf{h}_j \quad = \quad \delta_{ij}, \tag{2.21}$$

where $\mathbf{w}_i$ and $\mathbf{h}_j$ are column vectors of $\mathbf{W}$ and $\mathbf{H}$ and δ_{ij} is the Kronecker delta function

$$\delta_{ij} = \begin{cases} 1 & \text{if } i = j \\ 0 & \text{if } i \neq j. \end{cases}$$

The SINR for the m^{th} UE is [64]

$$\mathrm{SINR}_m^{(\mathrm{ZF})} = \mathrm{SNR}_m^{(\mathrm{ZF})} = \frac{1}{\sigma^2[(\mathbf{H}^H\mathbf{H})^{-1}]_{mm}}, \tag{2.22}$$

where $[\mathbf{T}]_{mm}$ denotes the $(m,m)^{\mathrm{th}}$ element of a matrix $\mathbf{T}$. With imperfect CSI, the ZF combiner uses the estimated channel so that it is defined as [21, page 48] $\mathbf{W} = \hat{\mathbf{H}}(\hat{\mathbf{H}}^H\hat{\mathbf{H}})^{-1}$.

Advantages and disadvantages: With ZF, the processing of the signal is simple and works well in interference limited cases [21, 60]. However, there is a noise enhancement, especially in the low SNR range [21, 60]. Therefore, ZF works poorly in noise limited cases. The inverse computation of the channel matrix increases the computation complexity [21, 60]. However, low complexity alternatives to inversion using Neumann series expansions are currently being developed for MM [62].

Minimum Mean-Squared Error Combiner

The MMSE combiner maximizes SINR [21] or equivalently minimizes the mean squared error between the estimated signal $\mathbf{w}^H\mathbf{y}$ and transmitted signal x_m. The MMSE combiner is obtained as [21, page 48]

$$\mathbf{W} = \mathbf{H}(\mathbf{H}^H\mathbf{H} + \sigma^2\mathbf{I})^{-1}. \tag{2.23}$$

The corresponding SINR of the m user is [64]

$$\mathrm{SINR}_m^{(\mathrm{MMSE})} = \frac{1}{[(\mathbf{I} + \sigma^2\mathbf{H}^H\mathbf{H})^{-1}]_{mm}} - 1. \tag{2.24}$$

With imperfect CSI, the MMSE combiner uses the estimated channel so that it is defined as $\mathbf{W} = \hat{\mathbf{H}}(\hat{\mathbf{H}}^H\hat{\mathbf{H}} + \sigma^2\mathbf{I})^{-1}$.

Advantages and disadvantages: MMSE has better performance than ZF at low SNR because it suppresses both noise and interference components [21, 60]. At high SNR, ZF approaches MMSE [21, 60]. Note that MMSE combining is not considered in this thesis because for MM ZF and MMSE are very similar [65].

Maximal Ratio Combining

MRC is the simplest linear combiner which is used to maximize the SNR and ignores the interference effect [60]. For instance, MRC requires only channel knowledge of the desired source signal while MMSE requires channel knowledge of the desired and interfering signals [60]. The MRC receiver is obtained as [60, page 331]

$$\mathbf{W} \;=\; \mathbf{H}. \tag{2.25}$$

The SINR for user m is given by

$$\mathrm{SINR}_m^{(\mathrm{MRC})} = \frac{|\mathbf{h}_m^H \mathbf{h}_m|^2}{\sum_{j \neq m} \mathbf{h}_m^H \mathbf{h}_j \mathbf{h}_j^H \mathbf{h}_m + \sigma^2 \mathbf{h}_m^H \mathbf{h}_m}. \tag{2.26}$$

With imperfect CSI, the MRC receiver uses the estimated channel so that it is defined as $\mathbf{W} = \hat{\mathbf{H}}$.

Advantages and disadvantages: At low SNR, the same array gain as in the case of the single UE system can be achieved with MRC [21, 60]. However, neglecting the interference gives a poor performance in interference limited cases [21, 60].

Figure 2.11 shows the mean average SINR for the three linear combiners versus transmit SNR (ρ), where the number of transmitters is $N_t = 3$ and the number of receivers is $N_r = 5$ in a MIMO system. We assume the channel elements are i.i.d. complex Gaussian distributed with zero mean and unit variance. MMSE has better performance than both ZF and MRC over the entire range of ρ. MRC is widely considered for MM due to its simplicity.

2.8.2 Vertical Bell Laboratories Layered Space Time (V-BLAST)

V-BLAST is a wireless architecture that detects the source signals iteratively and utilizes traditional detection techniques such as linear detectors at each iteration [17].

The two major computational bottlenecks in the V-BLAST algorithm are ordering for the nulling and cancellation process and matrix inverse computations for the receiver weights [66]. The classic approach to ordering the streams for detection in V-BLAST is to detect the stream with the highest output SINR first [66]. This classic approach is an optimal approach which requires ordering at each stage. From [66], let the ordered set $S = \{k_1, k_2, \ldots, k_{N_t}\}$ be a permutation of the integers 1, 2, ..., N_t specifying the order in which the transmitted symbols in $\mathbf{x}$ are extracted. In the optimal approach, the index k_i is chosen such that the SINR/SNR of the detected symbol at the i^{th} stage is maximized. Algorithm 1 shows the pseudocode for the

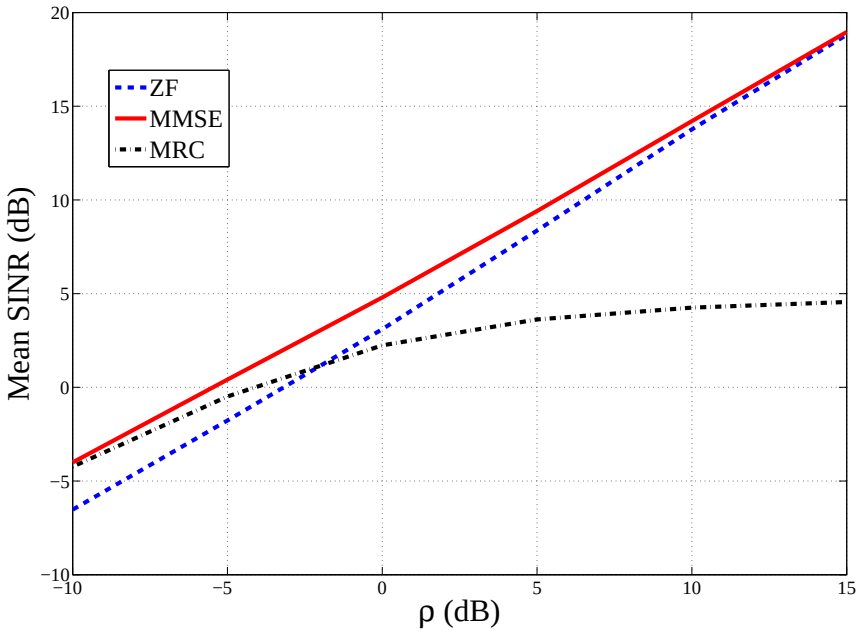

Figure 2.11: Average SINR of the three linear combiners vs transmit SNR (ρ), N_t =3 and $N_r = 5$. The linear combiners are ZF, MMSE and MRC.

V-BLAST detection algorithm.

In order to define the V-BLAST approach, we require the following notation. Let $\mathbf{H}_i$ represent $\mathbf{H}$ with columns $k_1, k_2, \ldots, k_{i-1}$ replaced by zeros and let $\mathbf{W}_i$ be given by $\mathbf{H}_i$ for MRC, $\mathbf{H}_i(\mathbf{H}_i^H\mathbf{H}_i)^{-1}$ for ZF and $\mathbf{H}_i(\mathbf{H}_i^H\mathbf{H}_i + \sigma^2\mathbf{I})^{-1}$ for MMSE. The SINR for user m at the i^{th} stage is given by (2.26), where the summation in the denominator of (2.26) is over $j \notin \{k_1, k_2, \ldots, k_{i-1}\}$ such that $j \neq m$. Maximizing the SINR at stage i gives

$$k_i^{(\mathrm{MRC/MMSE})} = \underset{m \notin \{k_1, k_2, \ldots, k_{i-1}\}}{\arg\max} \mathrm{SINR}_m^{(\mathrm{MRC/MMSE})}. \tag{2.27}$$

The optimal ordering for ZF is defined by [66]

$$k_i^{(\mathrm{ZF})} = \underset{j \notin \{k_1, k_2, \ldots, k_{i-1}\}}{\arg\min} ||(\mathbf{W}_i)_j||^2, \tag{2.28}$$

Algorithm 1 V-BLAST Algorithm

1) Initialization:	
$i = 1$	i is the iteration number.
$\mathbf{y}$	$\mathbf{y}$ is the received signal.
$\mathbf{H}$	$\mathbf{H}$ is the channel matrix.
2) Iterative Process:	
$\mathbf{W}$	Calculate the linear combiner. For ZF, $\mathbf{W} = \mathbf{H}(\mathbf{H}^H\mathbf{H})^{-1}$. For MMSE, $\mathbf{W} = \mathbf{H}(\mathbf{H}^H\mathbf{H} + \sigma^2\mathbf{I})^{-1}$. For MRC, $\mathbf{W} = \mathbf{H}$.
$\mathbf{G} = \mathbf{W}^H$	Find the Hermitian of the linear combiner, $\mathbf{W}$.
k_i	Find the selection index k_i. For ZF, $k_i = \underset{j \notin \{k_1, k_2, \ldots, k_{i-1}\}}{\arg\min} \|\|(\mathbf{W}_i)_j\|\|^2$. For MRC and MMSE, $k_i = \underset{j \notin \{k_1, k_2, \ldots, k_{i-1}\}}{\arg\max} \mathrm{SINR}_j^{(\mathrm{MRC/MMSE})}$.
$\mathbf{m}_{k_i} = (\mathbf{G}_i)_{k_i}$.	$\mathbf{m_{k_i}}$ is the i^{th} row of $\mathbf{G}$.
$\tilde{x_i} = \mathbf{m}_{ki}\mathbf{y}$	Calculate the estimated input signal $\tilde{x_i}$.
$\hat{x_i} = \hat{Q}[\tilde{x_i}]$	$\hat{Q}(.)$ is the quantization (slicing) operation appropriate to the constellation in use.
$\mathbf{y}_{i+1} = \mathbf{y}_i - \mathbf{h}_{k_i}\hat{x_{k_i}}$	The interference due to $\hat{x}_{k_i}$ is canceled.
$\mathbf{H}_{i+1} = \mathbf{H}_i^{\bar{k_i}}$	Update $\mathbf{H}$ at iteration i by zeroing the k_i column. This is denoted by $\mathbf{H}_i^{\bar{k_i}}$.
$i = i + 1$	Update i.

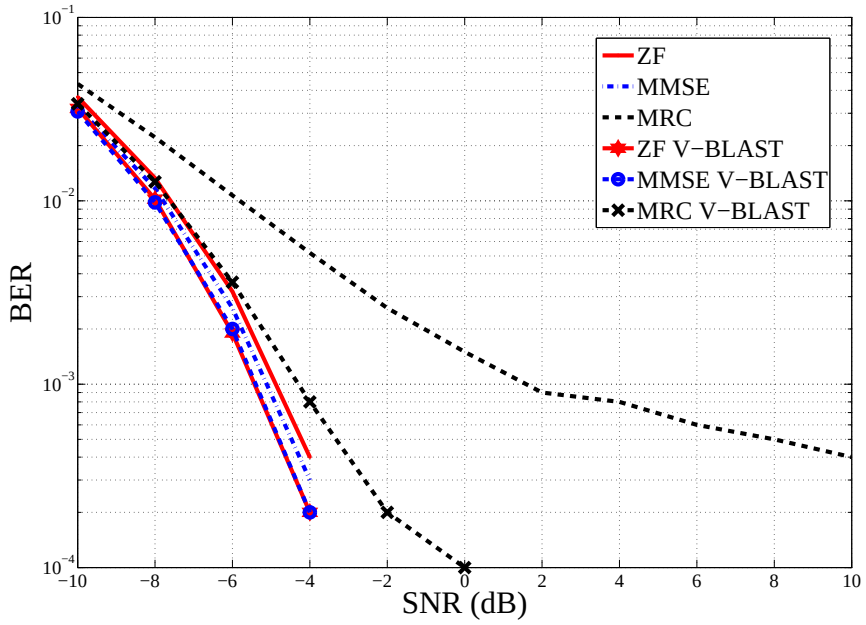

Figure 2.12: BER vs transmit SNR for the three different combiners and V-BLAST, $N_t = 4$ and $N_r = 20$. The linear combiners are ZF, MMSE and MRC.

where $(\mathbf{W}_i)_j$ represents column j of $\mathbf{W}_i$, the ZF combiner at stage i.

Figure 2.12 shows the bit error rate (BER) for the three linear combiners with V-BLAST versus transmit SNR, with $N_t = 4$, $N_r = 20$ in a MIMO system. A quasi-static flat Rayleigh fading channel model (channel elements are i.i.d. complex Gaussian distributed with zero mean and unit variance) is used. Binary phase shift keying (BPSK) is assumed for input modulation. The results are averaged over 100,000 coherence blocks. V-BLAST clearly improves the performance of linear combiners.

V-BLAST performance has also been studied with imperfect channel estimation [42] and with correlated channels [43]. Note that, repeated inverse computations are involved in the calculation for MMSE or ZF. With imperfect channel estimation, a similar strategy can be used except that the estimated channel replaces the perfect channel [42]. Hence, $\hat{\mathbf{H}}_i$ is used instead of $\mathbf{H}_i$ where $\hat{\mathbf{H}}_i$ represents $\hat{\mathbf{H}}$ with columns $k_1, k_2, \ldots, k_{i-1}$ replaced by zeros and $\mathbf{W}_i$

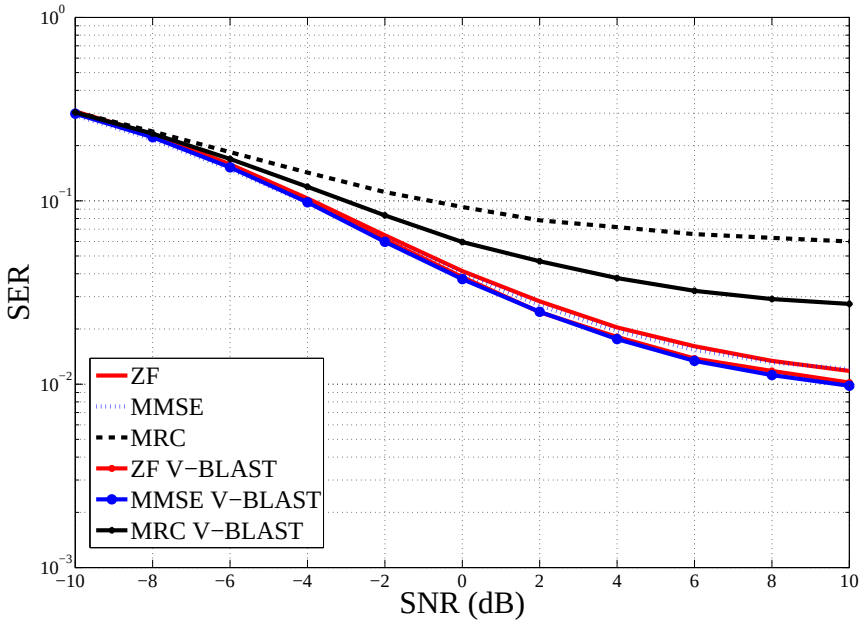

Figure 2.13: SER vs SNR for the three different combiners and V-BLAST with imperfect CSI, $N_t = 4$ and $N_r = 20$. The linear combiners are ZF, MMSE and MRC. The channel accuracy (r_0) equals 0.8.

is calculated from the estimated channel. For ZF, this means that detection is performed using $\mathbf{W}_i = \hat{\mathbf{H}}_i(\hat{\mathbf{H}}_i^H\hat{\mathbf{H}}_i)^{-1}$ and this estimated combining matrix is used in (2.28) for ordering. For MRC, detection is performed using $\mathbf{W}_i = \hat{\mathbf{H}}_i$ and ordering uses (2.26) with the true channels replaced by their estimates.

Figure 2.13 shows the symbol error rate (SER) versus transmit SNR for the three linear combiners with V-BLAST. This assumes a MIMO system with $N_t = 4$, $N_r = 20$ and with imperfect channel estimation. Imperfect channel model in (2.17) is used with $r_0 = 0.8$. Channel elements are assumed to be distributed as i.i.d. complex Gaussian with zero mean and unit variance. Quadrature phase shift keying (QPSK) is assumed for input modulation. The results are averaged over 100,000 coherence blocks. Receiver performance is impaired due to channel imperfection.

2.9 Performance Metrics

To investigate uplink MM performance, we consider the following metrics: SINR, SER and capacity. These are common measures found in the wireless literature [47, 67].

2.9.1 Signal-to-Interference-and-Noise-Ratio (SINR)

For any such linear combiner presented in Section 2.8.1, the output SINR for the m^{th} user is

$$\begin{aligned} \mathrm{SINR_m} &= \frac{E[|\mathbf{w}_m^H \mathbf{h}_m x_m|^2]}{E[|\mathbf{w}_m^H(\sum_{j\neq m}\mathbf{h}_j x_j + \mathbf{n})|^2]}, & (2.29)\\ &= \frac{\mathbf{w}_m^H \mathbf{h}_m \mathbf{h}_m^H \mathbf{w}_m}{\mathbf{w}_m^H[\sum_{j\neq m}\mathbf{h}_j\mathbf{h}_j^H + \sigma^2\mathbf{I}_{N_r}]\mathbf{w}_m}, & (2.30) \end{aligned}$$

where $\mathbf{w}_m$ is the m^{th} column of $\mathbf{W}$. However, with imperfect channel estimation used in (2.17), the SINR for the m^{th} user is [68]

$$\mathrm{SINR_m} = \frac{r_0^2|\mathbf{w}_m^H\hat{\mathbf{h}}_m|^2}{\mathbf{w}_m^H[(1-r_0^2)\mathbf{e}_m\mathbf{e}_m^H + \sum_{j\neq m}\mathbf{h}_j\mathbf{h}_j + \sigma^2\mathbf{I}_{N_r}]\mathbf{w}_m}, \quad (2.31)$$

where $\mathbf{e}_m$ is the m^{th} column of $\mathbf{E}$ and $\hat{\mathbf{h}}_m$ is the m^{th} column of $\hat{\mathbf{H}}$.

2.9.2 Symbol Error Rate

For M-ary quadrature amplitude modulation (M-QAM) or M-phase shift keying (M-PSK) modulations, the SER can be written in terms of expected values of the Gaussian Q-function and Q^2-function. The Q-function is calculated as [2]

$$\begin{aligned} Q(x) &= \frac{1}{\sqrt{2\pi}}\int_x^\infty e^{-\frac{u^2}{2}}du \\ &= \frac{1}{2}\mathrm{erfc}(\frac{x}{\sqrt{2}}). \end{aligned}$$

For example, the exact formula for the SER for the M-QAM family, when the number of bits (K) is even and $M = 2^K$, is given by [2, equation (4.2.144), page 282]

$$\begin{aligned} \mathrm{SER}^{\mathrm{MQAM}} &= 2(1-\frac{1}{\sqrt{M}})\mathrm{erfc}\left(\sqrt{\frac{3}{2(M-1)}K\gamma_b}\right) \\ &\times \left[1-0.5(1-\frac{1}{\sqrt{M}})\mathrm{erfc}\left(\sqrt{\frac{3}{2(M-1)}K\gamma_b}\right)\right], \end{aligned} \tag{2.32}$$

where γ_b is the SNR per bit.

2.9.3 Capacity

The ergodic capacity [69, page 36] can be defined as

$$\mathrm{E}[C] = \mathrm{E}[\log_2 \det(\mathbf{I} + \rho\,\mathbf{H}^H\mathbf{H})], \tag{2.33}$$

where $\det(.)$ is the determinant of a matrix and $[.]^H$ is the Hermitian operator. The capacity calculation is under the assumption of Gaussian noise and with no channel state information at the transmitter.

Note that the capacity matrix is not used for receiver evaluation.

Capacity Outage

The p-percentage outage capacity, C_{out}, is the defined as the transmission rate that can be supported by (100-p)% of the fading channel realizations [20, page 9], i.e., $P(C < C_{\mathrm{out}}) = p$ [69, page 36].

2.10 Power Control

Intelligent selection techniques for transmit power can be used to achieve good system performance [18]. The advantages of increasing transmit power are higher SNR and potentially a reduced BER in the communication system [18]. However, there are drawbacks of increasing the transmit power such as reducing the battery life of the transmitter and increasing interference to other UEs when sharing the same resources [47]. Power control in traditional MIMO, where the number of antennas is less than 10, has been extensively studied in the literature [18,47]. For example, closed form approximations for the power allocation are derived based on average total and block error rates in [70], where the base station and the UEs are co-located. For the two-cell downlink wireless system, transmit power allocation was analyzed under a sum-capacity maximization and peak power constraints at each base station [71]. Power control of the V-BLAST system [63], with SIC and per-antenna power constraint, was studied in [72]. Moreover, a power control method based on post detection SINR balancing in cellular V-BLAST systems was studied in [73]. Discrete PC and adaptive power control have been extensively studied to improve system performance as in [74–77].

In MM systems there are many UEs which are likely to have markedly different powers. This provides considerable potential scope for PC to improve the performance of MM systems. In Chapter 7, we investigate a low complexity receiver design under imperfect channel estimation including PC in MM.

2.11 Adaptive Modulation

Adaptive modulation (AM) is an instantaneous change of modulation level to match the system requirement [49]. Due to the continuous fluctuation of the wireless channel, AM can be used to improve the performance of the system [49]. For instance, AM aims to transmit more bits when the quality of the channel is good and fewer bits otherwise [49].

In MM systems, it is likely that UEs will have very different received signal strengths. Therefore, different modulation types are needed to transmit data in an effective manner across all values of SINR. By altering modulation types, a minimum requirement of SINR for a target BER can be identified. For example, a closed-form expression for the additive white Gaussian noise (AWGN) channel can be used to obtain the BER as a function of the SNR assuming ideal coherent detection (which is used when the receiver has knowledge of the carrier phase to detect the signal). The minimum required SNR for a target BER is defined as a threshold. In Chapter 7, we investigate a low complexity receiver design under imperfect channel estimation including PC with AM in MM.

Suppose K is the number of bits and $M = 2^K$. Define the SNR per symbol as $\gamma_s = K\gamma_b$, where γ_b is the SNR ber bit. The exact expression of BER for BPSK [67, equation (4.2.105), page 262] and the SER for QPSK [67, equation (4.2.107), page 263] are given by,

$$\mathrm{BER}^{\mathrm{BPSK}} = 0.5\,\mathrm{erfc}\left(\gamma_b\right), \tag{2.34}$$

$$\mathrm{SER}^{\mathrm{QPSK}} = \mathrm{erfc}\left(\sqrt{\gamma_b}\right)\left[1 - 1/4\,\mathrm{erfc}\left(\sqrt{\gamma_b}\right)\right]. \tag{2.35}$$

The BER with Gray coding is approximated as the SER divided by the number of bits per symbol (K). Therefore, the standard formula for the approximate BER of the M-PSK family in AWGN is [67, equation (4.2.109)-(4.2.110), page 265]

$$\mathrm{BER}^{(\mathrm{MPSK})} \approx 1/K\,\mathrm{erfc}\left(\sqrt{K\gamma_b}\sin(\pi/M)\right). \tag{2.36}$$

The exact formula for the SER of the M quadrature amplitude modulation (M-QAM) family, when K is even, is given by (2.32). With the rectangular constellation and when K is odd,

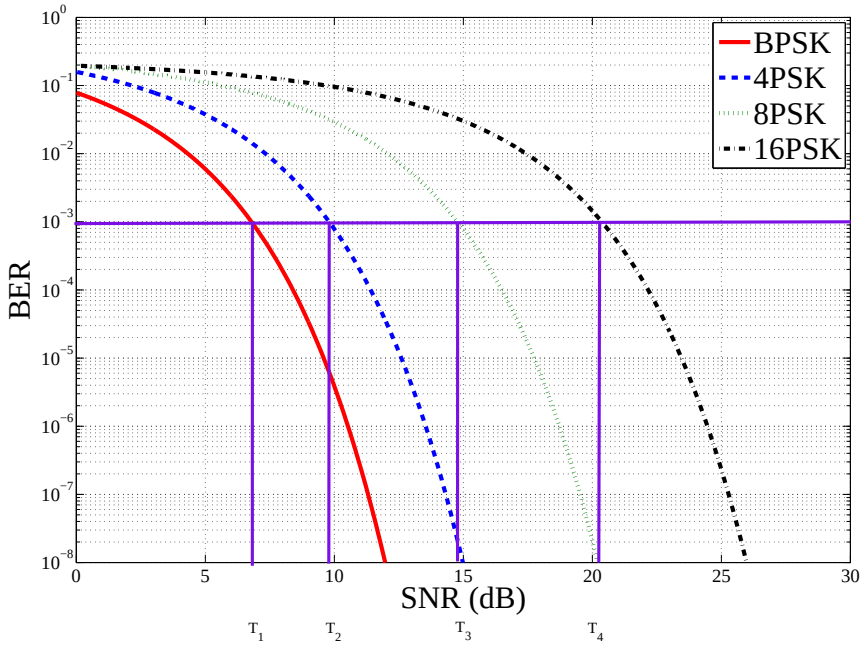

Figure 2.14: The BER for various M-PSK modulation levels as a function of SNR (γ_s) in dB.

an upper bound on the SER in (2.32) is given by [2, equation (4.2.145), page 283]

$$\mathrm{SER}^{\mathrm{MQAM}} \leq 2\mathrm{erfc}\left(\sqrt{\frac{3}{2(M-1)}K\gamma_b}\right). \tag{2.37}$$

Figure 2.14 shows the BER for various M-PSK modulation levels as a function of SNR (γ_s) in dB. The modulation levels are 2-PSK, 4-PSK, 8-PSK and 16-PSK. We use (2.34)-(2.37) to obtain the figure. Suppose that the target BER is 10^{-3} and the corresponding thresholds for the above modulations are T_1, T_2, T_3 and T_4. When the estimated SINR is less than T_1 then no modulation can be supported and the link is in outage. In the case of $T_1 \leq$ SINR $< T_2$, the modulation selected is BPSK. Similarly, if $T_2 \leq$ SINR $< T_3$, then the modulation is 4-PSK, if $T_3 \leq$ SINR $< T_4$, then the modulation is 8-PSK and when $T_4 \leq$ SINR, the modulation is 16-PSK.

Figure 2.15 shows the BER for various M-QAM modulation levels as a function of SNR

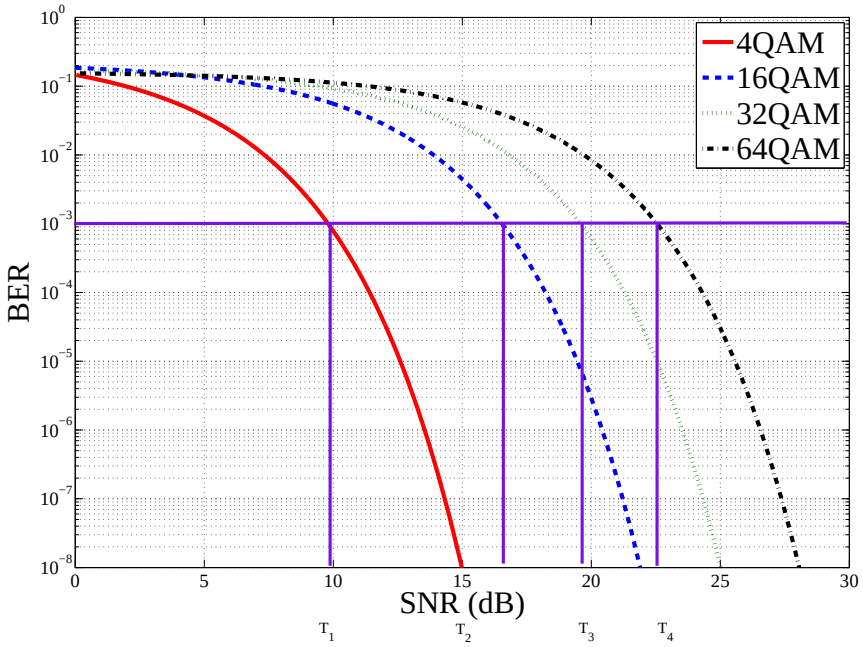

Figure 2.15: The BER for various M-QAM modulation levels as a function of SNR (γ_s) in dB.

(γ_s) in dB. The modulation levels are 4-QAM, 16-QAM, 32-QAM, 64-QAM. We use (2.34)-(2.37) to obtain the figure. The minimum required SNR to operate at a specified target BER is defined as a threshold. For example, the minimum thresholds at a target BER of 10^{-3} for QPSK, 16-QAM and 64-QAM are 9.8, 16.5 and 22.6 dB, respectively.

The performance of AM in cellular systems was studied in [78]. AM in correlated MIMO systems was studied in [79]. In [80], the effects of power reallocation and ordering in V-BLAST systems, with adaptive modulation and antenna selection, was discussed.

2.12 Parameter Values

In this section, we motivate and define the range of parameter values used throughout the thesis. In terms of system size, the number of transmitters, N_t, is usually selected to be 10 or 6 and the number of receivers is selected to be 100, 128 or 64. The reason for these selections is to

maintain the ratio of N_r/N_t as greater than or equal to 10, which is the ratio commonly assumed for MM [7]. Additionally, we investigate the effect of changing the ratio by also considering $N_t \in \{20, 40\}$.

For the large scale fading model in Section 2.6.5, where $P_{ij} = AL_{ij}d_{ij}^{-\gamma}$, A is a constant depending on transmitting power and antenna height. A also includes transmitting and receiving antenna gains and a reference distance loss [47]. The constant value of A is selected differently throughout the thesis. When a performance metric, such as SER or SINR, is used in an interference limited system, then the value of A is essentially canceled and we assume $A = 1$. In other scenarios, we relate the value of A to the median SNR of ZF (M_{ZF}) in such a way that gives a reasonable level of performance. For example, A might be chosen so that, $M_{\text{ZF}} \in \{5, 7, 10\}$ dB for $\rho = 0$ dB. We select the path loss exponent, $\gamma \in \{3, 4\}$ because these are typical values in the range of $[2, 4]$ commonly assumed for wireless systems [47]. The lognormal shadow fading variable, $\mathcal{L}_{ij} \sim \mathcal{CN}(0, \sigma_{SF}^2)$, has a standard deviation of σ_{SF}. We select σ_{SF} to be 8, which is a typical value for urban areas. In fact, typical values of σ_{SF} are in the range of $[4, 12]$ [47].

For the correlated channel model described in Section 2.6.7, where $\mathbf{H} = \mathbf{R}_r^{\frac{1}{2}}\mathbf{U}\mathbf{P}^{\frac{1}{2}}$ and the link gain is $P_j = \mathcal{A}\beta^{j-1}$, we assume the link gain of the strongest UE is $\mathcal{A} = 1$. This value is unimportant as the SNR, ρ, scales the strongest channel power to any desired value. β is a parameter which controls the rate of decay of the link gains and $0 < \beta \leq 1$. Therefore, we select $\beta \in \{0.1, 0.5, 0.7, 0.9\}$ in order to cover a wide range of behavior.

For the imperfect channel model described in Section 2.6.9, where $\mathbf{H} = r_0\hat{\mathbf{H}} + \sqrt{1 - r_0^2}\mathbf{E}$, we select the correlation coefficient between the true channel, $\mathbf{H}$, and the estimated channel, $\hat{\mathbf{H}}$ to be $r_0 = \{0.6, 0.8, 0.9, 0.99\}$. This is a much wider spread of r_0 values than would be considered for traditional MIMO since latency and pilot contamination issues could make channel estimation much more difficult in MM. Note that when $r_0 = 1$, the model is equivalent to perfect CSI.

Throughout the thesis results are averaged over a specific number of experiments, for example 1000-100,000 coherence blocks. In each case, the number of experiments are chosen to ensure statistically valid results and smooth curves in the resulting plots.

2.13 Summary

In this thesis, we focus on the uplink performance of MM with low complexity receivers, no precoding at the UEs and no CSI feedback to the UEs. We also assume that the UEs are uncoordinated, all UEs have single antennas and the receiver has a large number of antennas. At the receiver, we assume both single co-located arrays and multiple BSs back-hauled together to form a network MIMO system. In all cases, perfect or imperfect CSI is available to all collaborating BSs, but the effects of latency and imperfect backhaul are ignored. In addition, we only focus on simple receivers based on linear combiners and the V-BLAST technique [17] and we propose low complexity V-BLAST receivers, with ordering based on channel norms or link gains.

The relevant background information for this work has been presented in this chapter. This includes an overview of MIMO, multiuser MIMO, MM, MM deployment and MM arrays, channel models, the system model, receivers, performance metrics, PC and AM.

Chapter III

Distributed vs Co-located Base Station Deployment

3.1 Introduction

Most work on MM assumes co-located arrays but the distributed case has been proposed as a promising option for increased throughput and shadow fading diversity [81–84]. The advantage of distributed arrays has been investigated in traditional MIMO systems (less than 10 antennas) [85, 86] as well as in the context of remote radio heads/units [87] and cloud Radio Access Network [82]. In this chapter, we consider three MM deployment options: a co-located base station array (COL); B collaborative base stations with multiple antennas (BBS); and distributed arrays with geographically separated single antenna base stations (DIST). We assume a standard hexagonal cellular topology with two tiers of interference: a desired cell at the center and interference cells located in two surrounding tiers.

One of the advantages of large arrays is their ability to orthogonalize the channel vectors of different UEs at the co-located BS [24]. Here, the focus is on a different MM property, a type of averaging over the link gains, which enables us to demonstrate the gains of distributed over co-located deployment. In [81], a downlink finite system analysis was developed using randomly located BSs and in [82, 84], a downlink asymptotic analysis was derived for sum-rate and rate performance, respectively. In [83], an uplink distributed system analysis for SINR was derived from the asymptotic analysis in [88]. The work in [83] is the closest to this chapter but it focuses on spatial correlation effects and BS grouping. We take a different approach, simpli-

fying the analysis further while maintaining accuracy and deriving insights into MRC and ZF receivers, deployment options and propagation conditions. In this chapter, uplink performance is considered using linear receivers with fixed BS locations. MRC and ZF are used because they are particularly relevant in MM due to their relatively low complexity [7].

The main contributions of this chapter are: We

- develop remarkably simple and accurate analytic approximations to the SINR at the output of MM linear receivers;
- use the analytical results to explain the effects of path loss, shadowing, channel estimation error, channel correlation and system size;
- use analysis and simulation to evaluate the performance of an intermediate deployment, where the massive array is spread over B locations (BBS);
- use analysis and simulations to evaluate the deployment scenarios under differing levels of interference (different frequency re-use factors) and with different geographic spreads of the antenna arrays within the cell.

This chapter is organized as follows. The system model and deployment scenarios are given in Sections 3.2 and 3.3. Sections 3.4, 3.5 and 3.6 provide analysis, results and conclusions.

3.2 System Model

Consider a standard cellular structure with 19 hexagonal cells, where the center cell contains the desired UEs and there are two surrounding interference tiers (top left, Figure 3.1). In each cell a BS with N_r receive antennas serves N_t single antenna UEs. $N_{\mathrm{f}} \leq 18N_t$ is the number of interferers in the first and second interference tier that use the same resources, such as frequency and time, as the center cell. Single antenna UEs are uniformly distributed across each cell, with

a fixed number per cell. The intra-cell interference is the interference between UEs located in the center cell. The inter-cell interference is the interference from UEs located in different cells to the UEs in the center cell. For this uplink model which is a modified version from Section 2.7 with the inclusion of inter cell interference, the received signal is given by

$$\begin{aligned} \mathbf{y} &= \mathbf{H}\mathbf{x} + \mathbf{F}\mathbf{x}_I + \mathbf{n} \\ &= \underbrace{\mathbf{h}_1 x_1}_{\text{desired signal}} + \underbrace{\sum_{m=2}^{N_t} \mathbf{h}_m x_m}_{\text{intra-cell interference}} + \underbrace{\sum_{m=1}^{N_\text{f}} \mathbf{f}_m x_{I_m}}_{\text{inter-cell interference}} + \underbrace{\mathbf{n}}_{\text{noise}}, \end{aligned} \tag{3.1}$$

where $\mathbf{H}, \mathbf{x}$ and $\mathbf{n}$ have the same definitions in Section 2.7 and they are related to the center cell. $\mathbf{F} = [\mathbf{f}_1 \cdots \mathbf{f}_{N_f}]$ is the $N_r \times N_f$ channel matrix of UEs located in the other cells and $\mathbf{x}_I = [x_{I_1}, x_{I_2}, \ldots x_{I_{N_f}}]^T$ is the $N_f \times 1$ vector of transmitted symbols from other cell UEs. Without loss of generality the transmit symbols satisfy $\mathrm{E}[|x_j|^2] = \mathrm{E}[\left|x_{I_j}\right|^2] = 1$. The channel coefficient, f_{ij}, from UE j outside the center cell to receive antenna i has the link gain $\mathrm{E}[|f_{ij}|^2] = Q_{ij}$.

Obtaining accurate CSI is one of the challenges in MM due to pilot contamination [7] and in distributed scenarios there are likely to be latency issues also [10]. Hence, we assume the imperfect CSI model provided in Section 2.7.

In this chapter, we consider linear detectors and for any such combiner, the output SINR for the m^{th} user is calculated using a simple variation of the SINR in [68, equation (9)] as

$$\mathrm{SINR}_m = \frac{\mathrm{E}[|r_0 \mathbf{w}_m^H \hat{\mathbf{h}}_m x_m|^2]}{\mathrm{E}[|\mathbf{w}_m^H (r_0 \sum_{j \neq m} \hat{\mathbf{h}}_j x_j + \sqrt{1 - r_0^2}\mathbf{E}\mathbf{x} + \mathbf{F}\mathbf{x}_I + \mathbf{n})|^2]} \tag{3.2}$$

Note that the expectations in the numerator and denominator of (3.2) are with respect the transmitted symbols and the noise. The combiners considered are mainly ZF and MRC, but some results are also given for MMSE.

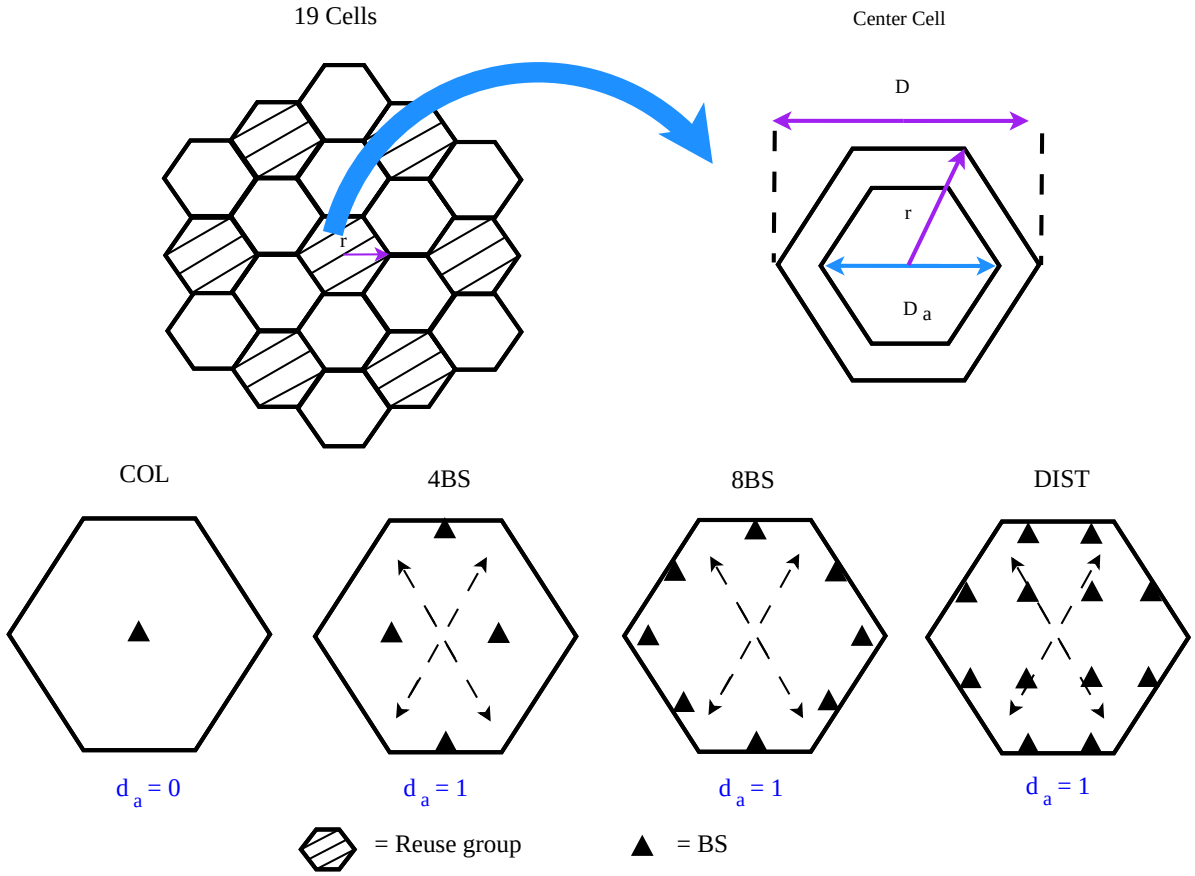

Figure 3.1: Example of deployment scenarios.

3.3 Deployment

The following scenarios are considered for simplicity and are also shown schematically in Figure 3.1.

- One massive co-located array (COL).
- B-collaborative base stations with multiple antennas at each BS (BBS).
- One massive array with geographically distributed single antenna BSs (DIST).

The UEs are located uniformly and randomly in all cells. Each cell has a radius of r (diameter $D = 2r$). The BSs are located in the inner indented hexagon of the center cell as in Figure 3.1 in order to study the effects of distributing antennas over varying proportions of the cell. Hence, the BSs are located inside a hexagon of diameter $D_a = d_a D$ where $0 \leq d_a \leq 1$ is a scaling factor. The special case of $d_a = 0$ corresponds to COL and, in DIST, $d_a = 1$ corresponds to spreading the array over the entire cell. Note that Figure 3.1 shows only 12 antennas in DIST for clarity. In this chapter we consider 128 antennas in the array because a regular grid of 128 points fits almost symmetrically in a hexagon giving an even spread of antennas over the cell in DIST. Hence, the specific deployments are: COL: 128 co-located antennas at the center of the coverage area; 4BS: 4 BS locations each with 32 antennas at each of the positions $(0, -\sqrt{3}/4)$, $(-0.25, 0)$, $(0, -\sqrt{3}/4)$ and $(0.25, 0)$ for $d_a = 1$ and $D = 1$; 8BS: 8 BS locations each with 16 antennas at each of the circular positions $(\sqrt{3}/4, 0)$, $(0.3062, 0.3062)$, $(0, \sqrt{3}/4)$, $(-0.3062, 0.3062)$, $(-\sqrt{3}/4, 0)$, $(-0.3062, -0.3062)$, $(0, \sqrt{3}/4)$ and $(0.3062, -0.3062)$ for $d_a = 1$ and $D = 1$; and DIST: 128 single antenna BSs. We consider various levels of interference from the two interference tiers in the cell layout of Fig. 3.1. The interference scenarios are: no interference (nCells = 1), interference from the 6 cells located in the first interference tier (nCells = 7), interference from the 18 cells located in both interference tiers (nCells = 19), and interference from the 6 shaded cells located in the frequency reuse group of size 3 (nCells = 19, reuse 3).

3.3.1 Channel Models

For all scenarios, we use the channel model from Section 2.6.6, where in (2.14) $\mathbf{H} = \mathbf{R}_r^{1/2}\mathbf{G}$, $G_{ij} = \sqrt{P_{ij}}U_{ij}$, the $U_{ij} \sim \mathcal{CN}(0, 1)$ are i.i.d. fast fading terms and $\mathbf{R}_r^{1/2}$ is the spatial correlation matrix at the receive array. For each scenario, the corresponding link gains are calculated as shown in Section 2.6.5, where $P_{ij} = AL_{ij}d_{ij}^{-\gamma}$ and A is a constant depending on transmit power,

antenna height, etc., L_{ij} is a lognormal shadow fading variable, d_{ij} is the link distance and γ is the path loss exponent. We assume L_{ij} in (2.9) to be spatially correlated lognormal shadow fading.

Note that including the effects of spatial correlation in the shadow fading is critical here because small values of d_a bring the antennas close together and in this situation independent shadowing is unrealistic. The correlation between the shadow fading terms at antennas i and j, is defined by $\bar{R}_{ij} = e^{-r_{ij}/(br)}$ with r_{ij} being the antenna separation and $b \in [0, 1]$ is the fraction of the cell radius at which decorrelation occurs i.e., at which $\bar{R}_{ij} = e^{-1}$. Note that $\bar{R}_{ij} = \mathrm{E}[10\log_{10}L_{ik} \times 10\log_{10}L_{jk}\ ]$ for any UE, $k = 1, 2, .., N_t$. This is the well-known exponential correlation model [89]. Typical values of b in the literature range from 0.1 to 0.5 [36, 90].

For simplicity, we assume a constant A and a constant path loss exponent, γ. In (2.14), the channel correlation matrix at the receiver has the block diagonal form $\mathbf{R}_r = \mathrm{diag}\,(\mathbf{R}_b, \ldots, \mathbf{R}_b)$, where $\mathbf{R}_b$ is the correlation matrix at each of the B arrays. Let $\mathbf{R}_b = (R_{ij})$, then the element R_{ij} is modeled by $R_{ij} = \alpha_u^{|i-j|}$, where α_u is the correlation between channels at adjacent antennas, $0 < \alpha_u < 1$ and $i, j = \{1, \ldots, N_r/B\}$. This is the simple exponential correlation model given in [58]. Therefore, $\mathbf{R}_b$ can be decomposed as $\mathbf{R}_b = \mathbf{\Psi}_b^H \mathbf{\Lambda}_b \mathbf{\Psi}_b$, where $\mathbf{\Psi}_b$ is a unitary matrix and $\mathbf{\Lambda}_b$ is a diagonal matrix containing the eigenvalues of $\mathbf{R}_b$.

3.4 Analysis

In this section we analyze the effects of propagation parameters and the BS deployment scenarios described in Section 3.3 on MRC and ZF performance.

3.4.1 Exact SINR Calculations

For a ZF receiver and UE 1, the general SINR in (3.2) collapses to [91]

$$\mathrm{SINR}_1^{(\mathrm{ZF})} = \frac{r_0^2}{[(\mathbf{W}^H((1-r_0^2)\mathbf{E}\mathbf{E}^H + \mathbf{F}\mathbf{F}^H + \sigma^2\mathbf{I})\mathbf{W}]_{11}}, \tag{3.3}$$

where $[.]_{11}$ denotes the (1,1)th element of a matrix. For an MRC receiver, the SINR for user 1 is given by

$$\mathrm{SINR}_1^{(\mathrm{MRC})} = \frac{r_0^2|\hat{\mathbf{h}}_1^H\hat{\mathbf{h}}_1|^2}{r_0^2\sum_{j=2}^{N_t}\hat{\mathbf{h}}_1^H\hat{\mathbf{h}}_j\hat{\mathbf{h}}_j^H\hat{\mathbf{h}}_1 + (1-r_0^2)\sum_{j=1}^{N_t}\hat{\mathbf{h}}_1^H\mathbf{e}_j\mathbf{e}_j^H\hat{\mathbf{h}}_1 + \sum_{j=1}^{N_f}\hat{\mathbf{h}}_1^H\mathbf{f}_j\mathbf{f}_j^H\hat{\mathbf{h}}_1 + \sigma^2\hat{\mathbf{h}}_1^H\hat{\mathbf{h}}_1}. \tag{3.4}$$

Every term in (3.3) and (3.4) is constructed from the cross products $\hat{\mathbf{h}}_i^H\hat{\mathbf{h}}_j$, $\hat{\mathbf{h}}_i^H\mathbf{e}_j$ and $\hat{\mathbf{h}}_i^H\mathbf{f}_j$. Since all UEs experience the same correlations, $\hat{\mathbf{h}}_j$, $\mathbf{e}_j$ and $\mathbf{f}_j$ all have the same correlation matrix. Hence, each cross product is of the form $\breve{\mathbf{x}}^H\breve{\mathbf{y}} = \tilde{\mathbf{x}}^H\mathbf{R}_r^{1/2}\mathbf{R}_r^{1/2}\tilde{\mathbf{y}}$ where $\tilde{\mathbf{x}}, \tilde{\mathbf{y}}$ have the same power structure as $\breve{\mathbf{x}}$, $\breve{\mathbf{y}}$, but are independent. Using the eigenvalue decomposition of $\mathbf{R}_r$ gives

$$\breve{\mathbf{x}}^H\breve{\mathbf{y}} = \tilde{\mathbf{x}}^H\mathbf{\Psi}^H\mathbf{\Lambda}\mathbf{\Psi}\tilde{\mathbf{y}}, \tag{3.5}$$

where $\mathbf{\Psi} = \mathrm{diag}\,(\mathbf{\Psi}_b, \ldots, \mathbf{\Psi}_b)$ and $\mathbf{\Lambda} = \mathrm{diag}\,(\mathbf{\Lambda}_b, \ldots, \mathbf{\Lambda}_b)$ are block diagonal. Furthermore, since $\mathbf{\Psi}$ is block diagonal and each UE has the same power in each block, $\mathbf{\Psi}\tilde{\mathbf{x}}$ is statistically identical to $\tilde{\mathbf{x}}$. Hence, $\breve{\mathbf{x}}^H\breve{\mathbf{y}}$ is statistically identical to $\tilde{\mathbf{x}}^H\mathbf{\Lambda}\tilde{\mathbf{y}} = \tilde{\mathbf{x}}^H\mathbf{\Lambda}^{1/2}\mathbf{\Lambda}^{1/2}\tilde{\mathbf{y}}$. Now $\mathbf{\Lambda}^{1/2}\tilde{\mathbf{y}}$ and $\tilde{\mathbf{x}}^H\mathbf{\Lambda}^{1/2}$ are simply scaled versions of the original $\tilde{\mathbf{x}}, \tilde{\mathbf{y}}$ values. Hence, for our uplink model of distributed single-antenna transmitters, the effect of correlation is equivalent to scaling the power at antenna i by Λ_{ii}. As a result, in the subsequent analysis, we replace P_{ij} by $\bar{P}_{ij} = \Lambda_{ii}P_{ij}$ and Q_{ij} by $\bar{Q}_{ij} = \Lambda_{ii}Q_{ij}$ and maintain the independence of the channel correlation coefficients as the correlation is catered for by the power scaling. Note that in the uncorrelated case, $\mathbf{R}_r = \mathbf{\Lambda} = \mathbf{I}$ and the power scaling has no effect, as desired.

3.4.2 SINR Approximation Analysis with ZF

Using the full SINR representation in (3.3) leads to a complicated analysis without any resulting insight. To avoid this complexity, we can approximate the interference from outside the desired cell as noise and replace the estimation error, interference and noise covariance matrix, $(1 - r_0^2)\mathbf{E}\mathbf{E}^H + \mathbf{F}\mathbf{F}^H + \sigma^2\mathbf{I}$, by an equivalent noise covariance matrix, $\sigma_{\text{eq}}^2\mathbf{I}$, where

$$\begin{aligned}\sigma_{\text{eq}}^2 &= 1/N_r \text{Tr}\left((1 - r_0^2)\mathbf{E}\mathbf{E}^H + \mathbf{F}\mathbf{F}^H + \sigma^2\mathbf{I}\right) \\ &= \sigma^2 + 1/N_r(1 - r_0^2)\sum_{i=1}^{N_r}\sum_{j=1}^{N_t}\bar{P}_{ij} + 1/N_r\sum_{i=1}^{N_r}\sum_{j=1}^{N_f}\bar{Q}_{ij}. \end{aligned} \tag{3.6}$$

Note that in (3.6) σ_{eq}^2 approaches σ^2 as N_r becomes large. The accuracy of this approximation investigated in Section 3.5 (see Figures 3.4 - 3.6). Thus,

$$\text{SINR}_1^{(\text{ZF})} \approx \frac{r_0^2}{\sigma_{\text{eq}}^2[(\hat{\mathbf{H}}^H\hat{\mathbf{H}})^{-1}]_{11}}. \tag{3.7}$$

Using the co-factor expression for $[(\hat{\mathbf{H}}^H\hat{\mathbf{H}})^{-1}]_{11}$, we obtain

$$\frac{r_0^2}{\sigma_{\text{eq}}^2[(\hat{\mathbf{H}}^H\hat{\mathbf{H}})^{-1}]_{11}} = \frac{r_0^2|\hat{\mathbf{H}}^H\hat{\mathbf{H}}|}{\sigma_{\text{eq}}^2|\hat{\mathbf{H}}_2^H\hat{\mathbf{H}}_2|}, \tag{3.8}$$

where $\hat{\mathbf{H}}_2$ is the channel matrix, $\hat{\mathbf{H}}$, with the first column removed. The mean SINR over the fast fading can be approximated using the Laplace approximation approach from [92], which was shown to be quite accurate for ratios of quadratic forms in [93], as

$$\text{E}[\text{SINR}_1^{(\text{ZF})}] \approx \frac{r_0^2\text{E}[|\hat{\mathbf{H}}^H\hat{\mathbf{H}}|]}{\sigma_{\text{eq}}^2\text{E}[|\hat{\mathbf{H}}_2^H\hat{\mathbf{H}}_2|]} = \frac{r_0^2\text{Perm}(\bar{\mathbf{P}})}{\sigma_{\text{eq}}^2\text{Perm}(\bar{\mathbf{P}}_2)}, \tag{3.9}$$

where $\text{Perm}(.)$ is the permanent of a matrix, $\bar{\mathbf{P}} = (\bar{P}_{ij})$, $1 \leqslant i \leqslant N_r$, $1 \leqslant j \leqslant N_t$, $\bar{\mathbf{P}}_2 = (\bar{P}_{ij})$, $1 \leqslant i \leqslant N_r$, $2 \leqslant j \leqslant N_t$ and the expectations are with respect to the fast fading. There are several

reasons for using the Laplace approximation. The results, shown in Figures 3.4 - 3.6, verify its accuracy for this situation and the analytical results in (3.12)-(3.16) verify the simple form of the resulting expressions. Furthermore, [92, 93] suggest that an exact analysis is intractable for more than two UEs. Rewriting the right hand side of (3.9) gives:

$$\begin{aligned}\frac{r_0^2\mathrm{Perm}(\bar{\mathbf{P}})}{\sigma_{\mathrm{eq}}^2\mathrm{Perm}(\bar{\mathbf{P}}_2)} &\approx \frac{r_0^2\sum_{i_1=1}^{N_r}\bar{P}_{i_11}\sum_{i_2\in s(1,1)}\bar{P}_{i_22}\cdots\sum_{i_{N_t}\in s(1,N_t-1)}\bar{P}_{i_{N_t}N_t}}{\sigma_{\mathrm{eq}}^2\sum_{i_2=1}^{N_r}\bar{P}_{i_22}\cdots\sum_{i_{N_t}\in s(2,N_t-1)}\bar{P}_{i_{N_t}N_t}} \\ &= \frac{r_0^2\sum_{i_1=1}^{N_r}\bar{P}_{i_11}[\bar{G}-\sum_{j=2}^{N_t}F_j(i_1)]}{\sigma_{\mathrm{eq}}^2\bar{G}} \\ &= \frac{r_0^2\sum_{i_1=1}^{N_r}\bar{P}_{i_11}}{\sigma_{\mathrm{eq}}^2} - \frac{r_0^2\sum_{i_1=1}^{N_r}\bar{P}_{i_11}\sum_{j=2}^{N_t}F_j(i_1)}{\sigma_{\mathrm{eq}}^2\bar{G}},\end{aligned} \tag{3.10}$$

where $s(k,l) = \{1,2,\ldots N_r\}\backslash\{i_k, i_{k+1},\ldots,i_l\}$, $\bar{G} = \sum_{i_2=1}^{N_r}\bar{P}_{i_22}\cdots\sum_{i_{N_t}\in s(2,N_t-1)}\bar{P}_{i_{N_t}N_t}$ and $F_j(i_1)$ is defined as

$$F_j(i_1) = \bar{P}_{i_1j}\sum_{i_2\in s(1,1)}\bar{P}_{i_22}\cdots\sum_{i_{j-1}\in s(1,j-2)}\bar{P}_{i_{j-1}j-1}\sum_{i_{j+1}\in s(1,j)}\bar{P}_{i_{j+1}j+1}\cdots\sum_{i_{N_t}\in s(1,N_t-1)}\bar{P}_{i_{N_t}N_t} \tag{3.11}$$

For $N_r \gg N_t$, the number of products of powers in $\bar{G}$ dominates the number in $\sum_{j=2}^{N_t}F_j(i_1)$ and therefore $\bar{G} \gg \sum_{j=2}^{N_t}F_j(i_1)$ so that

$$\mathrm{E}[\mathrm{SINR}_1^{(\mathrm{ZF})}] \approx r_0^2\sum_{i=1}^{N_r}\bar{P}_{i1}/\sigma_{\mathrm{eq}}^2. \tag{3.12}$$

Note that (3.12) relies on the equivalent noise model (see (3.7)), the Laplace approximation (see (3.9)) and the removal of lower order terms in (3.10). The latter two approximations are motivated by MM properties while the first is required for analytical progress. The overall accuracy and the accuracy of the Laplace approximation stage are evaluated in Section 3.5.

3.4.3 SINR Approximation Analysis with MRC

The mean SINR is again approximated using a Laplace approximation (as in (3.9)) to give

$$\mathrm{E}[\mathrm{SINR}_1^{(\mathrm{MRC})}] \approx \frac{r_0^2(\sum_{i=1}^{N_r}\bar{P}_{i1})^2+r_0^2\sum_{i=1}^{N_r}\bar{P}_{i1}^2}{r_0^2\sum_{i=1}^{N_r}\sum_{j=2}^{N_t}\bar{P}_{i1}\bar{P}_{ij}+(1-r_0^2)\sum_{i=1}^{N_r}\sum_{j=1}^{N_t}\bar{P}_{i1}\bar{P}_{ij}+\sum_{i=1}^{N_r}\sum_{j=1}^{N_f}\bar{P}_{i1}\bar{Q}_{ij}+\sigma^2\sum_{i=1}^{N_r}\bar{P}_{i1}}. \tag{3.13}$$

Similar results were obtained in [83] from a different approach, but were not expressed or used in the same way as in the following. In the MM scenario, the system is intra-cell interference limited and the leading term in both the numerator and denominator of (3.13) is dominant. As a result,

$$\mathrm{E}[\mathrm{SINR}_1^{(\mathrm{MRC})}] \approx \frac{r_0^2\sum_{i=1}^{N_r}\bar{P}_{i1}}{\frac{\sum_{i=1}^{N_r}\bar{P}_{i1}(-r_0^2\bar{P}_{i1}+\sum_{j=1}^{N_t}\bar{P}_{ij})}{\sum_{k=1}^{N_r}\bar{P}_{k1}}}. \tag{3.14}$$

3.4.4 Discussion

The simple approximations in (3.12) and (3.14) provide the following insights. Increasing the transmit SNR, ρ, does not scale (3.12) linearly as ZF only removes the intra-cell interference resulting in a ceiling on the ZF SINR. In addition, for MRC, (3.14) is independent of ρ as MRC is interference limited and a higher transmit SNR does not help. Consider the case of perfect CSI, $r_0 = 1$, for further insights. To evaluate the effects of distributed antennas, we substitute $\bar{P}_{ij} = \bar{P}_j$ into (3.12) and (3.14) to obtain the co-located results:

$$\mathrm{E}[\mathrm{SINR}_1^{(\mathrm{ZF})}] \approx \frac{N_r\bar{P}_1}{\sigma_{\mathrm{eq}}^2}, \quad \mathrm{E}[\mathrm{SINR}_1^{(\mathrm{MRC})}] \approx N_r\frac{\bar{P}_1}{\sum_{t=2}^{N_t}\bar{P}_t}. \tag{3.15}$$

In the BBS scenario, using $\bar{P}_{ij} = \bar{P}_j^{(k)}$, where $k \in \{1, \ldots, B\}$, (3.12) and (3.14) simplify to

$$\begin{aligned} \mathrm{E}[\mathrm{SINR}_1^{(\mathrm{ZF})}] &\approx \frac{N_r}{B} \frac{\sum_{k=1}^{B} \bar{P}_1^{(k)}}{\sigma_{\mathrm{eq}}^2}, \\ \mathrm{E}[\mathrm{SINR}_1^{(\mathrm{MRC})}] &\approx \frac{N_r}{B} \frac{\sum_{k=1}^{B} \bar{P}_1^{(k)}}{\sum_{k=1}^{B} \left(\frac{\bar{P}_1^{(k)}}{\sum_{i=1}^{B} \bar{P}_1^{(i)}} \right) \sum_{r=2}^{N_t} \bar{P}_r^{(k)}}. \end{aligned} \tag{3.16}$$

Note that the results in (3.12)-(3.16) are averaged over the fast fading. Nevertheless, we use these results as approximations to the instantaneous SINR at a system level as the variation due to the fast fading is negligible compared to the variation due to the long term powers.

The coefficient of variation (CV) is one type of measure of variation. For a random variable X, the CV can be calculated as $CV(X) = \sqrt{\mathrm{variance}[X]}/\mathrm{mean}[X]$. Here, the CV of the square of the absolute fast fading term, $|U_{ij}|^2$, is $CV = 1$ whereas for $\sigma_{SF} = 8$ dB, $\gamma = 3$ the CV of $\bar{P}_{ij}$, exceeds 50 (where the CV is computed using the moments derived in [94] for a circular cell). In fact, this difference is massive on the CV scale. The validity of the approximations is also supported by the accuracy of the results in Figure 3.4.

The MRC result in (3.15) is similar to the SINR of a large code division multiple access system [95, equation (8)]; however, the assumptions and channels are significantly different. The ZF result also differ from previously published results [83, 95]. Comparing (3.12) with (3.15) and (3.16) for $r_0 = 1$, we observe that the form of the ZF SINR is the same, but the co-located version has a single power, $\bar{P}_1$, scaled by $N_r/\sigma_{\mathrm{eq}}^2$; the BBS version has the average of B powers $\sum_{k=1}^{B} \bar{P}_1^{(k)}/B$ scaled by $N_r/(\sigma_{\mathrm{eq}}^2)$ and the distributed version has the average of N_r different powers, $\bar{P}_{i1}$, scaled by $N_r/\sigma_{\mathrm{eq}}^2$. Hence, the mean of the absolute SINR is very similar for the three cases, but in the BBS and the distributed case the variation is heavily reduced due to the increasing amount of averaging. Thus, the co-located case has higher maximum values (due to the fact that all N_r links are strong when the UE is in a good location) but suffers from

a poor lower tail (when all N_r links are weak). The lower tail of the cumulative distribution function (CDF) is critical and is emphasised with a dB scale showing that the distributed case will outperform the co-located case considerably (see Figures 3.4, 3.7, 3.8). Note that for each individual UE the CDF may not be an adequate representation of the expected performance, but here it is used as to assess the expected system wide performance across all UEs. The BBS scenario is important because it is much easier to locate a few BSs around the cell rather than use DIST. Hence, this scenario enables us to investigate how much of the fully distributed gains are achieved from a layout with only B sites. The same conclusions can be drawn for MRC, since the ratio of two single variables in (3.15) is being compared to the ratio of an average to a weighted average in (3.14) and (3.16). Again, with a distributed array, the averaging will reduce the variation leading to considerable improvement in the lower tail and in the dB values. Note that the averaging due to distributed antennas has a greater impact when the equivalent link gains are more variable, i.e., when the path loss exponent is higher or when the shadow fading correlation is smaller. The improvements of distributed arrays have been explained via (3.12) and (3.14)-(3.16) in terms of an averaging effect. This is closely linked to to the benefits of reduced link distances with distributed arrays. Spreading the antennas creates a range of link distances and most UEs will be in close proximity to some antennas and distant from others. As a result, extreme cases with all short or long links are removed and most UEs have a few short links. Therefore, these antenna proximity benefits can be viewed as an averaging effect.

3.5 Results

In this section, we verify the accuracy of the analysis and investigate the effects of system size, deployment and propagation parameters via Monte Carlo simulation. The baseline parameters are: $N_r = 128$, $N_t = 10$, $\rho = 0$ dB, $\gamma = 3$, $\sigma_{SF} = 8$ dB. Each cell is assumed to have a radius of $r = 0.5$ units, $b = 1/5$, d_a = 0 for the COL scenario, d_a = 0.7 for the 4BS scenario,

$d_a = 0.6$ for the 8BS scenario, and d_a = 1 for the DIST scenario. The value of d_a selected for the 4BS and 8BS scenarios is chosen as it is nearly optimal for both ZF and MRC. Where these parameters are changed, it is denoted in figure labels or captions. The link distance is calculated with an exclusion zone, so that $d_{ij} > 0.01$, and the scaling parameter, A, in (2.11) is set to 1. Note that the value of A has a very small impact on the results as in the interference limited cases considered, A is present in the numerator and denominator of the SINR and is essentially canceled out. This value is fixed across all simulations so we are essentially considering a fixed transmit power. Most of the results correspond to the ideal situation where perfect channel state information is available with zero latency. These assumptions are much harder to emulate for distributed arrays.

Figure 3.2 shows the SINR for DIST with MRC and ZF and differing levels of interference. For MRC, intra-cell interference is not nulled and is dominant. Hence, all four interference scenarios have similar SINR distributions. For ZF, intra-cell interference is nulled and so the interference scenarios have a large effect. Results for nCells = 7 and nCells = 19 are similar as the tier 1 interferers are dominant. The effect of reuse is large and the (nCells = 19, reuse 3) CDF is shifted up by around 10 dB. Finally, the nCells = 1 result is interference free due to ZF and this CDF gives much higher SNRs. Note that similar conclusions are found with COL, 4BS and 8BS deployments.

Figure 3.3 shows the SINR for DIST with MMSE and different levels of interference. Similar to the ZF results in Figure 3.2, results for nCells = 7 and nCells = 19 are similar as the tier 1 interferers are dominant. When the effect of reuse is large (the nCells = 19, reuse 3 case), the CDF is shifted up by around 10 dB. Finally, when nCells = 1 there is no inter cell interference and the CDF gives much higher SNRs similar to ZF in Figure 3.2. All the curves in Figure 3.3 are very similar to those in Figure 3.2 with MMSE giving a small performance improvement that is most noticeable in the upper tail.

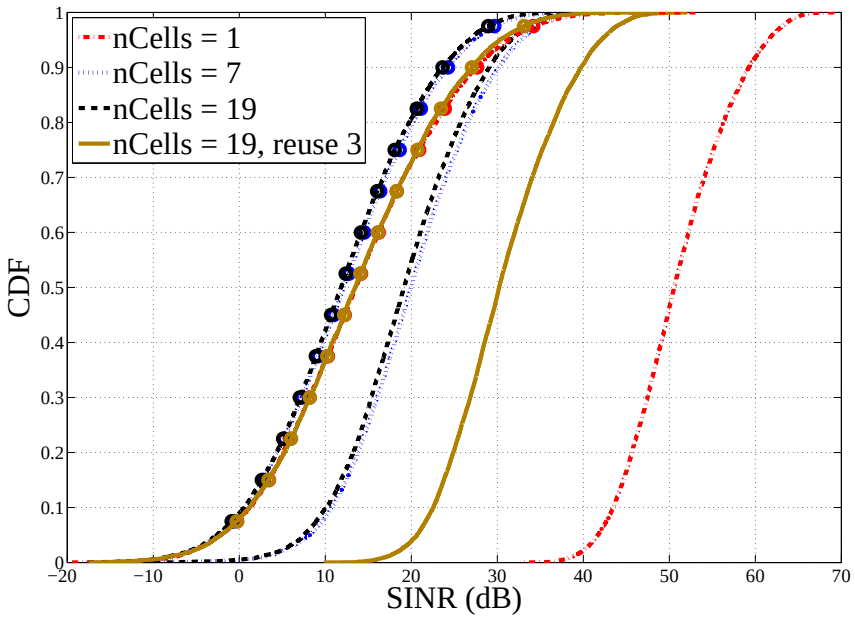

Figure 3.2: SINR CDFs for the DIST scenario with ZF and MRC and differing numbers of interfering cells. Lines alone represent ZF and lines with circles represent MRC. nCells $\in \{1, 7, 19\}$.

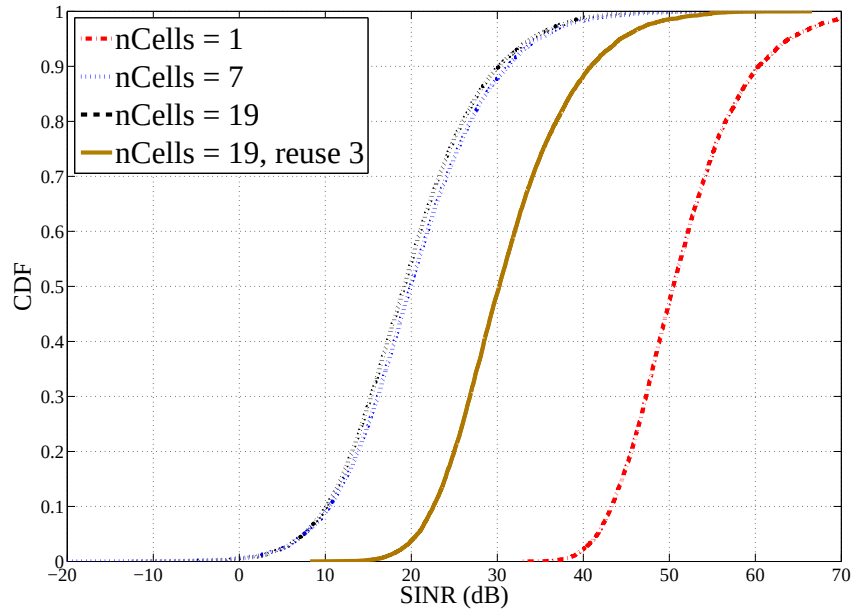

Figure 3.3: SINR CDFs for the DIST scenario with MMSE and differing numbers of interfering cells. nCells $\in \{1, 7, 19\}$.

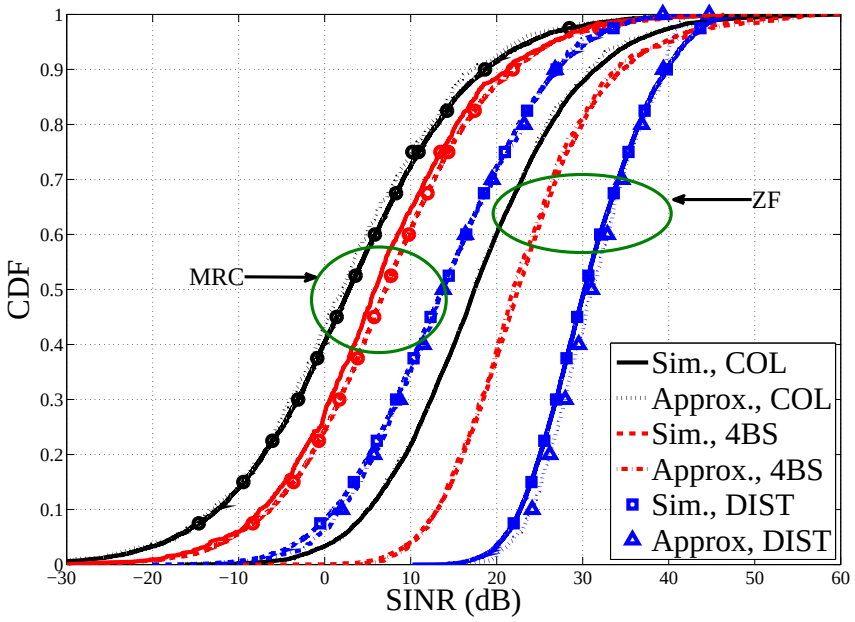

Figure 3.4: SINR CDFs for the three deployment scenarios with ZF and MRC and $r_0 = 1$. nCells = 19, reuse 3.

Figure 3.4 compares the SINR approximations (labeled Approx.) using (3.12) and (3.14) with the simulated instantaneous SINR values (labeled Sim.) for MRC and ZF. The remarkably simple approximations in (3.12) and (3.14) provide an excellent match to the SINR CDFs for both receivers. This validates the use of the simple approximation techniques in Section 3.4. The results in Figure 3.4 are for perfect CSI ($r_0 = 1$).

Figure 3.5 compares the SINR approximations using (3.12) and (3.14) with the simulated instantaneous SINR values for MRC and ZF with imperfect CSI, $r_0 = 0.99$. Simulation results suggest that the SINR obtained from the simple approximations in (3.12) and (3.14) is less accurate in the upper tail, particularly in more distributed scenarios, but works well in the COL case. For ZF, this may be due to the approximation of the interference from outside the desired cell as noise and the replacement of the estimation error, interference and noise covariance matrix, by equivalent noise as discussed in Section 3.4. Compared to the perfect CSI case,

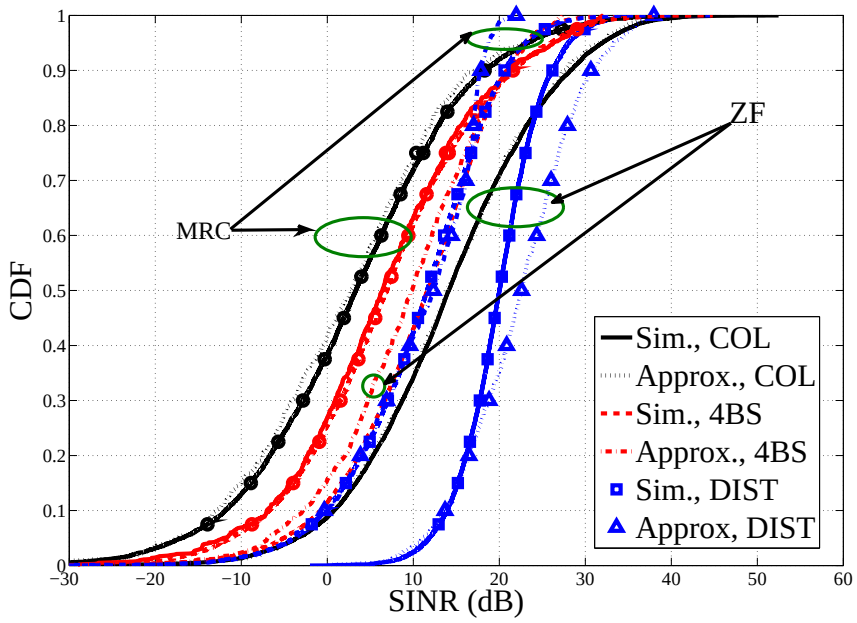

Figure 3.5: SINR CDFs for the three deployment scenarios with ZF and MRC and $r_0 = 0.99$. nCells = 19, reuse 3.

the estimation error is an extra term in this covariance matrix. Hence, imperfect CSI makes the covariance matrix larger and this makes the results more sensitive to the equivalent noise approximation. Compared to the results in Figure 3.4, imperfect CSI has a much greater impact on ZF than MRC.

When imperfect CSI is considered the analytical results are slightly less accurate as shown in Table 3.1. For $r_0 \in \{0.6, 1\}$, approximate results for the median SINR are accurate to within 1 dB for all MRC scenarios. For ZF, results are within 1 dB for COL, but have errors around 2 dB for 4BS and DIST. Two other features are shown in Table 3.1. First, the approximation error increases as r_0 reduces since greater channel estimation error inflates the $\mathbf{E}$ matrix making the equivalent noise model less accurate. Secondly, when the CSI is poor 4BS can outperform DIST. This is because DIST often results in a UE having a single dominant link and this situation is particularly susceptible to poor CSI.

Table 3.1: Simulated and approximated median SINR (dB) with imperfect channel estimation.

ZF (nCells = 19, reuse 3)						
	Sim.			**Approx.**		
r_0	**COL**	**4BS**	**DIST**	**COL**	**4BS**	**DIST**
1	17.2	22.2	30.1	17.3	22.2	30.8
0.99	14.1	18.5	20.0	14.1	17.7	22.4
0.9	7.7	11.6	10.3	7.5	10.0	12.6
0.8	4.6	8.1	6.7	4.2	6.3	8.8
0.6	-0.1	3.3	1.6	-0.5	1.6	3.9
MRC(nCells = 19, reuse 3)						
	Sim.			**Approx.**		
r_0	**COL**	**4BS**	**DIST**	**COL**	**4BS**	**DIST**
1	3.0	6.9	13.0	2.4	6.2	12.9
0.99	2.9	6.8	11.6	2.1	6.1	12.2
0.9	2.1	5.9	7.0	1.4	5.2	6.9
0.8	0.9	4.8	4.5	0.2	4.0	3.7
0.6	-1.5	2.2	0.4	-2.4	1.4	-0.5

For the COL scenario, Figure 3.6 compares the SINR approximations, (3.12), (3.7) and (3.14), with simulated instantaneous SINR values for MRC and ZF with imperfect CSI and correlation, $r_0 = 0.99$ and $\alpha_u = \{0.1, 0.9\}$. These results demonstrate that the SINR obtained from the simple approximations in (3.12) and (3.14) are less accurate for ZF when the correlation is high, but work well with low correlation. In addition, with low correlation the approximations in (3.7) are similar to (3.12) supporting the use of the Laplace approximation. However, for high correlation the ZF approximation is poor. This is caused by the effect of the correlation which makes the aggregate interference and noise more colored and less like simple additive noise. Overall, the simple closed form approximations are useful for all MRC scenarios and for ZF with low correlation.

Compared to the results in Figure 3.4, imperfect CSI has a much greater impact on ZF than MRC. In the DIST scenario, the correlation does not have an impact on the system performance

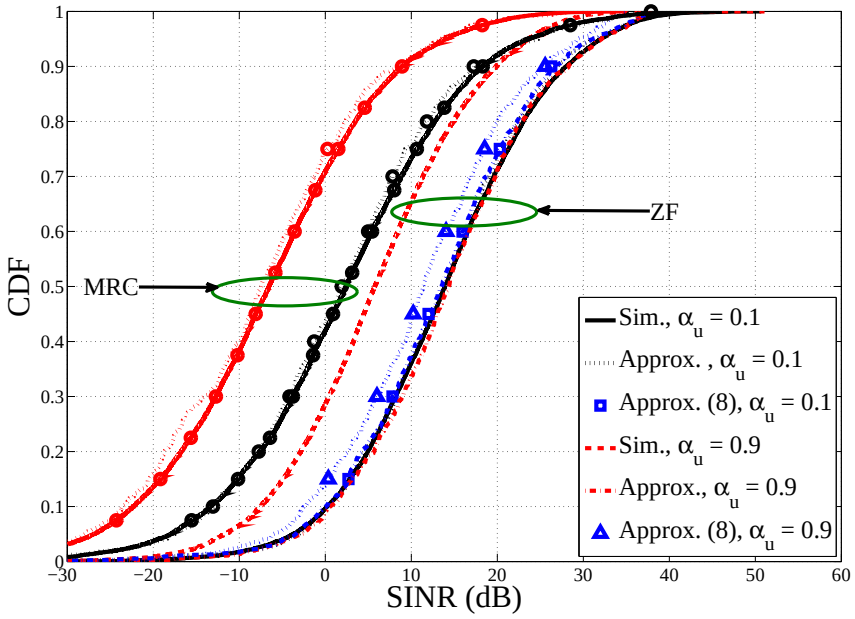

Figure 3.6: SINR CDFs for the COL scenario with ZF and MRC for $r_0 = 0.99$ and different correlation levels, $\alpha_u = \{0.1, 0.9\}$. nCells = 19, reuse 3.

because the correlation matrix $\mathbf{R}_r$ is the identity matrix.

Using a frequency reuse of factor 1 (nCells = 19), Figures 3.7 and 3.8 show the effect of γ on ZF and MRC. As shown in Section 3.4, increasing γ increases the gap between the co-located and distributed results. The changes between $\gamma = 3$ and $\gamma = 4$ are more noticeable for ZF than for MRC since an increased γ has a direct effect on SINR for ZF, whereas for MRC, increasing γ affects both the numerator and denominator of (3.14). Changes are also more noticeable for the distributed scenario. Increased path loss accentuates the variability in link gain. This is ideal for DIST where the different antenna locations mean that different UEs can tend to find different sets of antennas with reasonable link gains and the greater path loss from other UEs reduces the overall interference which must be mitigated. An interesting feature of Figures 3.7 and 3.8 is that they quantify the gains offered by 8BS and 4BS in comparison to DIST. In practice a fully distributed array may be impractical and only a partial distribution,

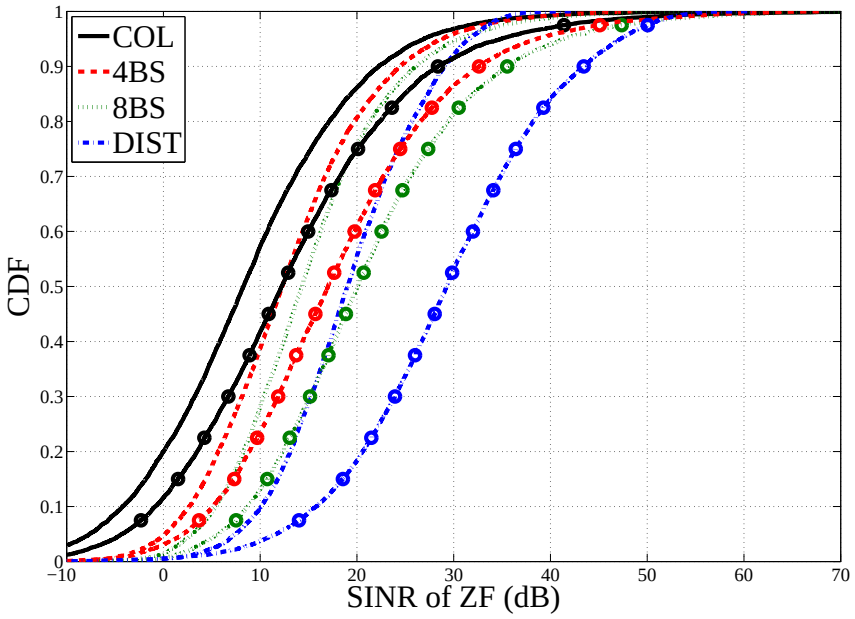

Figure 3.7: SINR CDFs for the four deployment scenarios with ZF, $\gamma \in \{3, 4\}$. Lines alone represent γ = 3 and lines with markers represent γ = 4. nCells = 19.

an intermediate deployment as in 4BS or 8BS, may be viable. Here, we observe that for ZF, moving from one BS site to four provides approximately 38% of the gains in moving from one site to 128 sites. The corresponding percentage gain is approximately 40% for MRC. Moving from one BS site to eight provides approximately 56% of the gains in moving from one site to 128 sites for ZF. The corresponding percentage gain is approximately 53% for MRC. With reuse 3, the percentage gains are similar.

Figure 3.9 shows the median SINR of ZF and MRC with different values of d_a and b for DIST, 4BS and 8BS. This explores the effect of spreading the antennas over increasing proportions of the cell area (increasing d_a) and the effect of increasing shadow fading correlation (increasing b). We observe that increasing the spread of the antenna array is more beneficial for DIST compared to 4BS or 8BS and for ZF compared to MRC. Both effects are due to the averaging effect explained by the closed form analysis in Section 3.4.

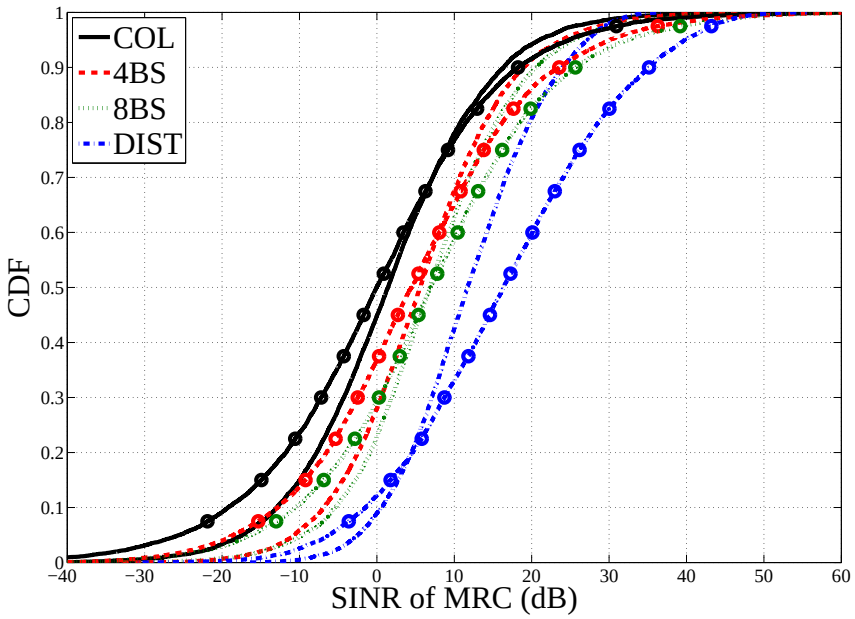

Figure 3.8: SINR CDFs for the four deployment scenarios with MRC, $\gamma \in \{3, 4\}$. Lines alone represent $\gamma = 3$ and lines with markers represent $\gamma = 4$. nCells = 19.

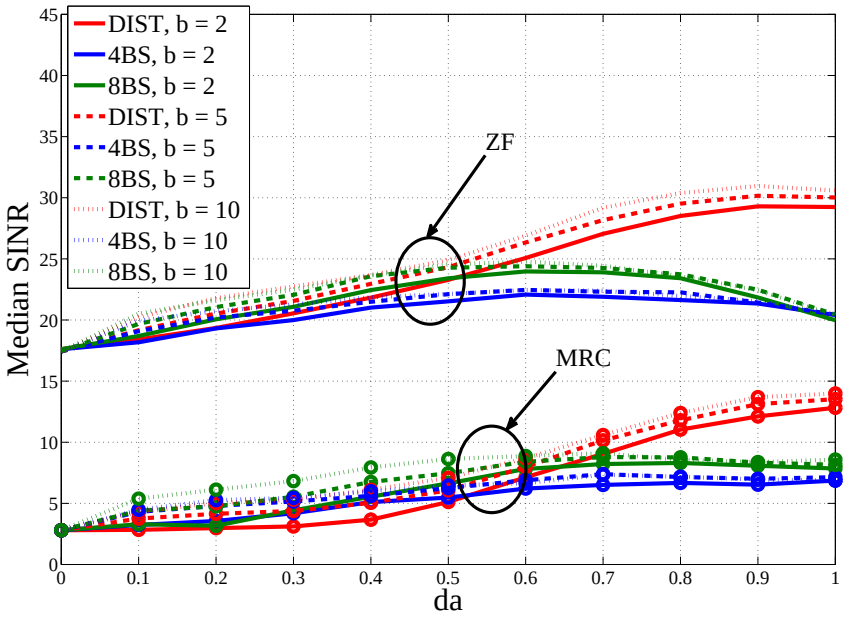

Figure 3.9: Median SINR vs d_a for ZF and MRC with DIST, 4BS and 8BS with $b \in \{1/2, 1/5, 1/10\}$. Lines alone represent ZF and lines with markers represent MRC. nCells = 19, reuse 3.

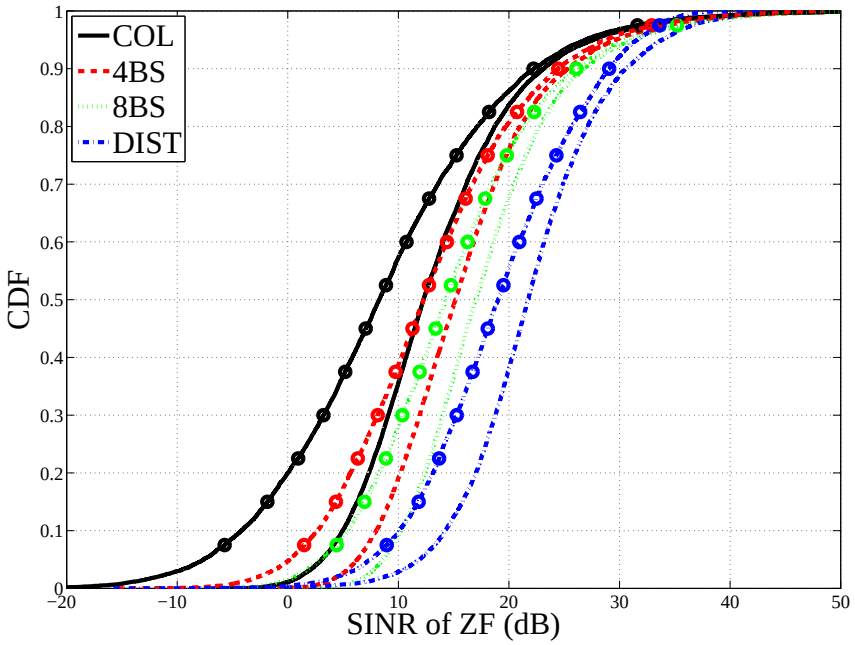

Figure 3.10: SINR CDFs for the four deployment scenarios with ZF, $\sigma_{\mathrm{SF}} \in \{4, 8\}$ dB. Lines alone represent σ_{SF} = 4 and lines with markers represent σ_{SF} = 8. nCells = 19.

Figures 3.10 -3.11 show the SINR CDFs for the four deployment scenarios with ZF and MRC respectively for $\sigma_{\mathrm{SF}} \in \{4, 8\}$ dB. The changes between $\sigma_{\mathrm{SF}} = 4$ and $\sigma_{\mathrm{SF}} = 8$ are more noticeable for ZF than for MRC since an increased σ_{SF} has a direct affect on SINR for ZF, whereas for MRC, increasing σ_{SF} affects both the numerator and denominator of (3.14). Changes are also more noticeable for the co-located scenario.

Obtaining accurate CSI is one of the challenges in MM as performance can be limited by interference arising from the re-use of pilots in neighboring cells [7]. Correlation is also an important factor when large numbers of antennas are deployed in a small physical volume. In Table 3.2, we give median SINR results for the four scenarios and both linear receivers for varying levels of CSI and correlation. Clearly, ZF is more sensitive to imperfect CSI in all deployments and the gains of ZF over MRC are reduced as r_0 decreases, particularly for DIST.

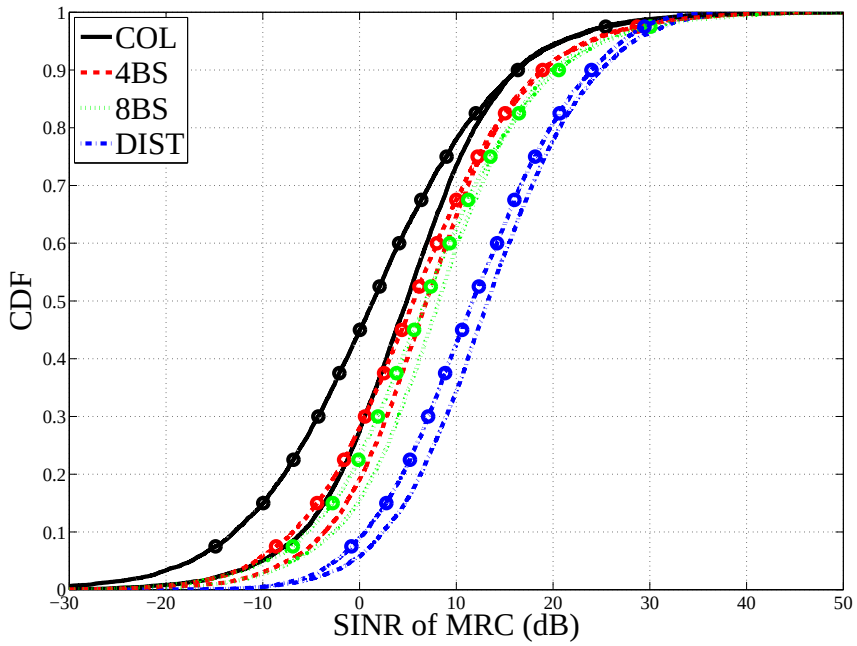

Figure 3.11: SINR CDFs for the four deployment scenarios with MRC, $\sigma_{\mathrm{SF}} \in \{4, 8\}$ dB. Lines alone represent σ_{SF} = 4 and lines with markers represent σ_{SF} = 8. nCells = 19.

Table 3.2: Median SINR (dB) with imperfect channel estimation and correlation.

$\alpha_u = 0.1$ (nCells = 19, reuse 3)								
	ZF				**MRC**			
r_0	**COL**	**4BS**	**8BS**	**DIST**	**COL**	**4BS**	**8BS**	**DIST**
1	17.5	22	24	30	3.0	7.1	8.3	13
0.99	14	18.5	20.1	20.2	2.8	6.9	7.9	12
0.9	7.6	11.5	12.3	10	1.9	5.8	7.2	7.0
0.8	4.7	7.9	8.9	6.6	1.4	4.9	5.8	4.4
0.6	0.1	3.4	3.9	1.7	-1.3	2.9	2.8	0.4
$\alpha_u = 0.9$ (nCells = 19, reuse 3)								
	ZF				**MRC**			
r_0	**COL**	**4BS**	**8BS**	**DIST**	**COL**	**4BS**	**8BS**	**DIST**
1	8.9	14	17	30	-6.4	-1.7	0.3	13
0.99	5.8	10	13	20	-6.7	-2.1	0.01	12
0.9	-0.5	3.5	5.5	10	-7.4	-3.2	-0.7	7.0
0.8	-3.6	0.3	1.9	6.6	-8.2	-3.9	-2.2	4.5
0.6	-8.1	-4.5	-3	1.7	-11	-6.5	-5.2	0.4

DIST is more heavily affected by imperfect CSI than COL. With imperfect CSI, the additive channel errors in the desired channel are of the form $\sqrt{1-r_0^2}\mathbf{e}_m$, where $\mathbf{e}_m$ is the m^{th} column of $\mathbf{E}$. The power of this term is $(1-r_0^2)\sum_{i=1}^{N_r}\bar{P}_{im}$ and as shown in Section 3.4, this is larger for DIST than COL. Hence, imperfect CSI has a greater impact on DIST than on COL as mentioned in the discussion of Table 3.1. Both r_0 and α_u have a serious impact on performance, although DIST is unaffected by correlation as there are no co-located antennas. Again, we observe that imperfect CSI can cause 4BS or 8BS to outperform DIST.

To summarize the practical implications of the numerical results, some level of distribution is preferable as averaging reduces variation and correlation has less impact on performance. Since urban channels tend to have higher σ_{SF} and γ values than most environments, they are usually more variable and therefore will benefit more from the averaging effects of distributed arrays. However, it is far easier to locate a few BSs around a cell than to use the full DIST ap-

proach. Hence, there is a performance-complexity trade-off which is also influenced by the fact that distributed arrays are likely to have less accurate CSI than co-located arrays. As a result, an intermediate deployment is an appealing design choice as it is simpler and less sensitive to CSI quality than DIST while avoiding the spatial correlation problems of COL.

3.6 Summary

In this chapter, we investigated the interactions between deployment scenarios, ZF, MRC and propagation parameters. A mixture of analysis, simulation and physical interpretations were used to show that the improvements offered by distributed arrays are largely due to an averaging effect which is more prominent for the ZF case. This averaging improves the lower tail of the SINR CDF of the distributed case relative to the co-located case. We also show that imperfect CSI has a significant impact which is greater for distributed arrays than for co-located arrays and reduces the improvements offered by ZF. In addition, correlation does not play a role in degrading the performance in distributed arrays but strongly affects co-located deployments. As a result, a partially distributed ZF system is an ideal candidate if the cost and CSI requirements could be met, providing performance benefits and robustness to errors in CSI.

Chapter IV

Array Size and Shape

4.1 Introduction

If the large arrays envisaged for MM are located within small volumes, then the channel correlations may become significant impacting on system performance [7, 25]. In this chapter, we look at the correlations present in massive uniform SQs and ULAs and evaluate the impact of correlation on capacity.

The advantages and disadvantages of different array configurations have been discussed in [1, 25, 30–34]. One-dimensional arrays, such as the ULA, have been shown to have some disadvantages such as front back ambiguity [32, 34] and an inability to resolve signal paths in azimuth and elevation [32, 34]. In contrast, two-dimensional and three-dimensional arrays, such as the SQ, offer extra degrees of freedom due to the variation in elevation angle [30] and a compact layout [31]. This work includes survey articles [1, 25, 30, 31] and research into precoding [32, 34, 96] and direction of arrival estimation [33]. In contrast, this chapter considers the joint effects of size and shape and focuses on the particular issue of how compact a two-dimensional array can be made relative to a ULA. Directly related work includes Chapter 5 where SQs and ULAs were compared in terms of antenna spacings. Here, we use capacity to perform a more meaningful comparison.

We consider an uplink MM deployment with a co-located BS array and distributed single antenna UEs. The performance of these systems is evaluated by ergodic capacity and capacity

outage. The key idea is to evaluate capacity under a range of correlation models and compare the performance of SQ and ULA. Square arrays offer two types of benefits relative to linear arrays. One benefit is compactness since a ULA of length b_{ULA} has approximately the same antenna spacing as a SQ with dimension $\sqrt{b_{\mathrm{ULA}}} \times \sqrt{b_{\mathrm{ULA}}}$. If size is not an issue, then a $b_{\mathrm{ULA}} \times b_{\mathrm{ULA}}$ SQ will deliver increased capacity compared to a ULA of length b_{ULA}. The main contributions of this chapter are:

- We evaluate these benefits for a range of correlation models and show that SQs always offer considerable space savings, usually requiring only 30% - 50% of the width of a ULA. When the correlations decay slowly at small distances, then SQ also offers a considerable increase in capacity compared to a ULA of the same width.

- We analytically quantify the potential effects of correlation and also prove the validity of a family of correlation models previously used in the literature [55].

The rest of the chapter is organized as follows. Sections 4.2 introduces the system model and Section 4.3 describes the correlation models. Section 4.4 defines the capacity metrics and evaluates ergodic capacity for some extreme cases. Results and conclusions are found in Sections 4.5 and 4.6, respectively.

4.2 System model

We consider the system model in Section 2.7, where the uplink received signal is

$$\mathbf{y} = \mathbf{H}\mathbf{x} + \mathbf{n} = \sum_{j=1}^{N_t} \mathbf{h}_j x_j + \mathbf{n}, \tag{4.1}$$

and $\mathbf{H}$, $\mathbf{x}$ and $\mathbf{n}$ are the channel, signal vector and noise, respectively.

Assume a large co-located array at the BS serving N_t UEs in the coverage region. The correlated channel model and link gains can be calculated as given in Section 2.6.7 where

$$\mathbf{H} = \mathbf{R}_r^{\frac{1}{2}} \mathbf{U} \mathbf{P}^{\frac{1}{2}}, \tag{4.2}$$

$\mathbf{P} = \text{diag}(P_1, P_2, \ldots, P_{N_t})$ and $P_j = \mathcal{A}\beta^{j-1}$ are the link gains. We use this simple model for the link gains in order to control the P_j's with a single parameter, β, which has a physical interpretation. $\mathbf{R}_r$ is the channel correlation matrix at the receiver.

4.3 Correlation Models

We consider the four common models described in Section 2.6.8. They are the Jakes, Gauss, Sqrt and Exp models. Note that when large arrays are deployed in a small volume, coupling may also become important. In this chapter, we do not model coupling explicitly but the aggregate effects of correlation and coupling may be captured by the broad range of correlation models considered here.

In [55,57,58], these models were explored without any formal verification that they are valid correlation models. The Jakes model is certainly valid by construction since it was derived from a physical scattering model [56]. However, to the best of our knowledge, the other three models including the widely used exponential model have not been validated. Hence, we prove their validity below.

Definition 1. *A correlation model for the channel vector,* $\mathbf{h}_i$*, is valid if* $\mathbf{R}_r = R_{ij}$ *satisfies* $R_{ij} = 1 \, \forall_i, |R_{ij}| \leq 1 \forall_{i,j}$ *and if* $\mathbf{R}_r$ *is positive semidefinite for all possible antenna numbers and locations.*

A more convenient approach to checking the validity of the Gauss, Sqrt and Exp models is given in the Theorem below.

Theorem 1. *The correlation model, $R_{ij} = e^{-a\bar{d}^c}$, for two antennas i and j separated by distance $\bar{d}$ is valid for all $a > 0$ and $0 \leq c \leq 2$.*

Proof. The spectral theorem for autocorrelation functions (ACF) [97, page 82] states that a given function is the ACF of a complex weakly stationary mean square continuous process in $\mathbb{R}^{\check{D}}$, where $\check{D}$ is a positive integer, if and only if it is the characteristic function (CF) of a certain random variable. Let $h(\check{x}, \check{y})$ refer to a channel coefficient from a given source to an antenna located at position $(\check{x}, \check{y})$. The Rayleigh channel assumptions imply that $\mathrm{E}[h(\check{x}, \check{y})] = 0$ and $\mathrm{E}\left[|h(\check{x}, \check{y})|^2\right] = 1$ for all $(\check{x}, \check{y})$. Furthermore, the ACF is defined as $\mathrm{E}[h(\check{x}_1, \check{y}_1)h^*(\check{x}_2, \check{y}_2)] = \exp\left(-a\bar{d}^c\right)$, where $\bar{d} = \sqrt{(\check{x}_1 - \check{x}_2)^2 + (\check{y}_1 - \check{y}_2)^2}$ is the distance between $(\check{x}_1, \check{y}_1)$ and $(\check{x}_2, \check{y}_2)$, and $(.)^*$ is the conjugate operator. Hence, the process is a weakly stationary two dimensional process. Since the ACF, $\exp\left(-a\bar{d}^c\right)$, is continuous at $\bar{d} = 0$ it follows from [97, page 81] that $h(\check{x}, \check{y})$ is mean square continuous. Hence, $\exp\left(-a\bar{d}^c\right)$ is valid if and only if it is the CF of a certain random variable. A stable random variable with parameters $\alpha\,(0 < \alpha \leq 2), \check{\sigma}\,(\check{\sigma} \geq 0), \check{\beta}\,(-1 \leq \check{\beta} \leq 1), \check{\mu}\,(-\infty < \check{\mu} < \infty)$ is denoted $S_\alpha(\check{\sigma}, \check{\beta}, \check{\mu})$ [98, page 5] and the particular stable variable $S_\alpha(\check{\sigma}, 0, 0)$ has the CF $\varphi(t) = \exp\left(-\check{\sigma}^\alpha |t|^\alpha\right)$ [98, page 9]. Hence, the ACF is the CF of a $S_c(a^{1/c}, 0, 0)$ variable and the ACF is valid for any $c \in (0, 2]$. □

The theorem demonstrates the validity of the Gaussian model (when $c = 2$, the Gauss correlation is the CF of a zero-mean Gaussian variable), the square root model (when $c = \frac{1}{2}$, the Sqrt correlation is the CF of a Levy variable) and the exponential model (when $c = 1$, the Exp correlation is the CF of a Cauchy variable). To understand why the model is invalid for $c > 2$, consider three closely spaced antennas in a ULA with antenna separation $\epsilon > 0$. The

correlation matrix, using $e^{-z} \approx 1 - z$ for small $z > 0$, is given by

$$\begin{aligned} \mathbf{R}_r &= \begin{bmatrix} 1 & e^{-a\epsilon^c} & e^{-a(2\epsilon)^c} \\ e^{-a\epsilon^c} & 1 & e^{-a\epsilon^c} \\ e^{-a(2\epsilon)^c} & e^{-a\epsilon^c} & 1 \end{bmatrix} \\ &\approx \begin{bmatrix} 1 & 1 - a\epsilon^c & 1 - a2^c\epsilon^c \\ 1 - a\epsilon^c & 1 & 1 - a\epsilon^c \\ 1 - a2^c\epsilon^c & 1 - a\epsilon^c & 1 \end{bmatrix}, \end{aligned} \tag{4.3}$$

where we have neglected lower order terms in the approximation. Taking the determinant of both sides of (4.3) and keeping dominant terms gives

$$|\mathbf{R}_r| \approx a^2 2^c \epsilon^{2c} (4 - 2^c). \tag{4.4}$$

From (4.4) we see that $c > 2$ causes $|\mathbf{R}_r|$ to be negative for a small enough spacing and violates the property that $\mathbf{R}_r$ must be positive semi-definite. The result also identifies the order of "roll off" of the correlation function at the origin which is allowable, with the Gaussian model giving the slowest valid decay at small spacings. Specifically, we observe that the correlation at a small spacing, ϵ, can take the form $1 - a\epsilon^c + o(\epsilon^c)$ only for $c \leq 2$ and $a > 0$. Hence, a quadratic roll-off is possible but not a cubic.

4.4 Capacity Metrics

In this chapter, we evaluate the effects of array size and shape through the corresponding effect of correlation on capacity. Hence, in this section we define the necessary capacity metrics.

4.4.1 Ergodic Capacity

As discussed in Section 2.9.3, the ergodic capacity [69, page 36] of the N_t UEs is given by

$$\mathrm{E}[C] = \mathrm{E}[\log_2 \det(\mathbf{I} + \rho\, \mathbf{H}^H \mathbf{H})], \tag{4.5}$$

where ρ is the SNR.

4.4.2 Capacity Outage

As mentioned in Section 2.9.3, the p-percentage outage capacity, C_{out}, is defined as the transmission rate that can be supported by (100-p)% of the fading channel realizations [20, page 9], i.e., $P(C < C_{\mathrm{out}}) = p$ [69, page 36]. For the model in (4.2) the ergodic capacity can be computed using results in [99] but no exact analytical results are known for C_{out}. Due to the complexity of [99] and the need to simulate C_{out}, simulations are used for both metrics.

4.4.3 Ergodic Capacity for Independent Channels

In the absence of correlation, $\mathbf{R}_r = \mathbf{I}$ and (4.5) reduces to

$$\begin{aligned} \mathrm{E}[C] &= \mathrm{E}[\log_2 \det(\mathbf{I} + \rho\, \mathbf{P}^{1/2} \mathbf{U}\mathbf{U}^H \mathbf{P}^{1/2})] && (4.6) \\ &= N_t\, \mathrm{E}[\log_2(1 + \rho \lambda_{\mathrm{arb}}), && (4.7) \end{aligned}$$

where λ_{arb} is an arbitrary (i.e., randomly selected) eigenvalue of $\mathbf{P}^{1/2}\mathbf{U}\mathbf{U}^H\mathbf{P}^{1/2}$ as derived in [100].

4.4.4 Ergodic Capacity for Perfectly Correlated Channels

In the limit, as the channel becomes perfectly correlated ($\mathbf{R}_r \to \mathbf{1}_{N_r \times N_r}$, where $\mathbf{1}_{N_r \times N_r}$ is the $N_r \times N_r$ matrix of ones), the channels from a UE to the antennas become identical and $\mathbf{H}$ has

the representation

$$\mathbf{H} = \mathbf{1}_{N_r \times N_r} \mathbf{U}_D \mathbf{P}^{1/2}, \tag{4.8}$$

where $\mathbf{U}_D$ is a diagonal matrix, $\mathbf{U}_D = \mathrm{diag}(U_1, U_2, \ldots, U_{N_t})$, where U_i is the common channel coefficient for user i. Substituting (4.8) in (2.33) and simplifying gives

$$\begin{aligned}
\mathrm{E}[C] &= \mathrm{E}\left[\log_2 \det(\mathbf{I} + \rho N_r \mathbf{P}^{1/2} \mathbf{U}_D^H \mathbf{1}_{N_r \times N_r} \mathbf{U}_D \mathbf{P}^{1/2})\right] && (4.9)\\
&= \mathrm{E}\left[\log_2(1 + \rho N_r \lambda)\right] && (4.10)\\
&= \mathrm{E}\left[\log_2\left(1 + \rho N_r \mathrm{Tr}\left(\mathbf{P}^{1/2} \mathbf{U}_D^H \mathbf{1}_{N_r \times N_r} \mathbf{U}_D \mathbf{P}^{1/2}\right)\right)\right] && (4.11)\\
&= \mathrm{E}\left[\log_2(1 + \rho N_r \sum_{i=1}^{N_t} P_i |U_i|^2)\right], && (4.12)
\end{aligned}$$

where $\mathrm{Tr}(.)$ is the trace operator. Note that (4.10) follows from (4.9) since $\mathbf{1}_{N_r \times N_r}$ is rank 1 and λ is the single non-zero eigenvalue of $\mathbf{P}^{1/2} \mathbf{U}_D^H \mathbf{1}_{N_r \times N_r} \mathbf{U}_D \mathbf{P}^{1/2}$. Similarly, (4.11) follows from (4.10) since $\mathrm{Tr}\left(\mathbf{P}^{1/2} \mathbf{U}_D^H \mathbf{1}_{N_r \times N_r} \mathbf{U}_D \mathbf{P}^{1/2}\right) = \lambda$. From (4.7) and (4.12), we observe that $\mathrm{E}[C]$ tends to grow linearly in the uncorrelated case with N_t whereas the growth is logarithmic in the perfectly correlated case. This difference is more noticeable for MM than for traditional MIMO and so the effects of correlation can be large. Furthermore, the effect of the $\mathbf{P}$ matrix can be inferred from (4.7) and (4.12). Large powers will clearly boost capacity. In contrast, increasing the spread of the powers tends to increase the variability of both λ_{arb} and $\sum_{i=1}^{N_t} P_i |U_i|^2$. The logarithm then penalizes the increased lower tail and the capacity tends to be reduced.

4.5 Results

In this section, we evaluate the performance of SQs and ULAs with different correlation models using ergodic capacity or 10% capacity outage. The system size is $N_r = 100$, $N_t = 10$ and the link gains are defined by $\mathcal{A} = 1$, $\beta \in \{0.1, 0.9\}$. The scale factor $\mathcal{A}$, is unity without loss of generality and $\beta = 0.1$, $\beta = 0.9$ correspond to a dominant UE and several similar strength

UEs, respectively. For most of the results, we assume $\rho = 0$ dB. Since SNR is essentially just a scaling factor, the trends discussed for $\rho = 0$ dB remain valid at other SNR values and this is supported by simulations at the end of the section. In order to compare the two arrays, the length of the ULA, (b_{ULA}), is given by $b_{\mathrm{ULA}} = 1$ without loss of generality. The SQ has width b_{SQ} expressed as a fraction of $b_{\mathrm{ULA}} = 1$, e.g., $b_{\mathrm{SQ}} = 0.3\, b_{\mathrm{ULA}}$. Varying levels of correlation are introduced by defining R_{target} as the correlation between the first and last ULA antennas, i.e., at separation 1. Varying R_{target} creates lightly or heavily correlated channels and a fixed value of R_{target} gives the value of μ required to define the four correlation models in Section 4.2.

In Figure 4.1, we show ergodic capacity and the 10% capacity outage vs R_{target} for the Jakes model with $\beta = 0.9$. Results are shown for a ULA with $b_{\mathrm{ULA}} = 1$ and a SQ with 30% ($b_{\mathrm{SQ}} = 0.3\, b_{\mathrm{ULA}}$) and 50% ($b_{\mathrm{SQ}} = 0.5\, b_{\mathrm{ULA}}$) of the width of the ULA. We observe that the ULA performs similarly to a SQ of 30% the width whereas 50% width gives a noticeable capacity improvement. Due to the stability of MM, the capacity distribution is not highly variable and the C_{out} results are simply a slightly shifted version of the ergodic capacity results. Since no further insights are found from C_{out}, we restrict the following results to ergodic capacity.

Figures 4.2 and 4.3 show mean capacity vs R_{target} for the Jakes and Gauss models. A comparison of Figure 4.2 and Figure 4.3 shows the obvious effect that ergodic capacity increases with β since the link gains grow with β. The results also show that ULA performance is usually bracketed by $b_{\mathrm{SQ}} = 0.3\, b_{\mathrm{ULA}}$ and $b_{\mathrm{SQ}} = 0.5\, b_{\mathrm{ULA}}$ and that a larger SQ is needed for $\beta = 0.1$ compared to $\beta = 0.9$.

Figures 4.4 and 4.5 repeat the results of Figures 4.2 and 4.3 for the Sqrt and Exp models. A comparison of Figures 4.2 and 4.3 with Figures 4.4 and 4.5 shows that the Jakes and Gauss models are more sensitive to correlation than Exp and Sqrt. This is shown by the substantial variation in capacity between the three SQs of varying widths. This difference is caused by the slow, quadratic roll-off of the correlation at small distances provided by Jakes and Gauss. Note

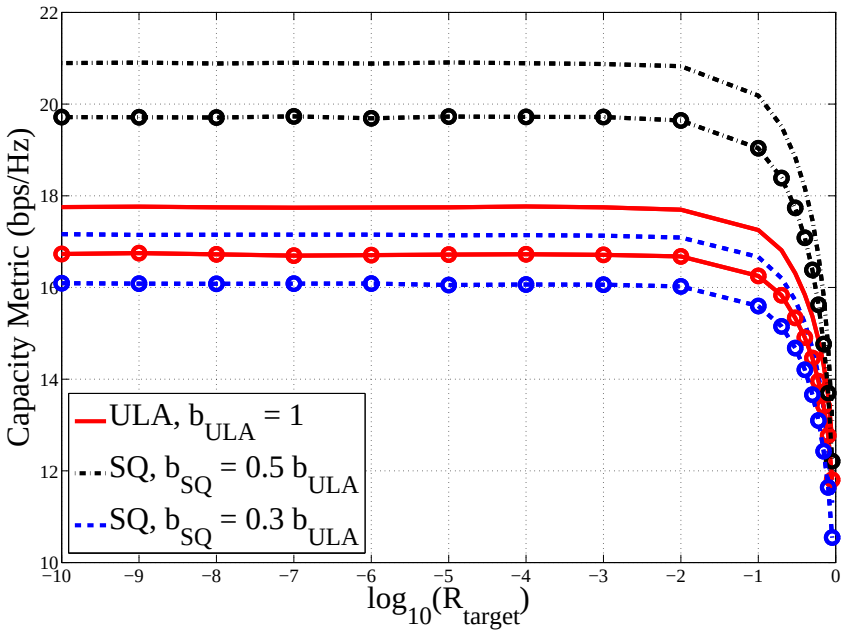

Figure 4.1: Capacity metrics vs R_{target} for the Jakes model. The metrics are mean capacity (given by lines) and C_{out} with p =10% (given by lines with points). $\beta = 0.9$.

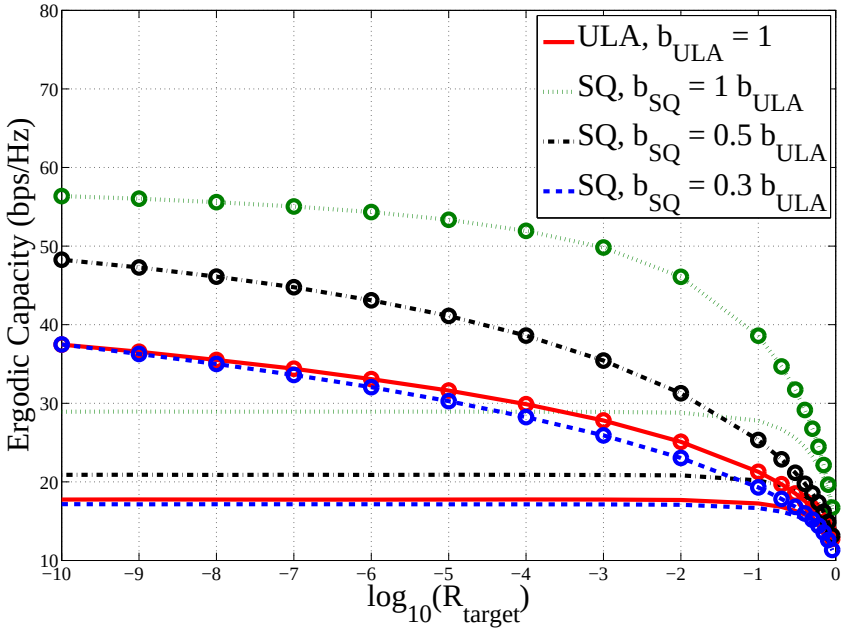

Figure 4.2: Ergodic capacity vs R_{target} for Jakes (lines only) and Gauss (lines with points) models. $\beta = 0.9$.

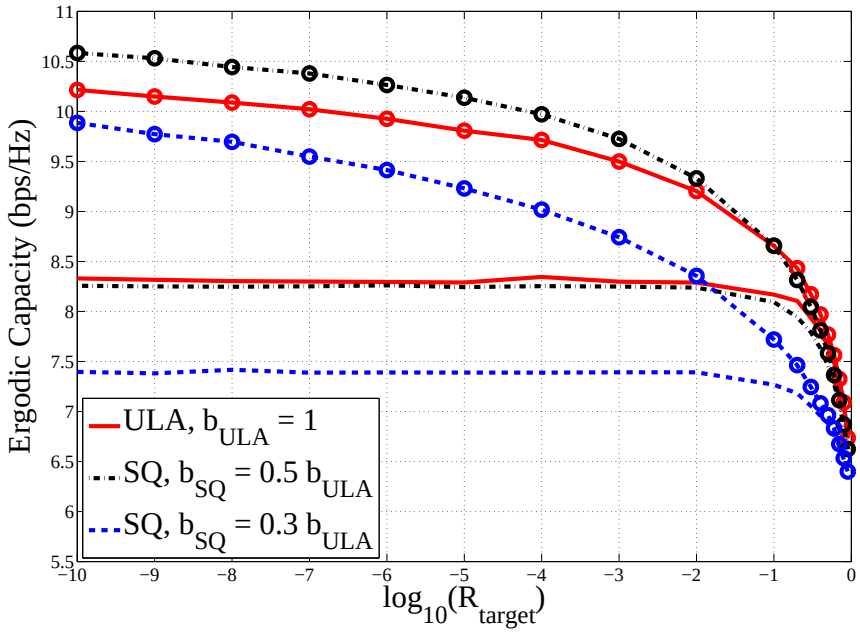

Figure 4.3: Ergodic capacity vs R_{target} for Jakes (lines only) and Gauss (lines with points) models. $\beta = 0.1$.

that the Sqrt and Exp models give lower correlation and this is why the observed capacity is higher.

Also shown in Figures 4.4-4.5 is the convergence of ergodic capacity to the Independent case, shown explicitly in Figure 4.5, which gives the plateau to the left of the figures as R_{target} becomes small. The Independent and Full Corr. results in Figure 4.5 are computed using (4.6) and (4.9) and show the potential variation in ergodic capacity as well as the extreme limits. Note that the Independent limit is approached faster by the Sqrt and Exp models as they decay more quickly. The Jakes model alone does not converge to the Independent limit since $J_0(2\pi\mu d_{ij})$ is not monotonic in d_{ij}. Hence, equating the Bessel function to R_{target} at $d_{ij} = 1$ does not provide small correlations as $R_{\text{target}} \to 0$ since the first lobe of the Bessel function does not diminish. An overview of Figures 4.1-4.5 shows that ULA performance is achieved for $b_{\text{SQ}} \in (0.3\, b_{\text{ULA}}, 0.5\, b_{\text{ULA}})$ for virtually all cases. Factors which tend to require a larger

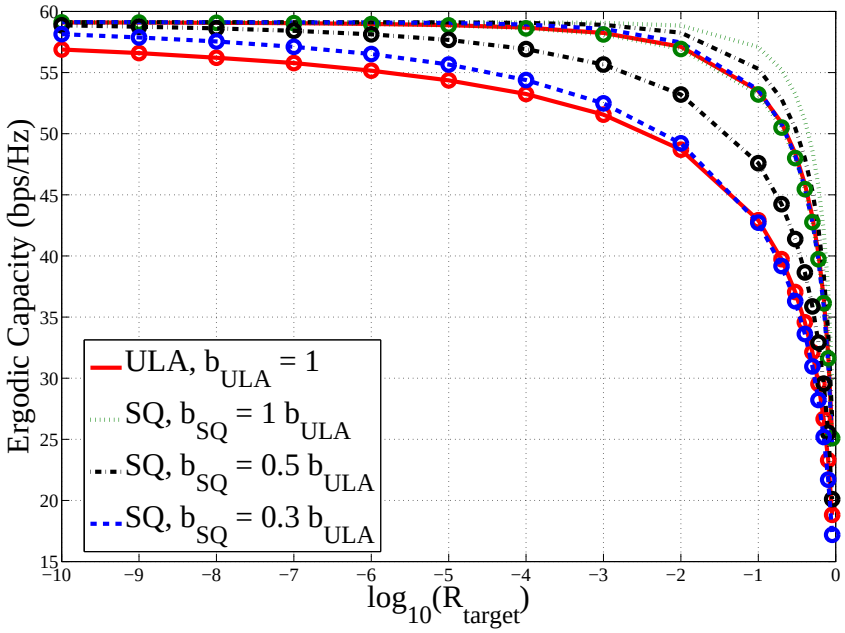

Figure 4.4: Ergodic capacity vs R_{target} for Sqrt (lines only) and Exp (lines with points) models. $\beta = 0.9$.

equivalent SQ are higher correlation and slowly decaying correlation.

Figures 4.1-4.5 also show that the benefits of SQs are dependent on the correlation models. For models with a quadratic roll-off (Jakes and Gauss) the high correlations at small spacing impact strongly on ULAs and a substantial capacity improvement is possible using SQs. For example, in Figure 4.2, 50% improvements are possible (comparing $b_{\text{ULA}} = 1$ with $b_{\text{SQ}} = 1b_{\text{ULA}}$). In contrast, for Sqrt and Exp the capacity improvements are much smaller. This contrasts to the space saving benefits which are between 30% and 50% for all correlation types.

For different values of ρ and different system sizes, the results remain similar, but the effects of correlation are more prominent as the ratio N_t/N_r increases. Figures 4.6 and 4.7 support this conclusion. In both figures we use the Exp model. In Figure 4.6 we vary $\rho \in \{-10, 0, 10\}$ dB and select $N_r = 100, N_t = 10$. In Figure 4.7 we fix ρ at 0 dB, and vary $N_r \in \{100, 200\}$ and $N_t \in \{10, 20, 40\}$.

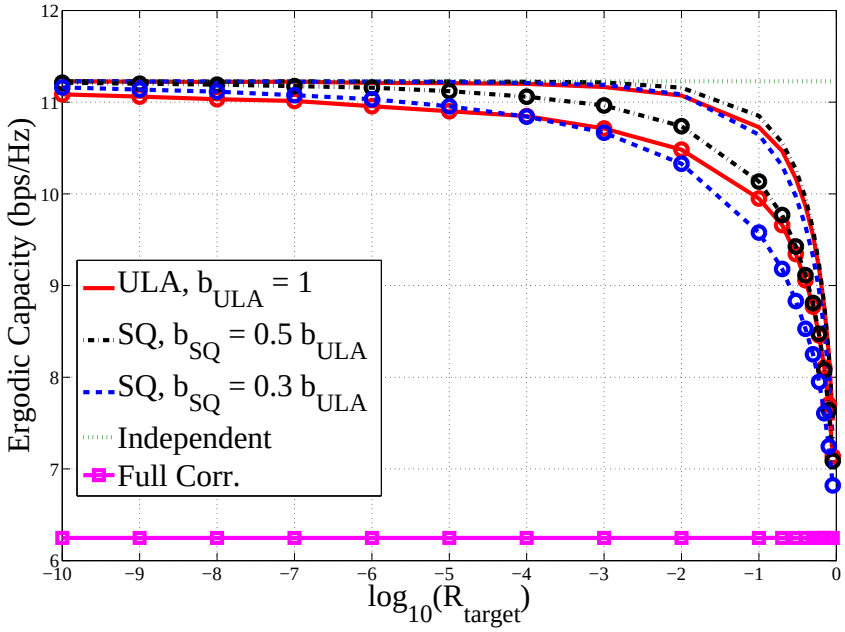

Figure 4.5: Ergodic capacity vs R_{target} for Sqrt (lines only) and Exp (lines with points) models. $\beta = 0.1$.

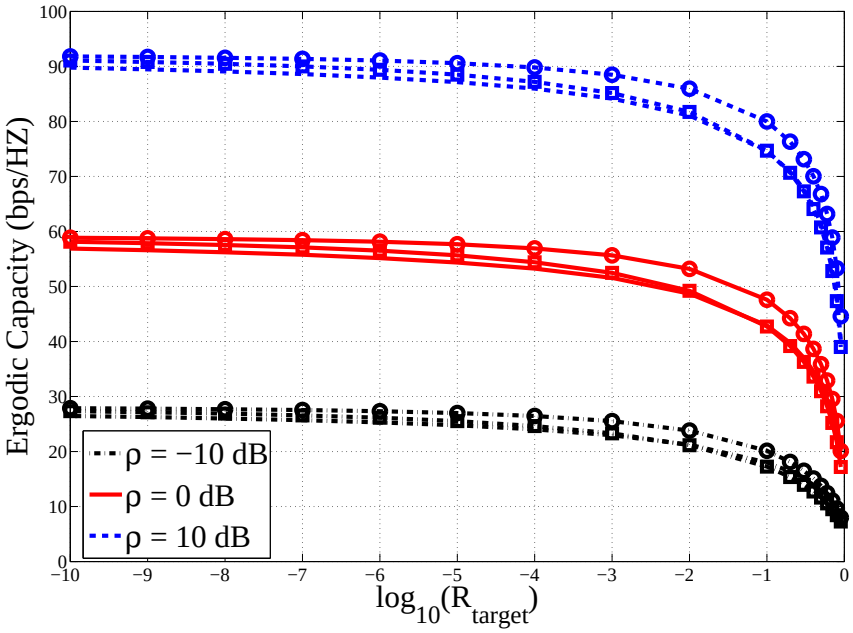

Figure 4.6: Ergodic capacity vs R_{target} for Sqrt (lines only) and Exp (lines with points) models. $\beta = 0.9$.

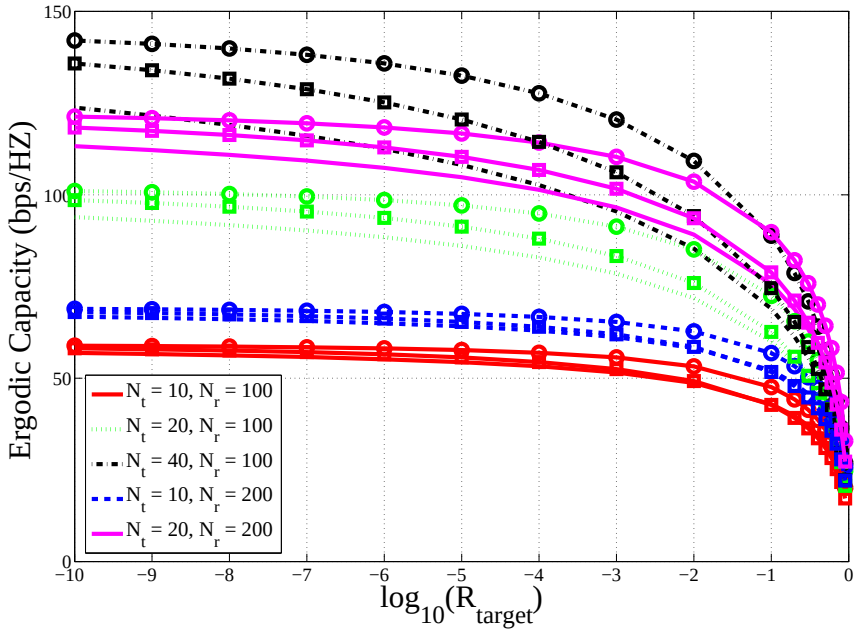

Figure 4.7: Ergodic capacity vs R_{target} for Sqrt (lines only) and Exp (lines with points) models. $\beta = 0.9$.

4.6 Summary

In this chapter, we have analytically justified a range of correlation models that have previously been used in the literature without verification. This analysis has also shown that correlation models must decay away from unity at zero separation with a power law behavior where the power is at most quadratic. Powers greater than two are invalid and so a quadratic roll-off is the slowest possible. Models such as Gaussian and Jakes which are quadratic near the origin are therefore extreme cases. This observation is closely tied to the differences between SQs and ULAs. We have shown that the capacity benefits of SQs are highly dependent on the correlation models. When the spatial correlation decays very slowly at the origin, then SQs offer substantial benefits in capacity. However, for more rapidly decaying correlations, the space savings offered by SQs are more important.

Chapter V

Performance of Traditional V-BLAST Based on Optimal Ordering

5.1 Introduction

The purpose of this chapter is to benchmark the performance of the traditional V-BLAST algorithm and take the first step towards simplification by substituting the ZF detector with the MRC detector. The effect of imperfect CSI is also investigated.

As shown in Section 2.8, the system performance of MM strongly depends on the accuracy of the CSI [7]. With imperfect channel estimation, the system performance can degrade severely due to pilot contamination [7] and latency effects [1]. Also, if the large arrays are located within a small area, then the channel correlations may become quite high, impacting system performance [7]. Finally, simple processing is very important for MM. Hence, our focus is to study a low complexity, MRC-based MM receiver with imperfect CSI and channel correlation.

We consider an uplink MM deployment of Section 2.7, with a co-located BS array and distributed single antenna UEs. Several studies which consider channel estimation and correlated channels have appeared in [101, 102] for traditional MIMO and in [96, 103] for MM. One of the most popular schemes in traditional MIMO is the V-BLAST approach, which is discussed in Section 2.8.2. Most of the work on traditional V-BLAST discusses ZF or MMSE combining and rarely considers MRC [44]. Also, very little work has appeared on V-BLAST with MM

probably because of the complexity of V-BLAST with large numbers of antennas. In this Chapter, we begin the development of a low-complexity version of V-BLAST which is suitable for MM. The baseline receiver is ZF V-BLAST and in this chapter we integrate V-BLAST with MRC in MM which gives similar performance to ZF V-BLAST with reduced complexity. This motivates our work to propose an improved low complexity MRC V-BLAST receiver design based on the channel norms in Chapter 6 and then simplify it further using link gain ordering as shown in Chapter 8.

Hence, in this chapter, we contribute as follows. We integrate MRC with V-BLAST for MM and compare its performance with ZF with V-BLAST. This work considers realistic MM scenarios with correlated channels and imperfect CSI. Furthermore, our results show that MRC with V-BLAST can approach the performance of ZF with V-BLAST in a MM context. In addition, following on from the work in Chapter 4, we provide analytical results which define the antenna spacings required for ULAs and SQs in order to obtain similar performance with MRC V-BLAST and ZF V-BLAST. For example, the SQ is dimensioned so that it gives a similar performance to the ULA with MRC V-BLAST and ZF V-BLAST. Note that we do not provide the closed-form results for the SER for this receiver because this is an intermediate receiver. However, for the final receiver which is discussed in Chapter 8, we provided the close-form results for the SER.

The rest of Chapter 5 is organized as follows. Section 5.2 introduces the system model while Section 5.3 describes the MM deployment and the channel model. Section 5.4 illustrates V-BLAST with optimal ordering. We provide analysis in Section 5.5, give simulation results in Section 5.6, and conclude in Section 5.7.

5.2 System Model

We consider the system model in Section 2.7, where the uplink received signal is

$$\mathbf{y} = \mathbf{H}\mathbf{x} + \mathbf{n} = \sum_{j=1}^{N_t} \mathbf{h}_j x_j + \mathbf{n}, \tag{5.1}$$

and $\mathbf{H}$, $\mathbf{x}$ and $\mathbf{n}$ are the channel, signal vector and noise, respectively. Also, we assume the imperfect CSI model described in Section 2.6.9 where

$$\hat{\mathbf{H}} = r_0\mathbf{H} + \sqrt{1 - r_0^2}\mathbf{E}, \tag{5.2}$$

and the SINR can be calculated as in (2.31).

5.3 Deployment and Channel Model

Assume a large co-located array at the BS serving N_t UEs in the coverage region. The correlated channel model and link gains can be calculated as given in Section 2.6.7 where

$$\mathbf{H} = \mathbf{R}_r^{\frac{1}{2}}\mathbf{U}\mathbf{P}^{\frac{1}{2}}, \tag{5.3}$$

$\mathbf{P} = \mathrm{diag}(P_1, P_2, \ldots, P_{N_t})$ and $P_j = \mathcal{A}\beta^{j-1}$ are the link gains. We use this simple model for the link gains in order to control the P_j's with a single parameter, β, which has a physical interpretation. Moreover, this model is useful because of the importance of the link gain decay rate in V-BLAST, where it is well-known that performance is heavily dependent on the differences between the link gains. $\mathbf{R}_r$ is the channel correlation matrix at the receiver. In the following, we provide two simple models for the correlation matrix, depending on the type of array used at the receiver.

5.3.1 Case 1: Uniform Linear Array (ULA)

Let $\mathbf{R}_r = (R_{ij})$, then the element R_{ij} is defined by $R_{ij} = \alpha_u^{|i-j|}$, where α_u is the correlation between channels at adjacent antennas and $0 < \alpha_u < 1$. This is the simple exponential correlation model given in [58].

5.3.2 Case 2 : Uniform Square Array (SQ)

Here, we assume a regularly spaced uniform square array and the element R_{ij} is defined by $R_{ij} = \alpha_s^{d_{ij}}$, where α_s is a correlation parameter and d_{ij} is the distance between the i^{th} and j^{th} antenna. To make the models comparable and ensure the correlation at a fixed separation is identical, we select $\alpha_s = \alpha_u^{1/\Delta}$, where Δ is the distance between adjacent antennas.

5.4 V-BLAST with Optimal Ordering

The two major computational bottlenecks in the V-BLAST algorithm are ordering for the nulling and cancellation process and matrix inverse computations for the receiver weights. The classic approach to ordering the streams for detection in V-BLAST is to detect the stream with the highest output SINR first [66]. From [66], let the ordered set $S = \{k_1, k_2, \ldots, k_{N_t}\}$ be a permutation of the integers 1, 2, ..., N_t specifying the order in which the transmitted symbols in $\mathbf{x}$ are extracted. In the optimal approach, the index k_i is chosen such that the SINR/SNR of the detected symbol at the i^{th} stage is maximized.

In order to define the optimal V-BLAST approach, we require the following notation. Let $\mathbf{H}_i$ represent $\mathbf{H}$ with columns $k_1, k_2, \ldots, k_{i-1}$ replaced by zeros and let $\mathbf{W}_i$ be given by $\mathbf{H}_i$ for MRC, $\mathbf{H}_i(\mathbf{H}_i^H\mathbf{H}_i)^{-1}$ for ZF. With this notation, MRC V-BLAST is based on (2.30). The SINR for user m at the i^{th} stage is given by (2.26), where the summation in the denominator of (2.26)

is over $j \notin \{k_1, k_2, \ldots, k_{i-1}\}$ such that $j \neq m$. Maximizing the SINR at stage i gives

$$k_i^{(\mathrm{MRC})} = \underset{m \notin \{k_1, k_2, \ldots, k_{i-1}\}}{\arg\max} \mathrm{SINR}_m^{(\mathrm{MRC})}. \tag{5.4}$$

The optimal ordering for ZF is defined by [66]

$$k_i^{(\mathrm{ZF})} = \underset{j \notin \{k_1, k_2, \ldots, k_{i-1}\}}{\arg\min} ||(\mathbf{W}_i)_j||^2, \tag{5.5}$$

where $(\mathbf{W}_i)_j$ represents column j of $\mathbf{W}_i$, the ZF combiner at stage i.

5.5 Analysis

5.5.1 Analysis of Imperfect CSI

In this section, we analyze the effects of imperfect CSI to see if MRC V-BLAST and ZF V-BLAST can have similar performance. Consider stage $m+1$ of V-BLAST detection where the symbols $x_{k_1}, x_{k_2}, \ldots, x_{k_m}$ have already been detected and assume that all m symbols in the previous stages are detected correctly. This assumption is used to simplify the analysis and to obtain insights into the effects of imperfect CSI.

In the subsequent simulations in Section 5.6, the full V-BLAST procedure is used and error propagation [104] may occur. The remaining UEs have link gains $P_{k_{m+1}}, P_{k_{m+2}}, \ldots, P_{k_{N_t}}$ which are denoted $P_{(m+1)}, P_{(m+2)}, \ldots, P_{(N_t)}$. Similarly, $P_{(1)}, P_{(2)}, \ldots, P_{(m)}$ are the link gains of UEs $k_1, k_2, \ldots, k_m$. Consider the noise inflation which occurs in V-BLAST with imperfect CSI in both the detection and cancellation stages. The noise inflation is defined as the difference in noise power between the imperfect CSI case and the perfect CSI case.

Detection Stage

During detection, the extra noise term due to imperfect CSI is given by $\sqrt{1-r_0^2}\mathbf{E}\mathbf{x}$. The covariance matrix of the extra noise is given by

$$\mathrm{E}\Big[(1-r_0^2)\mathbf{E}\mathbf{x}\mathbf{x}^H\mathbf{E}^H\Big] = (1-r_0^2)\mathrm{E}\left[\mathbf{E}\mathbf{E}^H\right]. \tag{5.6}$$

Since $\mathbf{E}$ has the same statistics as $\mathbf{H}$ in (5.3), it follows that

$$\begin{aligned}\mathrm{E}\Big[\mathbf{E}\mathbf{E}^H\Big] &= \mathrm{E}\left[\mathbf{R}_r^{1/2}\mathbf{U}\mathbf{P}\mathbf{U}^H\mathbf{R}_r^{1/2}\right] \\ &= \mathrm{tr}(\mathbf{P})\mathbf{R}_r. \end{aligned}\tag{5.7}$$

Hence, the power of the extra noise on each antenna is $\mathrm{tr}(\mathbf{P})$ as $(\mathbf{R}_r)_{ii} = 1$. Since the detection is at stage $m+1$, $\mathbf{E}$, $\mathbf{x}$,$\mathbf{U}$, $\mathbf{P}$ and $\mathbf{R}_r$ contain information about UEs $m+1$, $m+2, \ldots, N_t$. Therefore, the noise inflation for a ZF combiner is calculated as

$$(1-r_0^2)\sum_{j=m+1}^{N_t} P_{(j)}. \tag{5.8}$$

For an MRC receiver, adapting the result in [105], the noise inflation during detection is $(1-r_0^2)P_{(m+1)}$.

Cancellation Stage

The signal to be detected at stage $m+1$ is x_{m+1} and the corresponding received signal is

$$\mathbf{y}^{(m+1)} = \sum_{j=m+1}^{N_t} \mathbf{h}_{k_j} x_{k_j} + \mathbf{n}^{(m)}, \tag{5.9}$$

where $\mathbf{n}^{(m)} = \mathbf{n} + (\mathbf{h}_{k_1} - \hat{\mathbf{h}}_{k_1})x_{k_1} + \cdots + (\mathbf{h}_{k_m} - \hat{\mathbf{h}}_{k_m})x_{k_m}$ and $\mathbf{h}_j = r_0\hat{\mathbf{h}_j} + \sqrt{1-r_0^2}\mathbf{e}_j$, where $\mathbf{e}_j$ is the j^{th} column of $\mathbf{E}$. The definition of $\mathbf{n}^{(m)}$ uses the assumption that $\hat{x}_{k_j} = x_{k_j}$ for $j = 1, 2, \ldots, m$. Substituting for $\mathbf{h}_j$ in $\mathbf{n}^{(m)}$ gives

$$\begin{aligned}\mathbf{n}^{(m)} &= \mathbf{n} + \sum_{j=1}^{m}((r_0-1)\hat{\mathbf{h}}_{k_j} + \sqrt{1-r_0^2}\mathbf{e}_{k_j})x_{k_j} \\ &= (r_0-1)\sum_{j=1}^{m}\hat{\mathbf{h}}_{k_j}x_{k_j} + \mathbf{n} + \sqrt{1-r_0^2}\sum_{j=1}^{m}\mathbf{e}_{k_j}x_{k_j}.\end{aligned}$$

The covariance matrix of $\mathbf{n}^{(m)}$, denoted $\Sigma^{(\mathrm{m})}$, is given by

$$\begin{aligned}\Sigma^{(\mathrm{m})} &= (r_0-1)^2\mathrm{E}[\sum_{j=1}^{m}\hat{\mathbf{h}}_{k_j}x_{k_j}\sum_{j=1}^{m}x_{k_j}^H\hat{\mathbf{h}}_{k_j}^H] \\ &+ \mathrm{E}[\mathbf{n}\mathbf{n}^H] + (1-r_0^2)\mathrm{E}[\sum_{j=1}^{m}\mathbf{e}_{k_j}x_{k_j}\sum_{j=1}^{m}x_{k_j}^H\mathbf{e}_{k_j}^H] \\ &= (r_0-1)^2\sum_{j=1}^{m}\hat{\mathbf{h}}_{k_j}\hat{\mathbf{h}}_{k_j}^H + \sigma^2\mathbf{I} + (1-r_0^2)\sum_{j=1}^{m}P_{(j)}\mathbf{R}_r. \qquad (5.10)\end{aligned}$$

In (5.10), we have used $\mathrm{E}[\mathbf{e}_j\mathbf{e}_j^H] = P_{(j)}\mathbf{R}_r$ since $\mathbf{e}_j$ has the same statistics as $\mathbf{h}_j$. Taking the $(1,1)^{\text{th}}$ element of (5.10) gives the equivalent noise at stage $m+1$ as

$$(r_0-1)^2\sum_{j=1}^{m}|\hat{h}_{k_j1}|^2 + \sigma^2 + (1-r_0^2)\sum_{j=1}^{m}P_{(j)}, \qquad (5.11)$$

where $\hat{h}_{k_j1}$ is the first element of $\hat{h}_{k_j}$. Hence, the noise inflation due to cancellation is

$$(r_0-1)^2\sum_{j=1}^{m}|\hat{h}_{k_j1}|^2 + (1-r_0^2)\sum_{j=1}^{m}P_{(j)}. \qquad (5.12)$$

Overall Noise Inflation

Combining the noise inflation due to cancellation in (5.12) with the noise inflation during detection ($(1-r_0^2)P_{(m+1)}$ for MRC and $(1-r_0^2)\sum_{j=m+1}^{N_t}P_{(j)}$ for ZF) gives the overall noise inflation

results:

$$\text{MRC} : (r_0 - 1)^2 \sum_{j=1}^{m} |\hat{h}_{k_j 1}|^2 + (1 - r_0^2) \sum_{j=1}^{m+1} P_{(j)},$$
$$\text{ZF} : (r_0 - 1)^2 \sum_{j=1}^{m} |\hat{h}_{k_j 1}|^2 + (1 - r_0^2) \sum_{j=1}^{N_t} P_{(j)}.$$

Hence, imperfect CSI has a greater effect on ZF which suffers from a noise inflation at stage $m+1$ which is greater than MRC by $(1-r_0^2) \sum_{j=m+2}^{N_t} P_{(j)}$. A similar analysis was given in [106], but the simple form of (5.12) was not given.

The analysis shows that ZF is affected more by imperfect CSI and that the difference is weighted by the total remaining link gain, i.e., $\sum_{j=m+2}^{N_t} P_{(j)}$. When the $P_{(j)}$ terms are small, then the difference is small and the effect on ZF and MRC will be similar. When the $P_{(j)}$ terms are large then there is a larger difference in the effect of imperfect CSI. However, when the $P_{(j)}$ terms are large the SERs are likely to be small and will not contribute greatly to the overall V-BLAST SER.

For example, in Figure 5.2 with $\beta = 0.5$, the SERs were also calculated for each layer. In the first few layers as shown in Figure 5.3, where strong UEs are present, the $P_{(j)}$ terms are large but the SERs are low (below 10^{-3} for SNR $\leq$ 0 dB). Hence, the overall SER (approximately 2×10^{-1} at SNR = 0 dB) is not affected by these results. In contrast, in the later stages, the SERs are dominant (See Figure 5.3) and here the $P_{(j)}$ terms are much smaller. Note that the ZF and MRC results are indistinguishable. Overall, the analysis suggests that the effects of imperfect CSI are likely to be similar for ZF and MRC and this is supported by the simulations in Section 5.6. This is also supported in related work [26] where the asymptotic performance of MMSE and MRC receivers is shown to be equivalent (and ZF behaves similarly to MMSE [107]).

5.5.2 *Analysis of Correlation*

When comparing a ULA with a SQ, the SQ will suffer if the antenna spacing is held constant as there are many more near-neighbors in a square layout. Hence, it is of interest in a MM context to investigate SQ and ULA dimensions which lead to similar levels of correlations. To avoid relying on any particular correlation model, we define a ULA and a SQ to be "equivalent" if the median inter-element spacing is identical. Furthermore, since closed form results for median spacing in a SQ appear to be intractable, we employ a continuous approximation to the problem where the antenna locations are uniformly located on a line segment of length b_{ULA}, uniform on $[0, b_{\mathrm{ULA}}]$ for ULA, and on a square of width b_{SQ} uniform on $[0, b_{\mathrm{SQ}}] \times [0, b_{\mathrm{SQ}}]$ for SQ. The continuous approximation is particularly appealing for MM where a large number of antennas are considered.

For the ULA a random inter-element spacing can be given as $Z_{\mathrm{ULA}} = |X_1 - X_2|$, where X_1 and X_2 are i.i.d. uniform variables on $[0, b_{\mathrm{ULA}}]$. The CDF of Z_{ULA} is well-known as $X_1 - X_2$ is triangular. Using standard transformation theory [108, page 136 and 137] the CDF of Z_{ULA} is given by

$$F_{Z_{\mathrm{ULA}}}(z) = 2b_{\mathrm{ULA}}^{-2}(b_{\mathrm{ULA}} z - z^2/2), \quad 0 \leq z \leq b_{\mathrm{ULA}}. \tag{5.13}$$

For the SQ case, the inter-element spacing is defined by $Z_{\mathrm{SQ}} = \sqrt{(X_1 - X_2)^2 + (Y_1 - Y_2)^2}$, where X_1, X_2, Y_1 and Y_2 are i.i.d. uniform variables on $[0, b_{\mathrm{SQ}}]$. Using standard transformation theory [108, page 86-142 and 135-142], we obtain the CDF of Z_{SQ} as

$$F_{Z_{\mathrm{SQ}}}(z) = b_{\mathrm{SQ}}^{-4}(\pi b_{\mathrm{SQ}}^2 z^2 - \tfrac{8}{3} b_{SQ} z^3 + \tfrac{z^4}{2}), \quad 0 \leq z \leq b_{\mathrm{SQ}}. \tag{5.14}$$

To find the medians $(m_{\mathrm{ULA}}, m_{\mathrm{SQ}})$, solve $F_{Z_{\mathrm{ULA}}}(m_{\mathrm{ULA}}) = \frac{1}{2}$ using (5.13) and solve $F_{Z_{\mathrm{SQ}}}(m_{\mathrm{ULA}}) =$

$\frac{1}{2}$ using (5.14), giving

$$m_{\mathrm{ULA}} = (1 - \frac{\sqrt{2}}{2}) b_{\mathrm{ULA}}, \tag{5.15}$$

$$m_{\mathrm{SQ}} = 0.512\, b_{\mathrm{SQ}}. \tag{5.16}$$

To match the median spacing, $m_{\mathrm{ULA}} = m_{\mathrm{SQ}}$ and we obtain

$$b_{\mathrm{SQ}} = \frac{1 - \frac{\sqrt{2}}{2}}{0.512} b_{\mathrm{ULA}} = 0.572 b_{\mathrm{ULA}}. \tag{5.17}$$

This suggests that in order for a SQ to have a similar level of correlation as a ULA, the width of the square should be around 57% of the length of the ULA. We denote approach as "Adjusted SQ" in Figure 5.8. A SQ with the same antenna spacing as the ULA has a width of approximately 9% of the ULA length. This preliminary observation has some impact on MM design as the SQ is not as compact as might be hoped in comparison to a ULA. The usefulness of this result is also demonstrated in Section 5.6.

5.5.3 Complexity Calculation

A simple way to assess the computational complexity of V-BLAST with ZF and MRC is via the number of complex multiplications. In ZF V-BLAST, at stage 1, computing $\mathbf{H}^H\mathbf{H}$ requires $\frac{N_r N_t(N_t+1)}{2}$ multiplications and the inverse computation requires $\frac{N_t^3}{2} + \frac{3}{2}N_t^2$ multiplications based on [109]. Multiplying $(\mathbf{H}^H\mathbf{H})^{-1}$ with $\mathbf{H}^H$ requires $N_t^2 N_r$ multiplications. The ordering involves the $N_t N_r$ multiplications required to compute the column norms of the ZF combiner. Computing $\mathbf{w}_i^H\mathbf{y}$ and $\mathbf{w}_i\hat{x}_i$ both require N_r multiplications. Thus, stage 1 requires $\frac{N_r N_t(N_t+1)}{2} + \frac{N_t^3}{2} + \frac{3}{2}N_t^2 + N_t^2 N_r + N_t N_r + 2N_r$ multiplications. Similarly, stage 2 requires $\frac{N_r(N_t-1)(N_t-1+1)}{2} + \frac{(N_t-1)^3}{2} + \frac{3}{2}(N_t-1)^2 + (N_t-1)^2 N_r + N_t N_r + 2N_r$ multiplications which is simply obtained by replacing N_t by $N_t - 1$. Similarly, stage 3 requires

$\frac{N_r(N_t-2)(N_t-2+1)}{2} + \frac{(N_t-2)^3}{2} + \frac{3}{2}(N_t-2)^2 + (N_t-2)^2 N_r + N_t N_r + 2N_r$ multiplications where $N_t - 1$ is replaced by $N_t - 2$. Combining the $N_t - 1$ stages and considering the final stage which requires detection but no cancellation, ie. N_r multiplications, ZF V-BLAST requires $\frac{N_r \sum_{i=0}^{N_t-2}(N_t-i)(N_t-i+1)}{2} + \frac{\sum_{i=0}^{N_t-2}(N_t-i)^3}{2} + \frac{3}{2}\sum_{i=0}^{N_t-2}(N_t-i)^2 + \sum_{i=0}^{N_t-2}(N_t-i)^2 N_r + (N_t N_r + 2N_r)(N_t-1) + N_r$ multiplications. Since $N_r \gg N_t$, the term $\sum_{i=0}^{N_t-2}(N_t-i)^2 N_r$, which is equivalent to $\frac{N_r \sum_{i=0}^{N_t-2}(N_t-i)(N_t-i+1)}{2}$ in term of complexity order, is dominant and larger than $\frac{\sum_{i=0}^{N_t-2}(N_t-i)^3}{2}$. By using the fact that $\sum_{k=1}^{n} k^2 = \frac{n(n+1)(2n+1)}{6}$, the total complexity of ZF V-BLAST based on the dominant term becomes $O(N_r N_t^3)$.

In MRC V-BLAST, at stage 1, computing $\mathbf{h}_m^H \mathbf{h}_m$ requires N_r multiplications and squaring the term requires 1 multiply. Computing $\mathbf{h}_m^H \mathbf{h}_j \mathbf{h}_j^H \mathbf{h}_m$, requires $N_r + N_r + 1$ multiplications and the sum, $\sum_{j \neq m} \mathbf{h}_m^H \mathbf{h}_j \mathbf{h}_j^H \mathbf{h}_m$, requires $N_t - 1$ of such terms. Thus the total number of multiplications for ordering the SINR in stage 1 is $(N_t - 1)(2N_r + 1)$. Computing $\mathbf{h}_i^H \mathbf{y}$ and $\mathbf{h}_i \hat{x_i}$ both require N_r multiplications. Thus, stage 1 requires $(N_r + 1) + (N_t - 1)(2N_r + 1) + N_r + N_r + N_r$ multiplications. Similarly, stage 2 requires $(N_r + 1) + (N_t - 2)(2N_r + 1) + N_r + N_r + N_r$ multiplications and stage 3 requires $(N_r + 1) + (N_t - 3)(2N_r + 1) + N_r + N_r + N_r$ multiplications. As before, note that N_t is reduced by 1 at each stage. Combining the $N_t - 1$ stages and considering the final stage which requires detection but no cancellation, ie. N_r multiplications, MRC V-BLAST requires $(N_r + 1)(N_t - 1) + \sum_{i=1}^{N_t-1}(N_t - i)(2N_r + 1) + (N_r + N_r + N_r)(N_t - 1) + N_r$ multiplications. The dominant term is $\sum_{i=1}^{N_t-1}(N_t - i)(2N_r + 1) = (2N_r + 1)(N_t - 1 + N_t - 2 + \cdots + 1)$. By using the fact that $\sum_{i=1}^{k} i = 1 + 2 + \cdots + k = \frac{k(k+1)}{2}$, the total number of multiplications is $(N_t - 1)(4N_r + 1) + N_r + \frac{(2N_r+1)(N_t-1)N_t}{2}$. Thus, the total complexity of MRC V-BLAST based on the dominant term becomes $O(N_r N_t^2)$. As expected, the MRC V-BLAST complexity is less than ZF V-BLAST by an order of magnitude.

Table 5.1 summarizes the order of complexity calculations for ZF V-BLAST and MRC V-BLAST.

Table 5.1: Complexity calculations

Technique	**Complexity order of complex multipliers**
ZF V-BLAST	$O(N_r N_t^3)$
MRC V-BLAST	$O(N_r N_t^2)$

5.6 Results

In this section, we consider the performance of MM receivers with imperfect CSI and correlated channels using Monte Carlo simulations. Performance is measured by the SER assuming QPSK modulation. The results were averaged over the UEs and up to 10^5 independent channel realizations. The system size has $N_r = 100$ receive antennas and $N_t = 10$ transmit antennas. The baseline parameters are: the parameter which controls the rate of decay of the link gains $\beta = 0.5$, the correlation between adjacent antennas $\alpha_u = 0.1$, array type = uniform linear array (ULA). Where other parameters are used, they are given in the figure captions. In the figures, the signal to noise ratio (SNR) is the SNR of the strongest UE, given by $\frac{\mathcal{A}}{\sigma^2}$, where the link gain of the strongest UE is $\mathcal{A} = 1$ without loss of generality.

Figure 5.1 shows SER vs. SNR with MRC V-BLAST and ZF V-BLAST for different values of r_0, $r_0 \in \{1, 0.99, 0.9\}$. The effect of imperfect CSI on MRC V-BLAST and ZF V-BLAST is almost identical here when $\alpha_u = 0.1$ is used. Hence, with small correlation, the performance of MM using MRC V-BLAST and ZF V-BLAST is virtually the same and it is better to use MRC V-BLAST, which has a lower complexity. However, the MM performance is strongly affected by the level of CSI. When $r_0 = 0.9$, the performance of the system is extremely poor.

Figure 5.2 shows SER vs. SNR with MRC V-BLAST and ZF V-BLAST for different values of β, $\beta \in \{0.5, 0.7\}$ and $r_0 = 0.99$. The effect of changing the channel powers on MRC V-BLAST and ZF V-BLAST is very similar with small correlation ($\alpha_u = 0.1$). However, the system performance is strongly affected by β, with a better performance achieved when channel

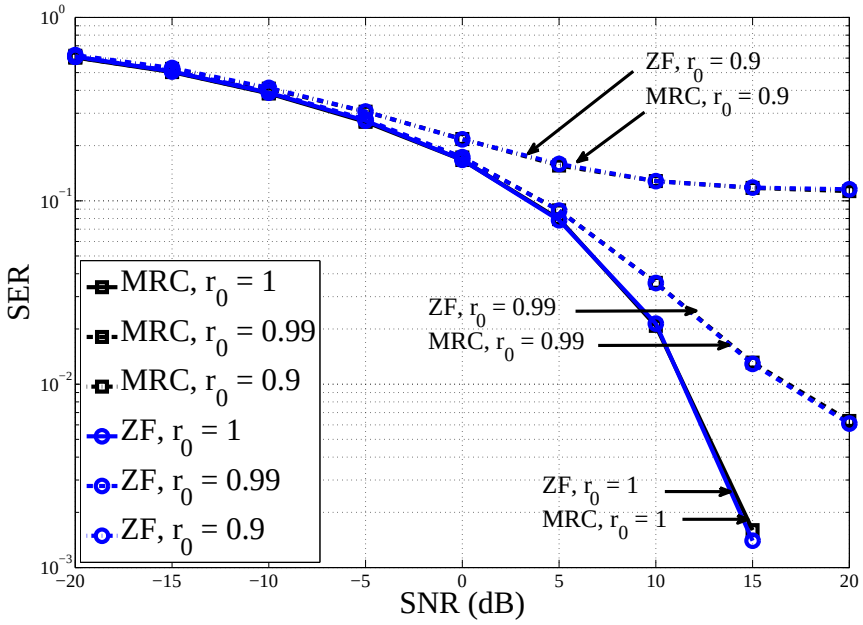

Figure 5.1: SER vs. SNR with MRC V-BLAST and ZF V-BLAST for different CSI accuracy (r_0).

powers are less distributed ($\beta = 0.7$).

Figure 5.3 shows SER at stage 1, 2, 9, 10 and SER vs. SNR with MRC V-BLAST and ZF V-BLAST for $\beta = 0.5$ and $r_0 = 0.99$. In the first two layers where strong UEs are present, the $P_{(j)}$ terms are large but the SERs are low (below 10^{-3} for SNR $\leq$ 0 dB). Hence, the overall SER (approximately 2×10^{-1} at SNR = 0 dB) is not affected by these results. In contrast, in the later stages, the SERs are dominant and here the $P_{(j)}$ terms are much smaller.

Figure 5.4 shows SER vs. SNR with MRC V-BLAST for SQ and ULA and $\alpha_u \in \{0.1, 0.9\}$. Inter-antenna spacing is the same for both configurations. The effect of changing the type of array on MRC V-BLAST and ZF V-BLAST is similar. From Figure 5.4, we observe that performance deteriorates as antenna correlation increases and that the ULA has lower SER for high α_u. Note that most antennas within the SQ have more neighbors than those within the ULA and this is why the ULA has lower SER for high α_u. For low α_u values, SQ and ULA are

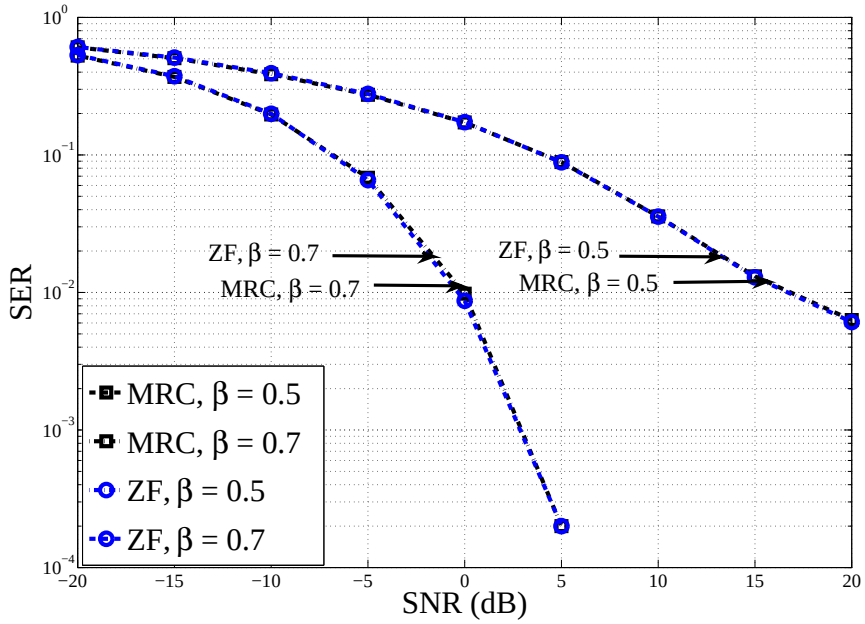

Figure 5.2: SER vs. SNR with MRC V-BLAST and ZF V-BLAST for different UE power distributions (β), $r_0 = 0.99$.

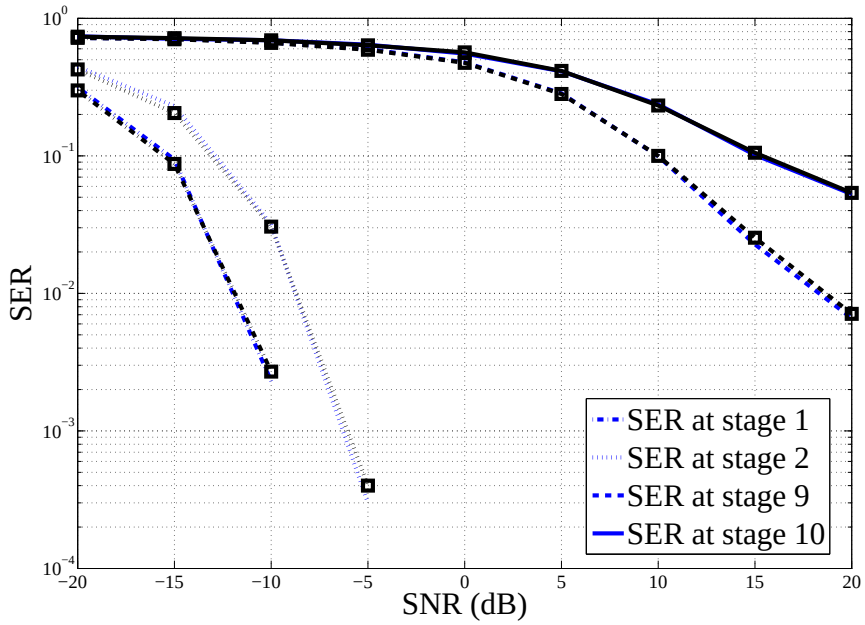

Figure 5.3: SER vs. SNR with MRC V-BLAST and ZF V-BLAST for $\beta = 0.5$, $r_0 = 0.99$. MRC V-BLAST is denoted by squares and lines in black color and ZF V-BLAST by lines in blue color.

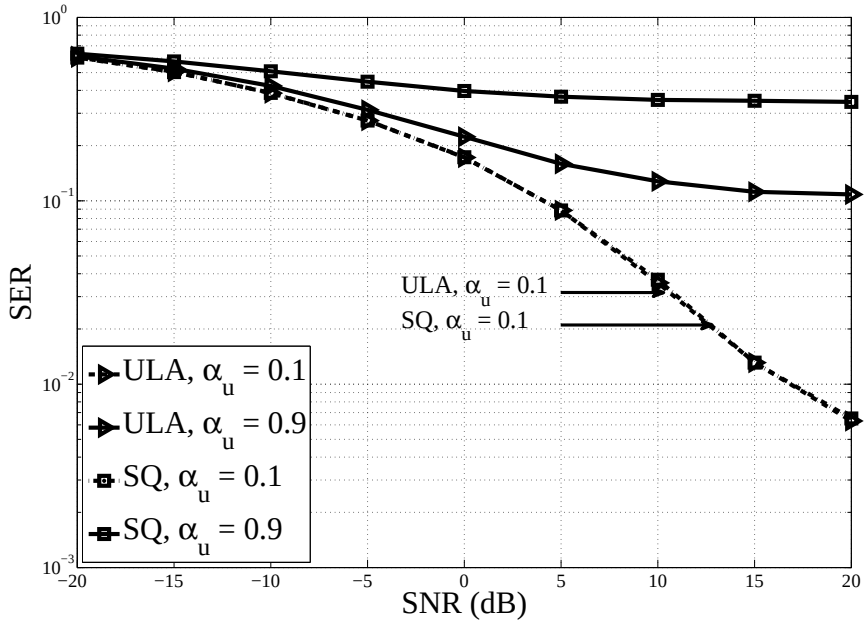

Figure 5.4: SER vs. SNR with MRC V-BLAST with different values of antenna correlation (α_u) and array types (SQ, ULA), $r_0 = 0.99$.

similar.

Figure 5.5 shows SER vs. SNR with MRC V-BLAST and ZF V-BLAST for different array types (SQ and ULA), $r_0 = 0.99$ and $\alpha_u = 0.9$. Here, the correlation is high ($\alpha_u = 0.9$) and the increased levels of correlation found in a SQ configuration mean that the SERs for SQ are worse than for the corresponding ULA for both MRC V-BLAST and MRC V-BLAST. The difference between ULA and SQ is increased as α_u increases, i.e., for $\alpha_u = 0.1$, the average correlation between two antennas is 0.016 (SQ) and 0.012 (ULA). However, for $\alpha_u = 0.9$, the average correlation is 0.60 (SQ) and 0.17 (ULA).

Figure 5.6 shows SER vs. SNR for $r_0 \in \{1, 0.99\}$ and $\alpha_u \in \{0.1, 0.5, 0.7\}$. By increasing the correlation level, the performance of the receiver deteriorates, especially in the imperfect CSI case. The correlation level has little effect in the case of perfect channel estimation and $\alpha_u = 0.1$ and 0.5.

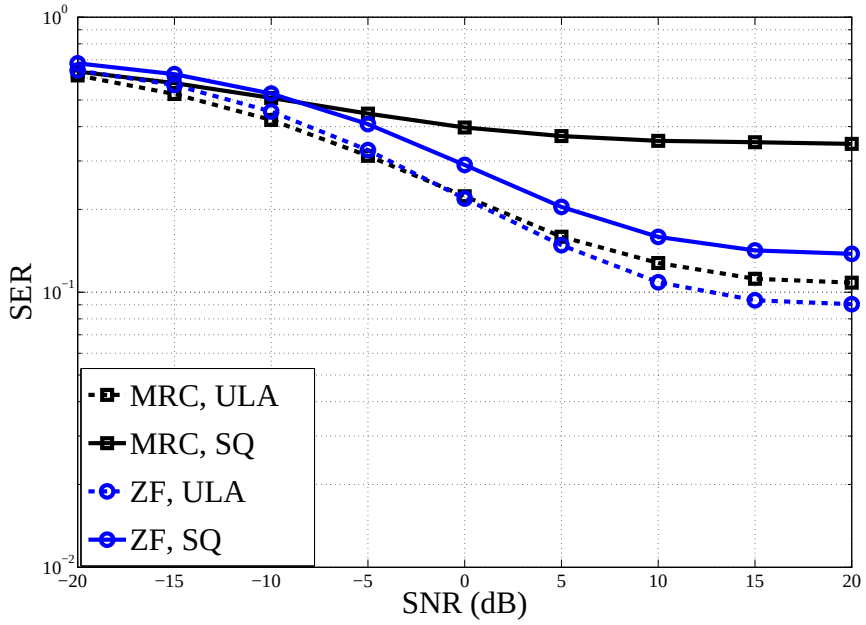

Figure 5.5: SER vs. SNR with MRC V-BLAST and ZF V-BLAST for different array types (SQ, ULA), $r_0 = 0.99$ and $\alpha_u = 0.9$.

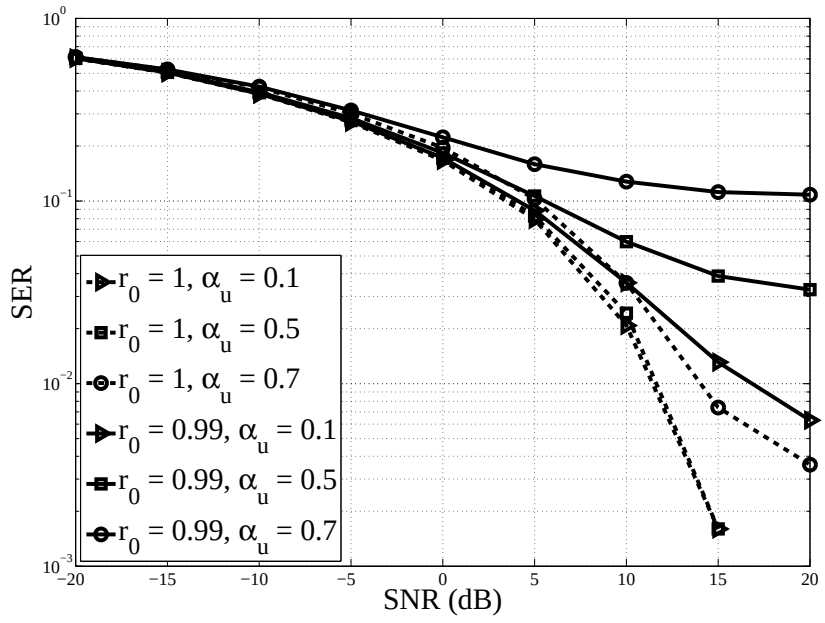

Figure 5.6: SER vs. SNR with MRC V-BLAST for different values of antenna correlation (α_u) and CSI accuracy (r_0).

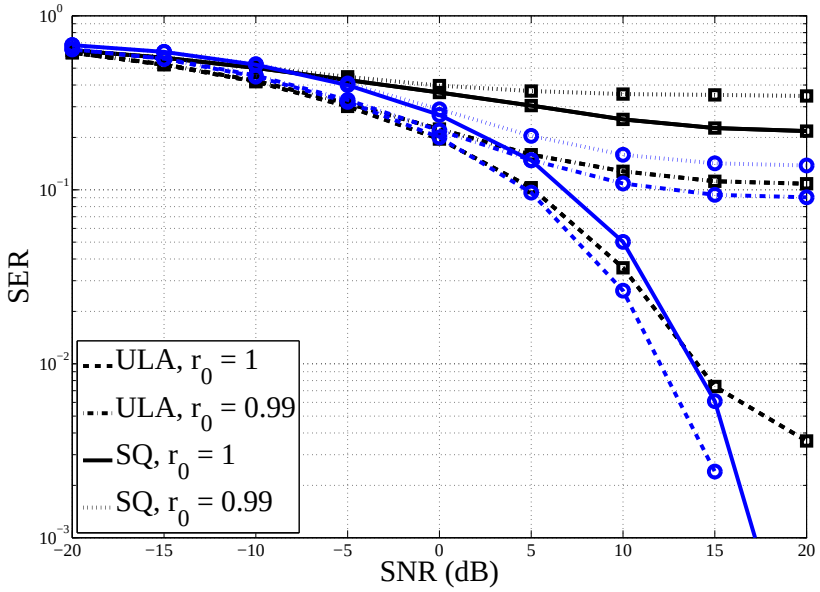

Figure 5.7: SER vs. SNR with MRC V-BLAST and ZF V-BLAST for different values of CSI accuracy (r_0) and array types (SQ, ULA). $\alpha_u = 0.9$, MRC V-BLAST is denoted by squares and lines and ZF V-BLAST by circles and lines.

Figure 5.7 shows SER vs. SNR with MRC V-BLAST and ZF V-BLAST for different values of r_0, $r_0 \in \{1, 0.99\}$ and array types (SQ and ULA), $\alpha_u = 0.9$. Squares and lines denote MRC V-BLAST and circles and lines denote ZF V-BLAST. Figure 5.7 demonstrates that MRC V-BLAST does not always perform in a similar way to ZF V-BLAST. For example, the ZF V-BLAST, SQ results with $r_0 = 1$ are far better than the MRC V-BLAST, SQ, $r_0 = 1$ results. Also, when $\alpha_u = 0.9$ and $r_0 = 1$ the performance of ZF V-BLAST with ULA is much better than it is with SQ. Both effects are due to correlation. Firstly, with equal antenna spacing the SQ has higher correlations and so the ZF results are worse for SQ compared to ULA. Secondly, correlation has a much greater impact on MRC for $r_0 = 1$ as ZF removes the interference while interference increases with correlation for MRC. To see this effect, the interference term $\sum_{j \neq m} \mathbf{h}_m^H \mathbf{h}_j \mathbf{h}_j^H \mathbf{h}_m$ in (2.26) is zero for ZF where as for MRC, each $\mathbf{h}_m^H \mathbf{h}_j \mathbf{h}_j^H \mathbf{h}_m$ is non-zero and is increased when $\mathbf{h}_m$ and $\mathbf{h}_j$ are correlated. This can be quantified numeri-

cally by considering the power of the interference term, $\mathrm{E}[\sum_{j\neq m}\mathbf{h}_m^H\mathbf{h}_j\mathbf{h}_j^H\mathbf{h}_m]$. From (2.16), we see that $\mathrm{E}[\sum_{j\neq m}\mathbf{h}_m^H\mathbf{h}_j\mathbf{h}_j^H\mathbf{h}_m] = \mathrm{Tr}(\mathbf{R}_r^2)P_m\sum_{j\neq m}P_j$. For independent channels this power is $N_rP_m\sum_{j\neq m}P_j$ whereas for perfectly correlated channels the power is $N_r^2P_m\sum_{j\neq m}P_j$. This shows the potential interference increase due to correlation and is particularly noticeable in MM where N_r is large. For the ULA, an exact calculation is possible giving $\mathrm{E}[\sum_{j\neq m}\mathbf{h}_m^H\mathbf{h}_j\mathbf{h}_j^H\mathbf{h}_m] = \frac{N_r-\alpha_u^2(N_r-2\alpha_u^{2N_r}+2)}{(1-\alpha_u^2)^2}P_m\sum_{j\neq m}P_j$.

Figure 5.8 shows SER vs. SNR with MRC V-BLAST and ZF V-BLAST for different SQ sizes (SQ, Adjusted SQ), $\alpha_u = 0.9$, $r_0 = 1$. MRC V-BLAST is denoted by squares and lines and ZF V-BLAST by circles and lines. By adjusting the width of the SQ, MRC V-BLAST and ZF V-BLAST can behave similarly and the Adjusted SQ SER results are similar for both ULA and SQ (See Figure 5.7). This shows that the simple closed form analysis in Section 5.5.2 may be beneficial in terms of dimensioning arrays. Increasing the gaps between antennas in two dimensions helps in reducing the correlation. In addition, the space can be used as much as it is allowed and hence better performance can be achieved compared to the compact SQs. Note that the MRC V-BLAST receiver may require a larger array dimension than the ZF V-BLAST receiver. Nevertheless, given enough spacing, the performance of MRC V-BLAST can approach ZF V-BLAST performance. We showed that by equating median antenna spacings (5.17) that a SQ needed to be increased in width from 9% of the ULA length (for equal inter-element spacing) to 57% in order to achieve similar performance.

5.7 Summary

In this chapter, we have investigated V-BLAST with MRC and ZF in a MM system with imperfect CSI and channel correlation. We found that MRC V-BLAST performance can approach ZF V-BLAST, despite its lower complexity, for a range of imperfect CSI levels, different channel powers and different types of array, as long as the antenna correlation is not too high. When

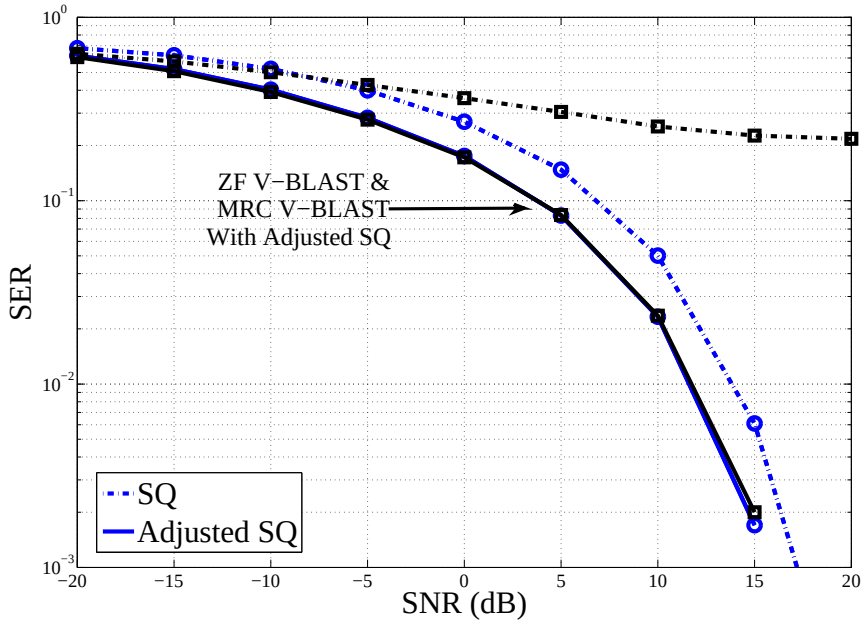

Figure 5.8: SER vs. SNR with MRC V-BLAST and ZF V-BLAST for different SQ sizes (SQ, Adjusted SQ). $\alpha_u = 0.9$, $r_0 = 1$, MRC V-BLAST is denoted by squares and lines and ZF V-BLAST by circles and lines.

the correlation level is increased, the performance of V-BLAST using either MRC or ZF is degraded and the gap between the two can become substantial. When the correlation is high, the ULA also offers large gains over the SQ if the same spacing is used. However, if the SQ is dimensioned using the closed form result derived, then MRC V-BLAST and ZF V-BLAST with SQ or ULA are shown to behave similarly.

Chapter VI

Low Complexity MRC V-BLAST Based on Channel Norm Ordering

6.1 Introduction

With the advent of MM, receiver complexity is becoming critical and in this chapter our focus is on reduced complexity receivers. We consider an uplink MM deployment with a co-located BS array and distributed single antenna UEs. We consider two types of linear receivers: MRC and ZF. We also consider the V-BLAST approach.

As we discussed in Chapter 5, very little work has appeared on V-BLAST with MM since the prime focus of MM is simplicity whereas V-BLAST requires repeated detection and ordering. Also, most of the work on traditional V-BLAST considers ZF or MMSE combining and rarely discusses MRC [44, 45].

In this Chapter, we integrate MRC with V-BLAST in MM and propose a simple, low complexity receiver design. The key contribution is that ZF performance can be reproduced using this approach with lower complexity. In support of this result, we characterize the SINR performance via simple closed form approximations which gives insight into the reasons why MRC and ZF behave similarly in the novel low complexity receiver. Note that in this chapter we ignore issues such as pilot contamination [7] and assume perfect CSI. Since ZF receivers are likely to be more affected by imperfect CSI (see Chapter 5), the proposed receiver may have

even greater benefits in the presence of imperfect CSI.

In [110], performance analysis based on average SER of the ordered V-BLAST approach over Nakagami-m fading channels was discussed. However in this chapter we are using a different channel model, different system size and a different ordering technique.

The rest of Chapter 6 is organized as follows. Section 6.2 introduces the system model. Section 6.3 describes the MM deployment and channel models. Section 6.4 describes the proposed receiver design. Section 6.5 provides analysis and a complexity comparison. We give simulation results in Section 6.6 and conclude in Section 6.7.

6.2 System Model

We consider the system model in Section 2.7, where the received signal $\mathbf{y}$ is calculated as

$$\mathbf{y} = \mathbf{H}\mathbf{x} + \mathbf{n}, \tag{6.1}$$

where $\mathbf{H}$, $\mathbf{x}$ and $\mathbf{n}$ are the channel, signal vector and noise, respectively. We assume perfect CSI and the SINR can be calculated as in (2.30). Without loss of generality, let the noise power be $\sigma^2 = 1$.

6.3 Deployment

Consider a large co-located antenna array at the BS serving N_t UEs in the coverage region.

6.3.1 Case 1: Unequal Received User Power

In this scenario, the UEs are located randomly in a circular coverage area, as shown in Figure 6.1. Due to shadowing and path loss effects, the received powers of the UE signals are all different. This is the standard multiuser MIMO scenario. The channel model is defined as

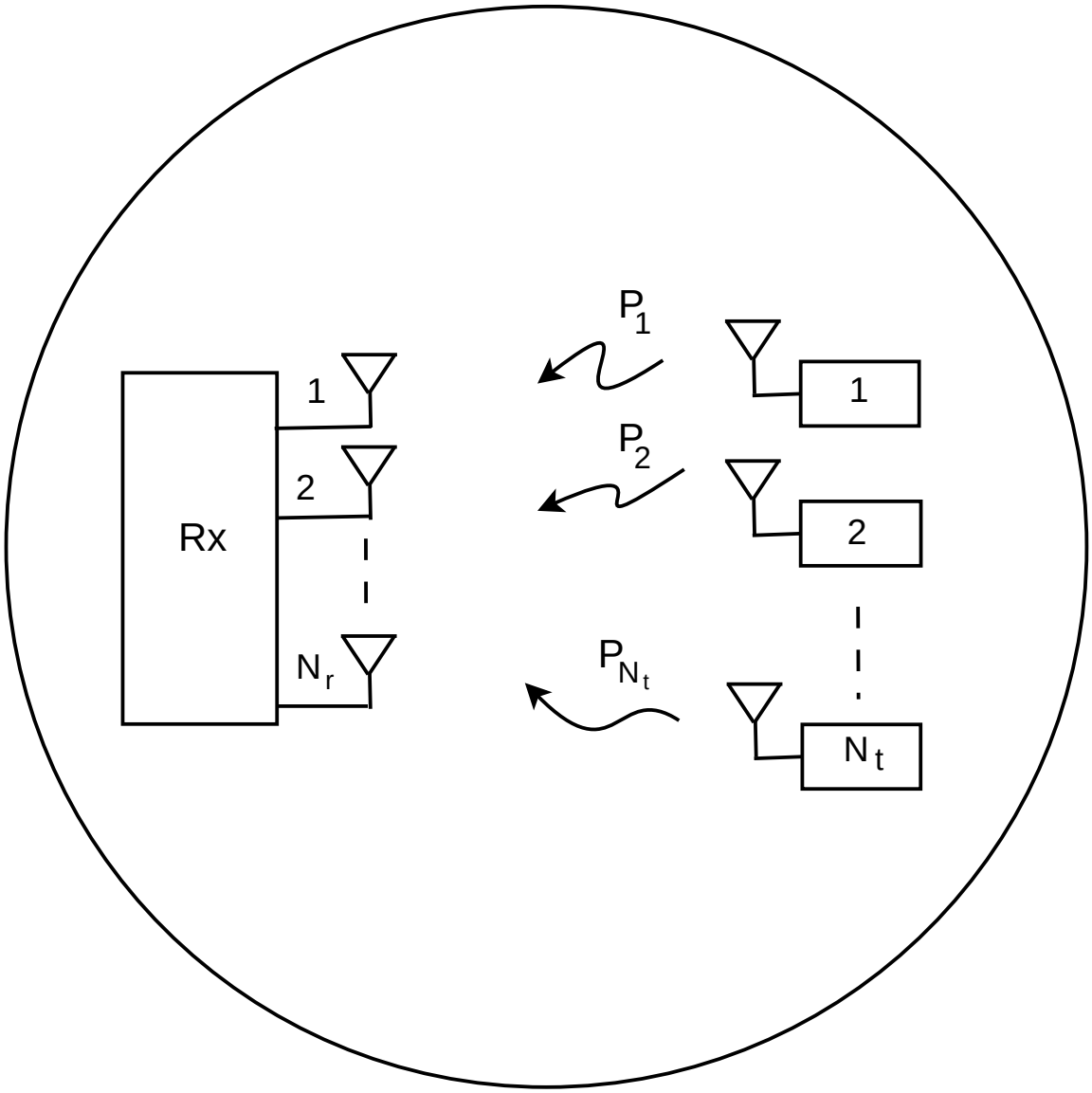

Figure 6.1: Case 1: System diagram where UEs are located randomly in a circular coverage area.

$\mathbf{H} = \mathbf{U}\mathbf{D}^{\frac{1}{2}}$, where the elements of $\mathbf{U}$ are i.i.d. $\mathcal{CN}(0,1)$ and $\mathbf{D} = \mathrm{diag}(P_1, P_2, \ldots, P_{N_t})$. Note that P_j is calculated as in (2.11), $P_j = AL_j d_j^{-\gamma}$, where j identifies the UEs, A is a constant depending on transmit power, antenna height, etc., L_j is a lognormal shadow fading variable, d_j is the link distance and γ is the path loss exponent.

6.3.2 Case 2: Equal Received User Power

Here, we assume that all link powers are the same. Hence, $h_{ij} = \sqrt{P}u_{ij}$, where $u_{ij} \sim \mathcal{CN}(0,1)$ are i.i.d. fast fading terms and P is the link power which is fixed for all UEs. This scenario corresponds to a single-user MIMO link or to situations where all UEs are essentially co-located, possibly arising in a small cell environment. It also provides a baseline case (equal powers) against which we can evaluate the effects of unequal powers.

6.4 The Proposed Receiver Design

In [45], the performance of V-BLAST with MRC was discussed in the context of traditional MIMO systems. These are small systems, typically using 2-8 antennas. Here, complexity issues are less important and ordering the SINRs at every stage, using a simple receiver such as MRC, is considered low complexity. With MM, there is a greater need for complexity reduction. Hence, we propose performing a single one-off ordering of the sources and then MRC detection at each stage. The proposed ordering simply ranks the sources by the corresponding column norms and detects the sources in this order.

Let the ordered set $S = \{k_1^{(\mathrm{C})}, k_2^{(\mathrm{C})}, \ldots, k_{N_t}^{(\mathrm{C})}\}$ be a permutation of the integers 1, 2, ..., N_t specifying the order in which the transmitted symbols in $\mathbf{x}$ are extracted. Hence, the approach for a single, channel norm ordering is labeled as C-V-BLAST and is defined by

$$k_i^{(\mathrm{C})} = \underset{j \notin \{k_1, k_2, \ldots, k_{i-1}\}}{\arg\max} ||\mathbf{h}_j||^2, \tag{6.2}$$

where $\mathbf{h}_j$ is the j^{th} column of $\mathbf{H}$.

6.5 Analysis

In this chapter, the focus is on comparing MRC based receivers with ZF. It is useful to understand when the two receivers, implemented in a V-BLAST framework, have similar performance. Hence, in this section, we consider a generic stage of the V-BLAST process and compare the SNR of ZF and the SINR of MRC. We also compare the complexity of the two simplest ZF and MRC techniques.

6.5.1 Comparison of ZF and MRC

At any stage of the V-BLAST decoding, assuming the previous stages were successful, the received signal is given by

$$\widetilde{\mathbf{y}} = \mathbf{H}_s \mathbf{x}_s + \mathbf{n}, \tag{6.3}$$

where $\mathbf{H}_s$ contains s columns of $\mathbf{H}$ and $\mathbf{x}_s$ contains the corresponding elements of $\mathbf{x}$ which have not been detected [1]. Without loss of generality, we label these elements from 1 to s so that $\mathbf{H}_s = [\mathbf{h}_1 \dots \mathbf{h}_s]$ and $\mathbf{x}_s = [x_1 \dots x_s]^T$. Now, denote $\mathbf{H}_s = \mathbf{V}\mathbf{P}^{\frac{1}{2}}$ where $\mathbf{P} = \text{diag}(P_1 \dots P_s)$ and the elements of $\mathbf{V}$ are i.i.d. $\mathcal{CN}(0,1)$. This gives

$$\widetilde{\mathbf{y}} = \mathbf{V}\mathbf{P}^{\frac{1}{2}} \mathbf{x}_s + \mathbf{n}, \tag{6.4}$$

and we further assume that $P_1 > P_2 > \cdots > P_s$ and the order of detection follows the order of the link gains. Note that these assumptions are completely general except for the assumption that the remaining s sources are detected in the order 1, 2, ..., s. However, this assumption is

[1] Hence, this is the $(N_t - s + 1)^{\text{th}}$ stage with s symbols left to be detected.

reasonable as the sources with larger link gains are usually detected first. Using the notation in (6.4), the SNR of a ZF detector for user 1 is given by [111]

$$\mathrm{SNR_{ZF}}^{(1)} = \frac{P_1 E_s}{\sigma^2 [(\mathbf{V}^H \mathbf{V})^{-1}]_{11}}, \tag{6.5}$$

where $\mathbf{V} = [\mathbf{v}_1 \mathbf{v}_2 \dots \mathbf{v}_s]$. Suppose $\bar{m} \in \{1, \dots, s\}$, then it is clear that $||\mathbf{v}_{\bar{m}}||^2$ is a Chi-Square random variable with $2N_r$ DOF, i.e., $||\mathbf{v}_{\bar{m}}||^2 \sim \chi^2_{2N_r}$. Note that $[(\mathbf{V}^H \mathbf{V})^{-1}]_{11}$ is given by [111]

$$[(\mathbf{V}^H \mathbf{V})^{-1}]_{11} = \frac{1}{\mathbf{v}_1^H \mathbf{v}_1 - \mathbf{v}_1^H \mathbf{V}_1 (\mathbf{V}_1^H \mathbf{V}_1)^{-1} \mathbf{V}_1^H \mathbf{v}_1}. \tag{6.6}$$

Accordingly, from [111, 112], $\frac{1}{[(\mathbf{V}^H \mathbf{V})^{-1}]_{11}}$ has a $\chi^2_{2(N_r - s + 1)}$ distribution. It follows that

$$\mathrm{E}[\mathrm{SNR_{ZF}}^{(1)}] = \frac{P_1 E_s (N_r - s + 1)}{\sigma^2}. \tag{6.7}$$

For an MRC detector, the SINR in (2.30) simplifies to

$$\mathrm{SNR_{MRC}}^{(1)} = \frac{P_1^2 E_s (\mathbf{v}_1^H \mathbf{v}_1)^2}{E_s P_1 \sum_{j=2}^{s} P_j |\mathbf{v}_1^H \mathbf{v}_j|^2 + P_1 (\mathbf{v}_1^H \mathbf{v}_1) \sigma^2}. \tag{6.8}$$

(6.8) gives

$$\mathrm{SINR_{MRC}}^{(1)} = \frac{P_1 \frac{(E_s \mathbf{v}_1^H \mathbf{v}_1)}{\sigma^2}}{1 + \frac{E_s}{\sigma^2} \sum_{j=2}^{s} \frac{P_j |\mathbf{v}_1^H \mathbf{v}_j|^2}{|\mathbf{v}_1^H \mathbf{v}_1|}}. \tag{6.9}$$

Using the Laplace approximation approach [92, equations (25) and (11)], which has been shown to be quite accurate for ratios of quadratic forms [93], the mean of the SINR in (6.9) can be approximated by the ratio of the means giving

$$\mathrm{E}[\mathrm{SINR_{MRC}}^{(1)}] \approx \frac{P_1 \frac{E_s N_r}{\sigma^2}}{1 + E_s \sum_{j=2}^{s} \frac{P_j}{\sigma^2}}. \tag{6.10}$$

Equation (6.10) is derived by conditioning on $\mathbf{v}_1$ in the denominator. Using this approach gives

$$\begin{aligned} \mathrm{E}[|\mathbf{v}_1^H\mathbf{v}_j|^2|\mathbf{v}_1^H\mathbf{v}_1|^{-1}] &= \mathrm{E}[\mathrm{E}[|\mathbf{v}_1^H\mathbf{v}_j|^2|\mathbf{v}_1^H\mathbf{v}_1|^{-1} \mid \mathbf{v}_1]] \\ &= \mathrm{E}[|\mathbf{v}_1^H\mathbf{v}_1|^{-1}\mathrm{E}[\mathbf{v}_1^H\mathbf{v}_j\mathbf{v}_j^H\mathbf{v}_1 \mid \mathbf{v}_1]] \\ &= \mathrm{E}[|\mathbf{v}_1^H\mathbf{v}_1|^{-1}\mathrm{E}[\mathbf{v}_1^H\mathbf{v}_1 \mid \mathbf{v}_1]] \\ &= 1 \end{aligned} \tag{6.11}$$

and (6.10) follows. In order for the ZF and MRC detectors to have similar performance, we require (6.7) and (6.10) to be similar. Hence,

$$\frac{P_1E_s(N_r-s+1)}{\sigma^2} \approx \frac{P_1E_sN_r}{\sigma^2+E_s\sum_{j=2}^{s}P_j}. \tag{6.12}$$

Solving (6.12) when $E_s = \sigma^2 = 1$ gives $\sum_{j=2}^{s} P_j = (s-1)(N_r-s+1)^{-1}$. As expected, the sum of the interference needs to be small before the MRC receiver is similar to the ZF receiver because MRC is corrupted by the aggregate interference while ZF removes it completely. Simulation results shown in Figure 6.2 support the accuracy of the SINR approximations used in (6.12) for ZF and MRC. This supports our conclusion that ZF performance and MRC performance will be similar when (6.12) holds.

.

6.5.2 Complexity Calculations

The simplest ZF-based detector is a simple ZF linear combiner with no V-BLAST structure. In comparison, the simplest MRC-based detector we consider uses C-V-BLAST. Here, we compare the computational complexity of these two techniques, with complexity measured by the number of complex multiplications. In ZF, computing $\mathbf{H}^H\mathbf{H}$ requires $\frac{N_rN_t(N_t+1)}{2}$ multiplications

and the inverse computation requires $\frac{N_t^3}{2} + \frac{3}{2}N_t^2$ multiplications based on [109]. Multiplying $(\mathbf{H}^H\mathbf{H})^{-1}$ with $\mathbf{H}^H$ requires $N_t^2 N_r$ multiplications and multiplying $(\mathbf{H}^H\mathbf{H})^{-1}\mathbf{H}^H$ by $\mathbf{y}$ requires $N_t N_r$ multiplications. Thus, the ZF algorithm requires $\frac{N_r N_t(N_t+1)}{2} + \frac{N_t^3}{2} + \frac{3}{2}N_t^2 + N_t^2 N_r + N_t N_r$ complex multiplications. In C-V-BLAST, computing $\mathbf{h}_i^H\mathbf{y}$ and $\mathbf{h}_i\hat{x}_i$ both require N_r multiplications. Repetition of this process for the first $N_t - 1$ stages requires $2N_r(N_t - 1)$ multiplications. The final stage requires detection but no cancellation, ie. N_r multiplications. The initial ordering involves the computation of N_t channel norms which requires $N_r N_t$ multiplications. Thus, C-V-BLAST requires $2N_r(N_t - 1) + N_r + N_r N_t$ multiplications. Table 6.1 summarizes the complexity calculations (where the complexity of the sort process in ordering is ignored).

Table 6.1: Complexity calculations

Technique	**Complexity: Number of complex multipliers**
ZF	$0.5N_t(N_t^2 + 3N_t(N_r + 1) + 3N_r)$
C-V-BLAST	$N_r(3N_t - 1)$

Even with no V-BLAST structure the ZF complexity is $O(N_r N_t^2)$ in comparison with the low complexity MRC approach which is $O(N_r N_t)$ without sorting. For example, with $N_t = 10$, $N_r = 100$, the number of multiplications are 18150 and 2900, respectively.

6.6 Results

In this section, we investigate the performance of several MM receivers via numerical simulation to measure the SER assuming QPSK modulation. The results are averaged over the UEs and over $10^4 - 10^6$ independent channel realizations. For Case 2, each set of realizations has a fixed power. For Case 1, each realization corresponds to a random drop where each drop creates a different set of link powers. We assume the noise power is $\sigma^2 = 1$. The system size is defined by the number of receive antennas, $N_r = 100$, and the number of transmit antennas,

$N_t \in \{10, 20, 40\}$. The propagation parameters are a constant path loss exponent of $\gamma = 3$ and the standard deviation of the shadowing factor is $\sigma_{SF} = 8$ dB. We employ an exclusion zone which prevents the UEs becoming too close to the BS. The radius of the coverage area is assumed to be 1. The link distance constraint used is $d_{ij} > 0.01$ and this avoids any unreasonably high link gains in (2.11) due to extremely short link distances.

In order to create the link powers for Case 2, we simply vary the SNR over the desired range and set $P_j = P = \mathrm{SNR}$. For Case 1, we use equation (2.11) to generate $P_1, P_2, \ldots, P_{N_t}$ and normalize by $P_{\mathrm{Avg}} = \frac{1}{N_t} \sum_{j=1}^{N_t} P_j$. Hence, the value of A, a constant depending on transmit power, is unimportant and we set $A = 1$. The normalized powers are then scaled by the desired SNR so that user j has $\mathrm{SNR}_j = \mathrm{SNR} \frac{P_j}{P_{\mathrm{Avg}}}$. This makes the average SNR over all UEs equal to the target SNR and enables a fair comparison of Case 1 and Case 2.

Figure 6.2 compares simulated instantaneous SINR values for MRC and ZF in stage 1 of a V-BLAST detector assuming that the UE with the highest link power is detected first. In these simulations, we have not normalized the link powers by P_{Avg} and simply use (2.11) to create the random drops with $A = 1$. Also shown are the simple mean SINR approximations using (6.7) and (6.10). Note that the ZF analysis is visually indistinguishable from the simulated results whereas the MRC results have a very slight offset. Hence, (6.7) and (6.10) provide excellent approximations to the SINR cumulative distribution functions (CDFs) for both receivers and this supports the use of (6.12) which suggests that ZF and MRC will be similar only when the link powers are small, of the order of $\sum_{j=2}^{s} P_j \approx (s-1)(N_r - s + 1)^{-1}$, where s is the number of undetected sources.

Figure 6.3 shows that the SER of a simple ZF combiner is almost the same as ZF V-BLAST for $N_r = 100$, $N_t = 10$. Hence, the V-BLAST structure is unnecessary in this scenario and a simple ZF combiner performs equally well. For ZF, the equal power scenario performs better, because ZF removes the interference and with equal power there are no sources with small

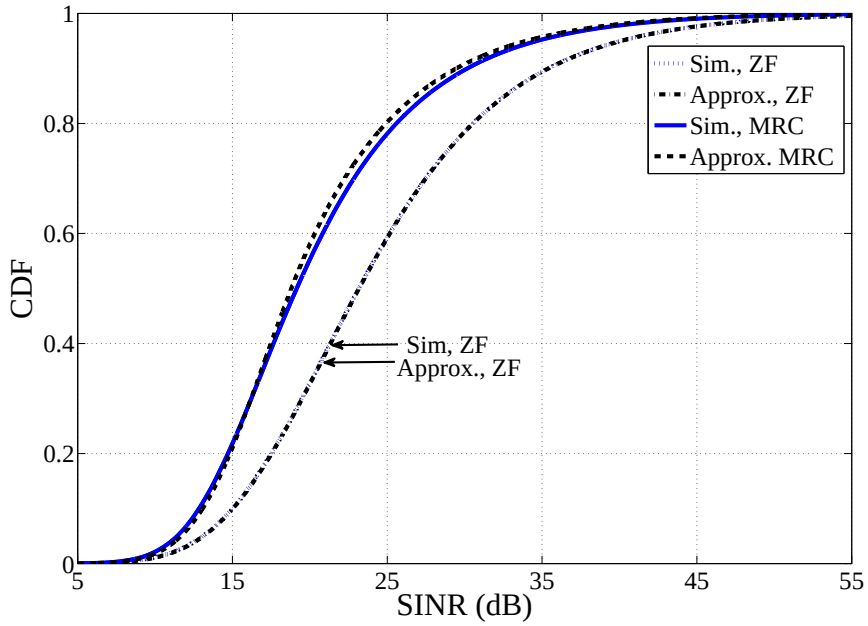

Figure 6.2: SINR CDFs for Case 1 with ZF and MRC, N_t = 10.

power, unless all sources are weak.

Figure 6.4 shows the key result that in the unequal power case (Case 1) the C-V-BLAST is almost identical to ZF and ZF V-BLAST. This can be seen by comparing the Case 1 SER curves in Figure 6.3 with the Case 1 C-V-BLAST results in Figure 6.4. Hence, with distributed UEs, C-V-BLAST achieves the same performance as ZF with a much smaller complexity (see Table 6.1). This rather unexpected result can be explained using (6.12). From (6.12), MRC and ZF should only give similar performance when the sum of the interferers is small. In general, with random drops of distributed UEs, there is no reason why this should be the case. In fact, what is happening is that the SER is dominated by the occasions when all the UEs have weak link powers and in this situation the sum of the interferers is small. At low SNR, all UEs have weak link powers and so the total interference is small and MRC and ZF are similar. At higher SNR, the UEs do not have weak link powers and in the early V-BLAST stages the interference can be

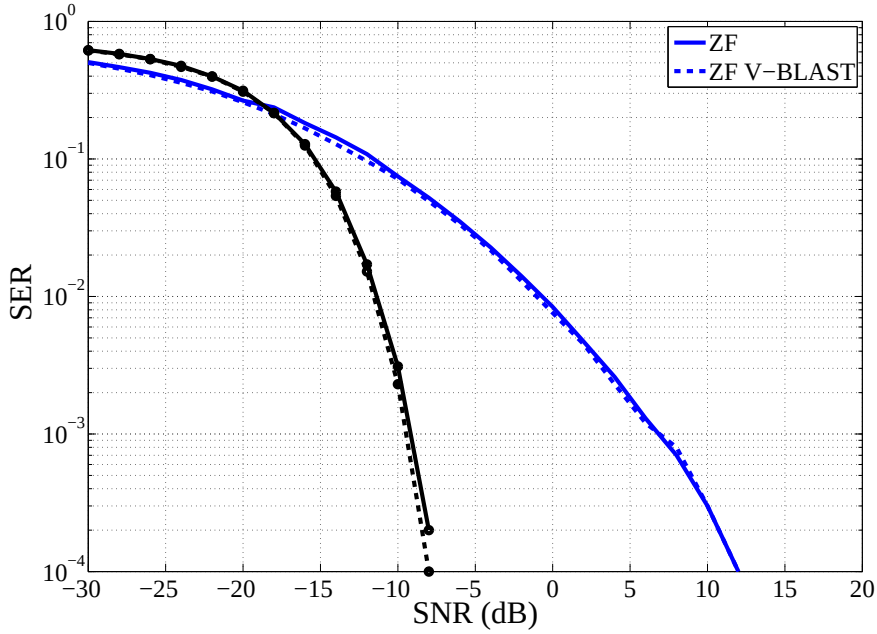

Figure 6.3: SER vs. SNR with ZF and ZF V-BLAST, N_t = 10. Lines represent Case 1 and lines with circles represent Case 2.

quite large. However, due to the long-tailed shadowing/path-loss model, there are large power discrepancies between UEs. Hence, the strongest UE dominates and experiences a high SINR. Hence, ZF and MRC are not similar, but this is a low SER scenario which does not have a great impact on the overall SER. In the later V-BLAST stages, the UEs experience a lower SINR and the contribution to the overall SER is greater. Here, the total interference is small as there are fewer, weaker undetected UEs. Hence, in the situations which contribute most to the overall SER, MRC and ZF tend to be similar.

Also shown in Figures 6.4-6.6 is the very poor performance of a single MRC receiver in both Case 1 and Case 2 and the presence of a floor which becomes worse as the loading increases from 10 to 40 UEs. For MRC, a spread of powers helps the performance of V-BLAST at higher loadings and in all cases C-V-BLAST is impressive. Also shown in Figures 6.4-6.6 is V-BLAST with MRC where a single ordering is performed at the start based on the initial SINRs (labeled

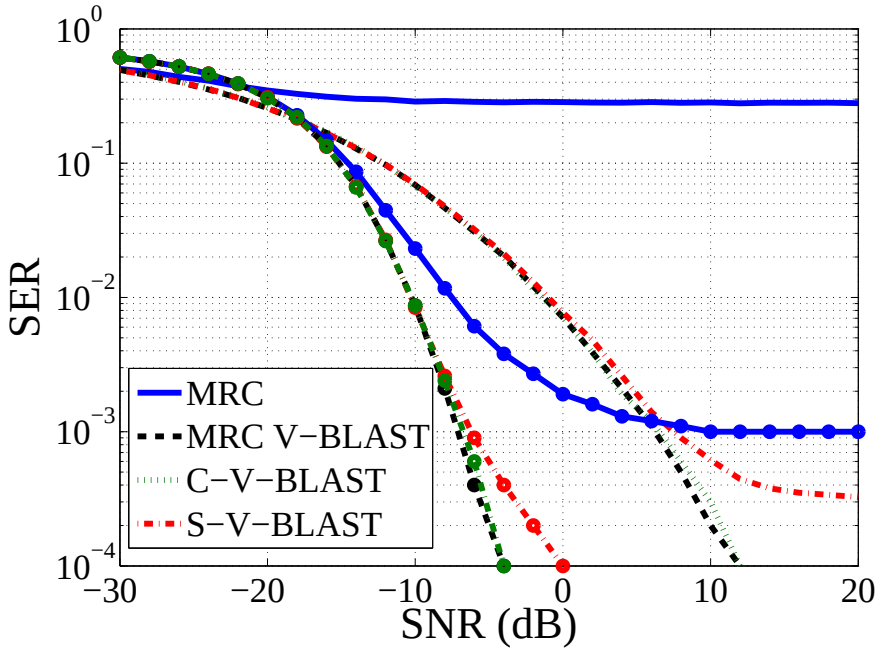

Figure 6.4: SER vs. SNR with MRC with different ordering techniques, N_t = 10. Lines represent Case 1 and lines with circles represent Case 2.

single SINR ordering (S-V-BLAST)). It is interesting that this is worse than C-V-BLAST and is due to the fact that the power-based ordering remains valid throughout the iterations while the SINR keeps changing as the detection and cancellation steps occur.

6.7 Summary

In this chapter, we have investigated a variety of simple linear combiners and V-BLAST structures based on MRC and ZF. We have found that the performance of ZF can approach ZF V-BLAST with lower computation. Additionally, we have shown that MRC V-BLAST has a similar performance to ZF when the link powers are different. Note that MRC V-BLAST has the same complexity as the linear ZF receiver (see Section 5.5.3, Section 6.5.2 and Table 6.1). C-V-BLAST, which has a lower complexity than MRC V-BLAST, can achieve a similar performance to MRC V-BLAST and therefore to the linear ZF receiver as well. When using S-V-BLAST,

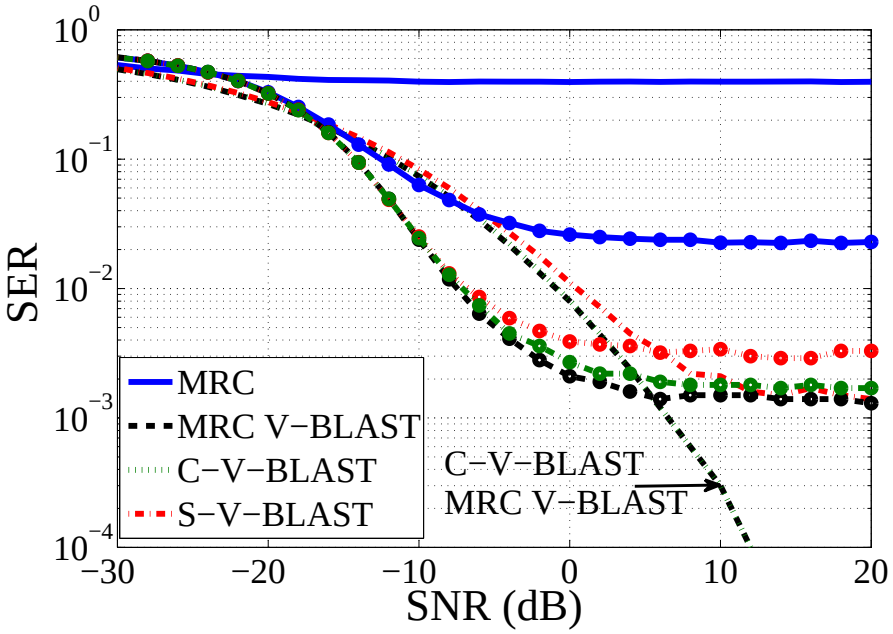

Figure 6.5: SER vs. SNR with MRC with different ordering techniques, N_t = 20. Lines represent Case 1 and lines with circles represent Case 2.

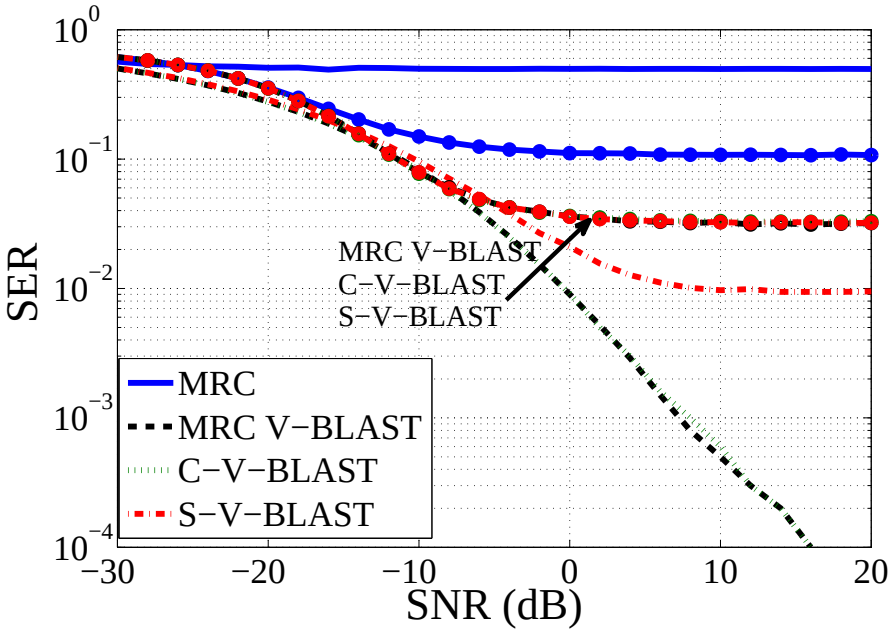

Figure 6.6: SER vs. SNR with MRC with different ordering techniques, N_t = 40. Lines represent Case 1 and lines with circles represent Case 2.

the performance becomes worse as the SINR keeps changing as the detection and cancellation steps occur. Thus, ZF performance can be reproduced using the C-V-BLAST approach with a much lower complexity in the most important scenario, where UEs are distributed and experience different link powers. This SER equivalence is found on a system-wide basis due to the fact that high SERs are dominated by low UE link powers. In this situation, we show that the SNR/SINR of the ZF/MRC receivers can become very similar.

Chapter VII

Low Complexity MRC V-BLAST Based on Channel Norm Ordering with Adaptive Modulation and Power Control

7.1 Introduction

In this chapter, we consider the low complexity V-BLAST receiver using MRC and a single channel norm ordering (C-V-BLAST) proposed in Chapter 6. We evaluate its performance in the presence of imperfect CSI in an uplink MM deployment with a co-located BS array and distributed single antenna UEs. This receiver has shown promising performance in Chapter 6 for a simple fixed transmit power, fixed modulation scenario. In this chapter, we explore the performance of C-V-BLAST with both PC and AM.

PC with SIC was studied in [72], and PC with V-BLAST detection was studied in [113]. In these works, ZF and MMSE combining are considered. However, MRC which is used in C-V-BLAST was not considered. Some work is now emerging for PC with MM [114, 115]. These studies focus on PC for downlink [114] and uplink systems [115] without adaptive modulation, which is a key component of the system in this chapter. There is little previous work on V-BLAST based approaches to MM since these structures are usually considered too complex, However, in Chapter 6 it was shown that the C-V-BLAST approach based on a single up-front ordering based on channel norms, standard V-BLAST cancellation and an MRC was an order of magnitude less complex than a linear ZF combiner. Results in Chapter 6 also showed that

for MM systems the C-V-BLAST approach could achieve a similar performance to a linear ZF receiver and also to conventional ZF V-BLAST. These results were limited to QPSK modulation and perfect CSI and are extended in this chapter.

The main contributions of the chapter are as follows

- We develop an idealized bound for PC performance by developing an exhaustive search procedure for the AM system which maximizes the number of transmitted bits.

- We evaluate the performance of the promising low-complexity receiver (C-V-BLAST) in a more realistic system environment including AM and imperfect CSI.

- We show that C-V-BLAST can achieve similar performance to a linear ZF receiver with low complexity and without the need for additional PC.

The system model and details of the adaptive modulation are given in Section 7.2 and 7.3, respectively. Sections 7.4, 7.5, 7.6 and 7.7 provide the PC method for adaptive modulation, analysis, results and conclusions.

7.2 System Model

We consider the system model in Section 2.7 and the imperfect CSI structure

$$\hat{\mathbf{H}} = r_0\mathbf{H} + \sqrt{1 - r_0^2}\mathbf{E}, \tag{7.1}$$

where r_0 is the correlation coefficient between the true channel, $\mathbf{H}$, and the estimated channel, $\hat{\mathbf{H}}$, and $\mathbf{E}$ has the same statistics as $\mathbf{H}$. We assume that the UEs are located randomly in a circular coverage area of radius $\breve{R}$ surrounding the co-located BS array. The link gain P_j is calculated as in (2.11), $P_j = AL_j d_j^{-\gamma}$, where j identifies the UEs, A is a constant depending

on transmit power, antenna height, etc., L_j is a lognormal shadow fading variable, d_j is the link distance and γ is the path loss exponent.

We also consider an exclusion zone radius, R_0, such that $d_j > R_0$ to prevent UEs being too close to the BS. In the absence of power control, we assume the transmitted symbol $\mathbf{x}$ is given as in Section 2.7, i.e., $\mathrm{E}[|x_j|^2] = 1$. With power control, each UE transmits $\sqrt{\alpha_j}x_j$, i.e. user j scales the data, x_j, by $\sqrt{\alpha_j}$, where $0 \leq \alpha_j \leq 1$. The received signal can be written as

$$\mathbf{y} = \mathbf{H}\mathbf{x} + \mathbf{n} = \sum_{j=1}^{N_t} \mathbf{h}_j \sqrt{\alpha_j} x_j + \mathbf{n}, \tag{7.2}$$

where $\mathbf{n}$ is a noise vector with $n_i \sim \mathcal{CN}(0, \sigma^2)$. The SINR for the m^{th} user using linear combining is calculated using a simple variation of (2.31) [68] as

$$\mathrm{SINR}_m = \frac{\mathrm{E}[|\mathbf{w}_m^H r_0 \hat{\mathbf{h}}_m \sqrt{\alpha_m} x_m|^2]}{\mathrm{E}[|\mathbf{w}_m^H (\sqrt{1 - r_0^2}\mathbf{e}_m \sqrt{\alpha_m} x_m + \sum_{j \neq m} \mathbf{h}_j \sqrt{\alpha_j} x_j + \mathbf{n})|^2]}. \tag{7.3}$$

We consider a simple linear receiver (ZF) and the C-V-BLAST approach given in Chapter 6.

7.3 Adaptive Modulation

Due to the continuous fluctuation of the wireless channel, AM can be used to improve the performance of the system. Here, we assume that each UE selects from seven modulation options: outage, BPSK, QPSK, 8-PSK, 16-QAM, 32-QAM and 64-QAM based on the estimated SINR. Based on the discussion in Section 2.11, the SINR thresholds for this AM scheme can be derived and are given in Table 7.1 for a target BER of 10^{-3}. These thresholds make the assumption that interference, estimation error and noise can be approximated by additive white Gaussian noise.

Table 7.1: Modulation switching thresholds for a target BER value (from [2], see Section 2.11).

Modulation	**Bits**	**Modulation switching thresholds**
	#	Target BER = 10^{-3}
Outage	0	$0 \leq \text{SINR} < 4.8$
BPSK	1	$4.8 \leq \text{SINR} < 9.6$
QPSK	2	$9.6 \leq \text{SINR} < 30.1$
8-PSK	3	$30.1 \leq \text{SINR} < 45.1$
16-QAM	4	$45.1 \leq \text{SINR} < 90.8$
32-QAM	5	$90.8 \leq \text{SINR} < 179.9$
64-QAM	6	$179.9 \leq \text{SINR}$

7.4 Power Control For Adaptive Modulation

Here, we derive an exhaustive search algorithm for PC with V-BLAST. A slightly simpler form also holds for ZF. In order to implement AM the BS estimates the SINR of the UEs and feeds back the modulation levels to the UEs using Table 7.1. The SINR evaluation at the m^{th} V-BLAST stage assumes that there are no errors in detection in the first $m-1$ stages. For ease of notation, the ordered set of UEs $\{k_1, k_2, \ldots, k_{N_t}\}$ for V-BLAST detection is assumed to be $\{1, 2, \ldots, N_t\}$ so that the UEs are labeled in terms of decreasing channel norms. With this notation, user m is detected at stage m and its SINR, from (7.3), is given by

$$\text{SINR}_m = \frac{\alpha_m S_m}{\alpha_m E_m + \sum_{j=m+1}^{N_t} \alpha_j I_{mj} + N_m}, \tag{7.4}$$

where $S_m = r_0^2 \mathbf{w}_m^H \hat{\mathbf{h}}_m \hat{\mathbf{h}}_m^H \mathbf{w}_m$, $E_m = (1 - r_0^2) \mathbf{w}_m^H \mathbf{e}_m \mathbf{e}_m^H \mathbf{w}_m$, $I_{mj} = \mathbf{w}_m^H \mathbf{h}_j \mathbf{h}_j^H \mathbf{w}_m$, $N_m = \mathbf{w}_m^H \mathbf{w}_m / \rho$ and $\rho = 1/\sigma^2$. Note that the BS can only obtain $\hat{\mathbf{H}}$ so that I_{mj} and E_m, which involve knowledge of the true channel, are not known. However, since we are interested in the maximum performance improvement possible due to power control, we allow the use of (7.4) in the power control process. With the available information, optimal power control will adjust the

transmit powers of the UEs (varying $\alpha_1, \alpha_2, \ldots, \alpha_{N_t}$) so that $\mathrm{SINR}_1, \mathrm{SINR}_2, \ldots, \mathrm{SINR}_{N_t}$ corresponds to the maximum total number of transmitted bits from the N_t UEs using Table 7.1. Note that any SINR that lies between the modulation switching thresholds corresponds to wasted power. Hence, without loss of generality, the only SINR values of interest in power control use the seven thresholds in Table 7.1, i.e., the thresholds in the set $\mathcal{T} = \{0, 4.78, \ldots, 179.89\}$. This makes the exhaustive search for $\alpha_1, \alpha_2, \ldots, \alpha_{N_t}$ finite. Setting SINR_m equal to T_m, where $T_m \in \mathcal{T}$, gives

$$\alpha_m(S_m - T_m E_m) - \sum_{j=m+1}^{N_t} \alpha_j T_m I_{mj} = T_m N_m. \tag{7.5}$$

Define $\beta_m^{(m)} = S_m - T_m E_m$ and $\beta_j^{(m)} = -T_m I_{mj}$, then (7.5) becomes $\alpha_m(\beta_m^{(m)}) + \sum_{j=m+1}^{N_t} \alpha_m \beta_j^{(m)} = T_m N_m$. In compact form, we can write (7.5) for all N_t stages as

$$\begin{bmatrix} \beta_1^{(1)} & \beta_2^{(1)} & \ldots & \beta_{N_t}^{(1)} \\ 0 & \beta_2^{(2)} & \ldots & \beta_{N_t}^{(2)} \\ 0 & 0 & \ldots & \\ 0 & 0 & 0 & \beta_{N_t}^{(N_t)} \end{bmatrix} \begin{bmatrix} \alpha_1 \\ . \\ . \\ \alpha_{N_t} \end{bmatrix} = \begin{bmatrix} T_1 N_1 \\ T_2 N_2 \\ . \\ T_{N_t} N_{N_t} \end{bmatrix}. \tag{7.6}$$

If (7.6) is soluble and leads to a solution where each $0 \leq \alpha_i \leq 1$, then this set of thresholds is feasible and corresponds to a certain number of transmitted bits. Hence, power control can in principle be achieved by an exhaustive search over all possible thresholds for all UEs. For each possibility, (7.6) is checked for feasibility and the maximum number of feasible transmitted bits is recorded. Of course, this is computationally intensive involving a search over $n_M^{N_t}$ possibilities (n_M = # of modulations). Hence, this gives an upper bound on power control performance rather than a practical methodology.

$$
\begin{aligned}
F(p) &= 1 - F_G\left(\frac{w_1}{\sigma_{SF}}\right) + \frac{\breve{R}^2}{\breve{R}^2 - R_0^2}\Bigg[\left\{F_G\left(\frac{w_1}{\sigma_{SF}}\right) - F_G\left(\frac{w_0}{\sigma_{SF}}\right)\right\} \\
&- \left(\frac{A}{p}\right)^{\frac{2}{\gamma}} e^{\left(\frac{2\sigma_{SF}^2}{\gamma^2}\right)}\left\{F_G\left(\frac{w_1 + 2\sigma_{SF}^2/\gamma}{\sigma_{SF}}\right) - F_G\left(\frac{w_0 + 2\sigma_{SF}^2/\gamma}{\sigma_{SF}}\right)\right\}\Bigg] \qquad (7.7) \\
f(p) &= \frac{1}{\sigma_{SF}}\Bigg[f_G\left(\frac{w_1}{\sigma_{SF}}\right) + \frac{\breve{R}^2}{\breve{R}^2 - R_0^2}\left\{-f_G\left(\frac{w_1}{\sigma_{SF}}\right) + f_G\left(\frac{w_0}{\sigma_{SF}}\right)\right\} \\
&- \left(\frac{A}{p}\right)^{\frac{2}{\gamma}} e^{\left(\frac{2\sigma_{SF}^2}{\gamma^2}\right)}\left\{-f_G\left(\frac{w_1 + 2\sigma_{SF}^2/\gamma}{\sigma_{SF}}\right) + f_G\left(\frac{w_0 + 2\sigma_{SF}^2/\gamma}{\sigma_{SF}}\right)\right\}\Bigg] \\
&+ \frac{2}{\gamma} A^{\frac{2}{\gamma}} p^{\frac{-2-\gamma}{\gamma}} e^{\left(\frac{2\sigma_{SF}^2}{\gamma^2}\right)}\left\{F_G\left(\frac{w_1 + 2\sigma_{SF}^2/\gamma}{\sigma_{SF}}\right) - F_G\left(\frac{w_0 + 2\sigma_{SF}^2/\gamma}{\sigma_{SF}}\right)\right\} \qquad (7.8)
\end{aligned}
$$

7.5 Analysis

It is well known that V-BLAST performance is enhanced when there are large differences between the SINRs of the UEs as discussed in Chapter 6. This is strongly related to power control. If the UEs have similar SINRs power control can be used to artificially separate them, whereas if they are very distinct already, power control may not be necessary. The largest factor affecting the SINRs of the UEs is the long term power. Hence, we consider the order statistics of the link gains to investigate the size of the difference between UEs. The CDF of P_j is given by (7.7) [94, equation (6)], where $F_G(.)$ is the CDF of a standard Gaussian, The parameters in (7.7) are $w_0 = \ln(w\breve{R}^{-\gamma})$, $w_1 = \ln(wR_0^{-\gamma})$ and $w = A/p$. Differentiating (7.7) gives the PDF as in (7.8), where $f_G(.)$ is the PDF of a standard Gaussian. Since $P_1 \ldots P_{N_t}$ are N_t independent variates, each with CDF $F(p)$, then $P_{(1)} < P_{(2)} < \cdots < P_{(N_t)}$ are the order statistics and $P_{(j)}$ has PDF $f_{(j)}(p)$ given by [116, equations (2.1.6)]

$$
f_{(j)}(p) = C_j F^{j-1}(p)[1 - F(p)]^{N_t - j} f(p), \qquad (7.9)
$$

where $C_j = \frac{N_t!}{(j-1)!(N_t-j)!}$. Hence, using (7.7) and (7.8) in (7.9) provides a closed form solution for the PDFs of $P_{(j)}$.

7.6 Results

In this section, the baseline parameters are: $N_r = 64$, $N_t = 6$, $\rho = 0$ dB, $\gamma = 3$, $\sigma_{SF} = 8$ dB $r_0 = 1$, $\breve{R} = 1$, $R_0 = 0.01$ and $A = 0.015$. The value $A = 0.015$ is chosen to correspond to a reasonable level of performance such that the median SNR of ZF (M_{ZF}) is equal to 5 dB. Note that we use $N_t = 6$, which is rather small for MM, to make the complexity of the exhaustive power control search manageable.

The PDFs of $P_{(j)}$ computed from (7.9) are shown in Figure 7.1 for $j = \{1, 2, \ldots, 6\}$. The PDFs have been scaled to have the same maximum value to make a visual comparison possible. It is clear from Figure 7.1 that there are substantial differences in the means of the order statistics since the SINRs of the UEs are heavily dependent on the $P_{(j)}$'s. This suggests that there are likely to be large differences in the UE SINRs and in turn this suggests that power control may not have much impact on performance. This is supported by the results in Figures 7.2-7.4.

Figure 7.2 shows the CDF of the total number of transmitted bits for ZF, C-V-BLAST with no PC and C-V-BLAST with power control (labeled C-V-BLAST (PC)). Perfect CSI is assumed. Here, we see that C-V-BLAST with no PC performs a little worse than ZF but offers lower complexity. PC makes little difference as suggested by the analytical results in Figure 7.1. As M_{ZF} increases (i.e., A increases) the gap between ZF and C-V-BLAST with no PC also increases. This is the result of two key properties. First, with perfect CSI, ZF is noise limited and increased transmit power improves performance. Secondly, C-V-BLAST with no PC is interference limited, as it relies on MRC, and so is not helped so much by increased power.

Figure 7.3 shows similar results for the case of imperfect CSI, $r_0 = 0.9$. It is notable that here, C-V-BLAST with no PC performs better than ZF as well as having reduced complex-

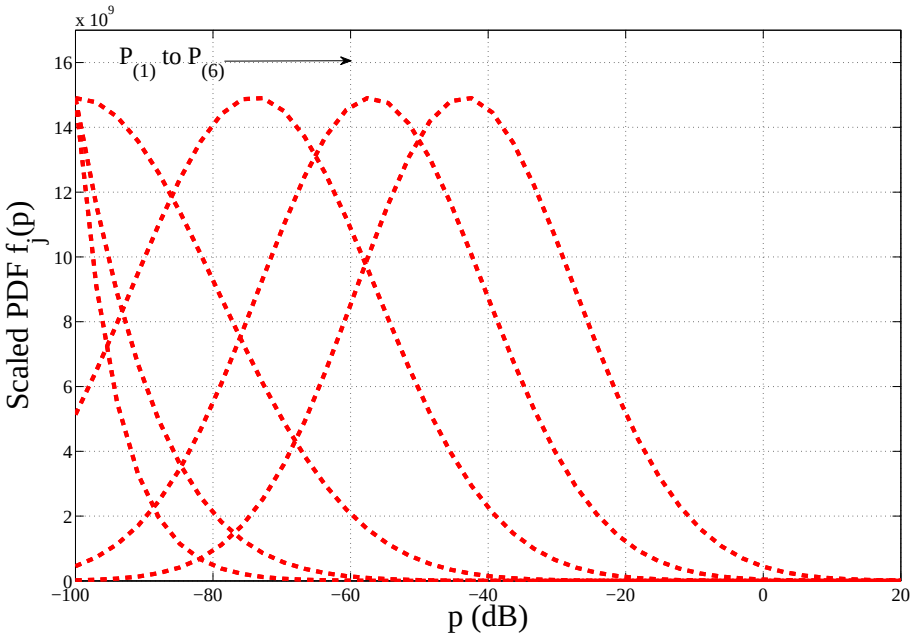

Figure 7.1: Scaled PDFs of the order statistics, $P_{(j)}$.

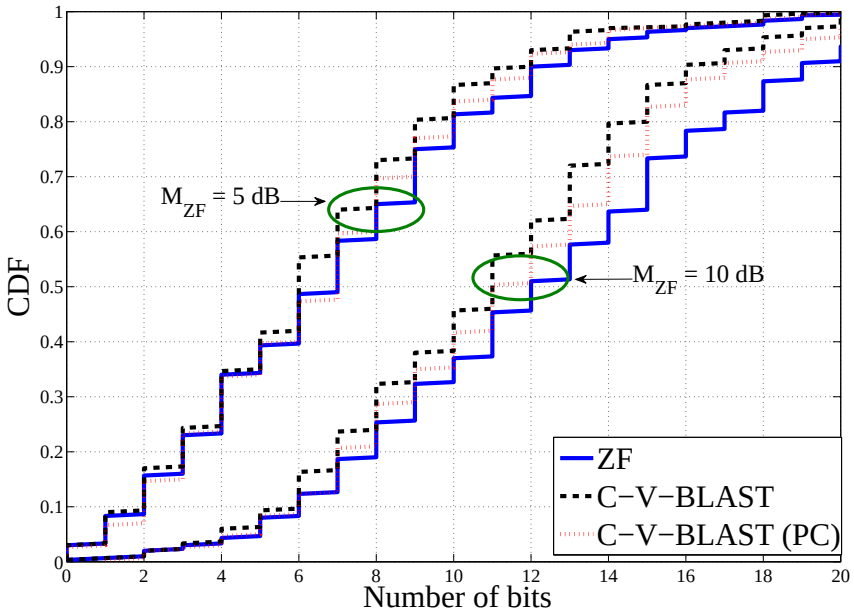

Figure 7.2: The CDF of the total number of bits under perfect CSI ($r_0 = 1$). The median SNR for ZF is $M_{\text{ZF}} \in \{5, 10\}$ dB.

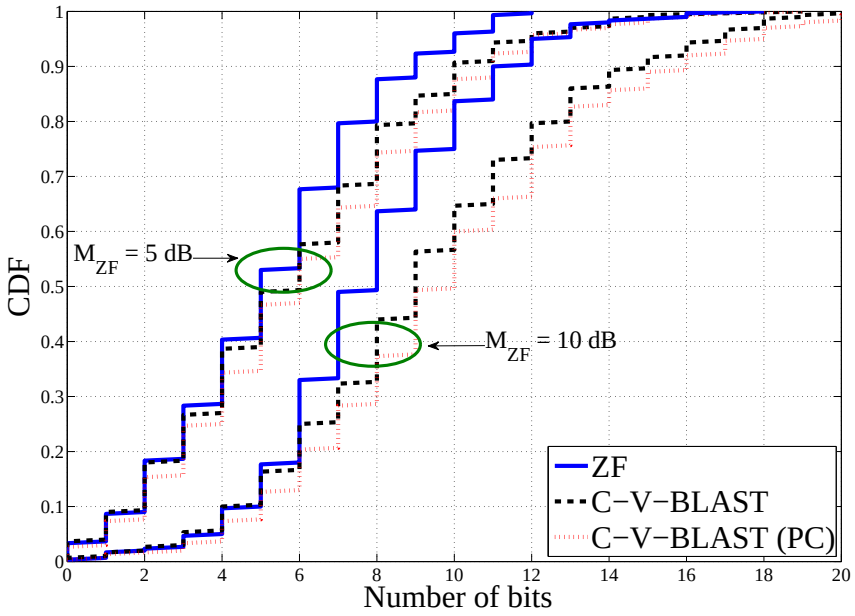

Figure 7.3: The CDF of the total number of bits under imperfect CSI ($r_0 = 0.9$). The median SNR for ZF is $M_{\text{ZF}} \in \{5, 10\}$ dB.

ity. This is because MRC is less sensitive to the introduction of the estimation error than ZF. Again, PC offers a small gain and the differences between receivers grows as the transmit power increases.

In Figure 7.4 the same CDFs are given using field measurements for the link gains. The data was obtained from a drive test of a suburban cell in a long term evolution (LTE) network. Link gains were measured over a drive route covering an entire cell using equipment in the vehicle to measure received signal strength at a mobile. The measured link gains were then randomly sampled to create a drop of $N_t = 6$ link gains and this was repeated 300 times. For equivalence with Figure 7.2-7.3 and for confidentiality reasons, the link gains are scaled so that $M_{\text{ZF}} = 10$ dB. Here also, we observe the limited impact of PC and a small performance gap between C-V-BLAST with no PC and ZF which tends to disappear with imperfect CSI. In all the results shown, the improvement in the total number of bits transmitted is less than 1 bit on average.

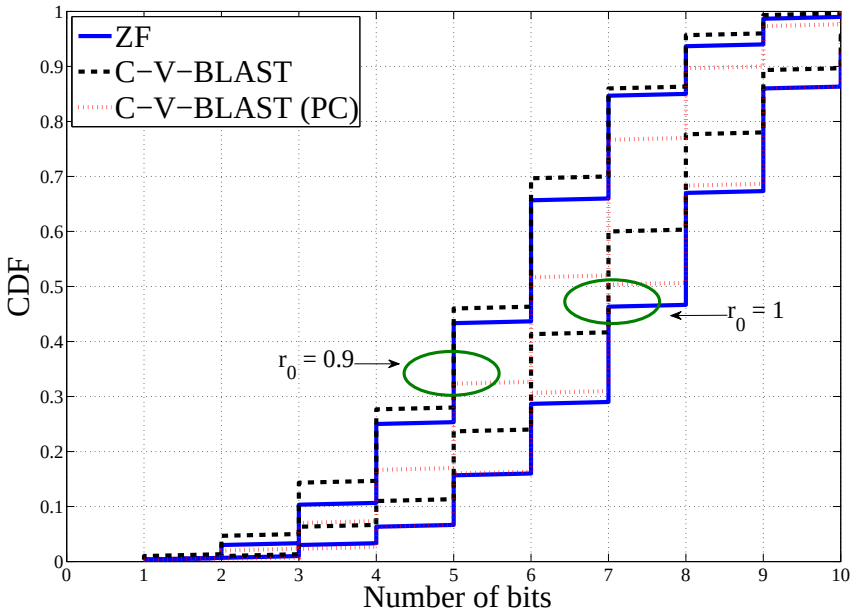

Figure 7.4: The CDF of the total number of bits using field data for the link gains with $M_{\mathrm{ZF}} = 10$ dB. The channel accuracy: $r_0 \in \{1, 0.9\}$.

7.7 Summary

The C-V-BLAST receiver is known to have reduced complexity compared to standard ZF. In this chapter, we have also investigated its performance in terms of throughput in an AM system. Here, we show that the performance loss relative to ZF is small for perfect CSI and that C-V-BLAST can potentially provide both complexity reduction and performance improvement when the CSI is imperfect. In addition, gains due to PC are limited and so C-V-BLAST is a promising option, without the need for additional PC.

Chapter VIII

Analysis of Low Complexity MRC V-BLAST based on Link Gain Ordering

8.1 Introduction

With the advent of MM, receiver complexity is becoming critical and in this chapter our focus is on further reducing the complexity of the V-BLAST receivers developed and analyzed in Chapters 5-7. We consider an uplink MM deployment with either a co-located or distributed BS array and distributed single antenna UEs. Note that distributed scenarios in this chapter include both the BBS deployment and the fully distributed (DIST) deployment.

As we discussed in Chapter 5 and Chapter 6, very little work has appeared on V-BLAST with MM since computationally efficient receiver structures are essential to make MM viable. Conventional V-BLAST requires repeated detection and reordering. Furthermore, most work on traditional V-BLAST considers the use of ZF or MMSE detection. Hence, traditional V-BLAST is too computationally intensive for MM. However, by replacing ZF or MMSE receivers by MRC and using a one-shot ordering method based on channel norms, a V-BLAST scheme was proposed in Chapter 6 which has lower complexity than linear ZF detection and similar performance. This system is denoted C-V-BLAST. Note that the use of both MRC and the single ordering technique was needed in Chapter 6 to produce the complexity reduction relative to a linear ZF receiver. Here, we propose a variation on C-V-BLAST where the ordering is simplified

further by using the long term powers or link gains rather than the instantaneous channel norms. This approach is denoted P-V-BLAST and analysis of this system leads to a remarkably simple and comprehensive error rate evaluation for both co-located and distributed arrays. The P-V-BLAST approach also opens up other possibilities for system gains as discussed in Section 8.3.

There is considerable related analytical work in the V-BLAST literature [44, 104, 117–121], but not of direct relevance to the P-V-BLAST system with MM. For example, most work considers ZF in the detection stage [44, 104, 117–121] and much of the work neglects ordering [44, 117, 120]. Due to the difficulties of V-BLAST analysis, most of the results are bounds [44, 104, 118] and some make restrictions to 2 UEs [44, 119] to develop closed form results. Error propagation is handled to at least some extent in [104, 117, 119, 120]. In this chapter, the use of MRC and a single deterministic ordering makes analytic progress more tractable. The MM context both simplifies and hinders the analysis as discussed in Sections 8.4 and 8.5. The main technical difficulty introduced by MM is the lack of numerical stability in established analytical approaches. Hence, we develop novel approximate techniques which are accurate and stable.

The main contributions in this chapter are as follows:

- We propose a simplified ordering scheme compared to the low complexity V-BLAST receiver in Chapter 6.

- We evaluate the probability of disagreement between the channel norm based ordering in Chapter 6 (C-V-BLAST) and our proposed ordering based on link gains (P-V-BLAST) for both co-located and distributed arrays.

- Based on the new ordering scheme, we derive a simple, accurate, closed form approximation to the error rate of P-V-BLAST for both co-located and distributed arrays.

- The analysis also provides an approximation to the SER of an MRC receiver which is useful in MM for both co-located and distributed arrays.

- We show that the performance of a distributed array can be approximated by an equivalent co-located array and derive this equivalence.

The rest of the chapter is organized as follows. Section 8.2 introduces the system model. Section 8.3 a gives an overview of the proposed low complexity receiver. Section 8.4 and Section 8.5 provide an analysis of the P-V-BLAST error rate and the accuracy of the ordering method, respectively. We give simulation results in Section 8.6 and conclude in Section 8.7.

8.2 System Model

We consider the system model in Section 2.7, where

$$\mathbf{y} = \mathbf{H}\mathbf{x} + \mathbf{n} = \sum_{m=1}^{N_t} \mathbf{h}_m x_m + \mathbf{n}, \tag{8.1}$$

and $\mathbf{H}$, $\mathbf{x}$ and $\mathbf{n}$ are the channel, signal vector and noise, respectively. We assume perfect CSI and the SINR can be calculated as in (2.30). Let the noise power be $\sigma^2 = 1$. We focus on MRC receivers within a low complexity V-BLAST structure (similar to C-V-BLAST) and also compare MRC to ZF.

8.2.1 Deployment

MM can result from a large number of antennas deployed at one location or from an array of distributed antennas linked together to form a massive network MIMO system. Hence, the following scenarios are considered.

- *Scenario 1*: one massive co-located array.

- *Scenario 2*: B-collaborative base stations with multiple antennas at each BS (BBS).

In each scenario, the UEs are located randomly in the coverage area (assumed to be a circle for simplicity). For all scenarios, the channel coefficient h_{ij} can be calculated as in (2.9), so that $h_{ij} = \sqrt{P_{ij}}U_{ij}$ where U_{ij} is the fast fading term. In addition, for each scenario, the corresponding link gains are calculated as shown in Section 2.6.5, where $P_{ij} = AL_{ij}d_{ij}^{-\gamma}$ and A is a constant depending on transmit power, antenna height, etc., L_{ij} is a lognormal shadow fading variable, d_{ij} is the link distance and γ is the path loss exponent.

8.3 P-V-BLAST

With MM, it is shown in Section 8.5 that ordering based on the instantaneous channels (as in (6.2)) is very similar to ordering based on the link gains or long term channel powers. This motivates us to define an alternative, simplified ordering scheme. Assume the ordered set $S^{(P)} = \{k_1^{(P)}, k_2^{(P)}, \ldots, k_{N_t}^{(P)}\}$ decides the order in which the transmitted symbols in $\mathbf{x}$ are detected [66]. The simplified ordering scheme based on long term powers is defined by

$$k_i^{(\mathrm{P})} = \underset{j \notin \{k_1, k_2, \ldots, k_{i-1}\}}{\arg\max} \left(\sum_{r=1}^{N_r} P_{rj}\right). \tag{8.2}$$

The V-BLAST MRC receiver using the single power ordering in (8.2) is denoted P-V-BLAST. Note that P-V-BLAST is simply C-V-BLAST using ordering based on the mean column norms rather than the instantaneous values. The complexity is somewhat lower than C-V-BLAST as the column norms are not required but it has the same order $(O(N_r N_t))$. Other potential advantages exist since ordering and potentially scheduling can be performed based only on the long term channel powers which are quicker and easier to obtain. For example, with P-V-BLAST the ordering can be performed as soon as the link gains are available. Also, it is possible that mean SINR values could be used for scheduling and other link control functions [122,

123]. These mean values are solely functions of the link gains and hence, scheduling, power adaptation, rate adaptation, etc. can all be performed more rapidly with P-V-BLAST. Hence, the P-V-BLAST structure may have further advantages beyond a lower complexity compared to C-V-BLAST.

8.4 P-V-BLAST Error Analysis

In this section, we derive the error rate for P-V-BLAST. We consider the group error probability defined by $P_G = P(K \geq 1)$, where K is the number of UEs in the group of N_t UEs that are incorrectly detected. Hence,

$$\begin{aligned} P_G &= 1 - P\left(\text{no errors for the } N_t \text{ UEs}\right) \\ &= 1 - P(s_1) \prod_{i=2}^{N_t} P(s_i | s_1, s_2, \ldots, s_{i-1}), \end{aligned} \tag{8.3}$$

where s_i denotes the event that the UE detected in the i^{th} V-BLAST stage is detected correctly. Note that error propagation [104] does not affect P_G since the group error rate corresponds to 100% error propagation [44]. For standard MIMO systems the conditioning in (8.3) makes analysis very complex. The dependence on $s_1, s_2, \ldots, s_{i-1}$ is complicated as successful detection in the first $i-1$ stages has a subtle impact on s_i. More importantly, with standard V-BLAST, ordering is performed after each detection and the UE to be detected at stage i is variable.

With MM, both of these complications become less important. First, the SINR values in (2.30) become less variable due to the averaging effect of large numbers of antennas. This reduces the effect of conditioning on the probability of error. Secondly, with large numbers of antennas the ordering of UEs becomes very similar to ordering based on the link gains (see Section 8.5). This is a deterministic ordering and allows the UE to be detected at stage i to be

identified in advance. Hence, we approximate (8.3) by

$$P_G \approx 1 - \prod_{i=1}^{N_t} P(s_i), \tag{8.4}$$

where UE $k_i^{(\mathrm{P})}$ is detected at stage i with $k_i^{(\mathrm{P})}$ defined by (8.2). Note that $(1 - P(s_i))$ is the standard SER for detecting UE $k_i^{(\mathrm{P})}$ with MRC in the presence of interferers $k_{i+1}^{(\mathrm{P})}, k_{i+2}^{(\mathrm{P})}, \ldots, k_{N_t}^{(\mathrm{P})}$. Hence, we now develop SER results for MRC with interference.

8.4.1 General Symbol Error Rate Formulation

For ease of notation, consider the SER of the first UE to be detected and assume, without loss of generality, that $k_1^{(\mathrm{P})} = 1$. The SER for QPSK modulation can be calculated using [124, equation (50)]

$$\mathrm{SER} = 2\mathrm{E}[Q(\sqrt{\bar{\gamma}})] - \mathrm{E}[Q^2(\sqrt{\bar{\gamma}})], \tag{8.5}$$

where $Q(.)$ is the Gaussian Q-function and

$$\bar{\gamma} = \frac{\left(\mathbf{h}_1^H \mathbf{h}_1\right)^2}{\mathbf{h}_1^H \left(\sum_{j=2}^{N_t} \tilde{\mathbf{P}}_j + \sigma^2 \mathbf{I}\right) \mathbf{h}_1}. \tag{8.6}$$

In (8.6), $\tilde{\mathbf{P}}_j = \mathrm{diag}(P_{1j}, P_{2j}, \ldots P_{N_r j})$. Using the notation, $\mathbf{h}_1 = \tilde{\mathbf{P}}_1^{1/2} \mathbf{u}_1$, where the elements of $\mathbf{u}_1$ are i.i.d. $\mathcal{CN}(0,1)$, $\bar{\gamma}$ in (8.6) can be written as

$$\bar{\gamma} = \frac{\left(\mathbf{u}_1^H \tilde{\mathbf{P}}_1 \mathbf{u}_1\right)^2}{\mathbf{u}_1^H \tilde{\mathbf{P}}_1^{1/2} \left(\sum_{j=2}^{N_t} \tilde{\mathbf{P}}_j + \sigma^2 \mathbf{I}\right) \tilde{\mathbf{P}}_1^{1/2} \mathbf{u}_1}. \tag{8.7}$$

8.4.2 Symbol Error Rate Calculation for Co-located Scenario

In the co-located scenario $\tilde{\mathbf{P}}_j = P_j\mathbf{I}$ and (8.6) collapses to

$$\bar{\gamma} = P_1\hat{t}/I_f, \tag{8.8}$$

where I_f is the interference and noise power, $I_f = \sum_{j=2}^{N_t} P_j + \sigma^2$ and $\hat{t} = \mathbf{u}_1^H\mathbf{u}_1$ has a complex chi-squared distribution with $2N_r$ DOF. Hence, (8.5) becomes

$$\begin{aligned} \text{SER} &= 2\text{E}\left[Q\left(\sqrt{\frac{P_1}{I_f}\hat{t}}\right)\right] - \text{E}\left[Q^2\left(\sqrt{\frac{P_1}{I_f}\hat{t}}\right)\right], \\ &= 2\int_0^\infty \frac{Q\left(\sqrt{\bar{b}\hat{t}}\right)\hat{t}^{N_r-1}e^{-\hat{t}}}{\Gamma(N_r)}d\hat{t} - \int_0^\infty \frac{Q^2\left(\sqrt{\bar{b}\hat{t}}\right)\hat{t}^{N_r-1}e^{-\hat{t}}}{\Gamma(N_r)}d\hat{t}, \end{aligned} \tag{8.9}$$

where $\bar{b} = P_1/I_f$ and $\Gamma(.)$ is the gamma function. The SER in (8.9) is known (see [125–127]) and for low SER values the first term in (8.9) is often used as an approximation or upper bound. Hence, we can write [126]

$$\text{SER} \leq 2\left(\frac{1-\mu_c}{2}\right)^{N_r}\sum_{k=0}^{N_r-1}\binom{N_r-1+k}{k}\left(\frac{1+\mu_c}{2}\right)^k, \tag{8.10}$$

where $\mu_c = \bar{\gamma}_c/(1+\bar{\gamma}_c)$ and $\bar{\gamma}_c = 0.5P_1/(\sigma^2 + \sum_{j=2}^{N_t} P_j)$. We can also use (8.10) for the no interference case with $\mu_c = 0.5P_1/\sigma^2$. This occurs in the final V-BLAST stage. This analysis can be easily extended to M-QAM modulation. Note that the second integral in (8.9) can be found in [126] and involves a sum of hypergeometric functions. Unfortunately, for MM the arguments of the hypergeometric functions become large and the result is unstable. Hence, in Section 8.6 the numerical results use a numerical integral to evaluate (8.9) whereas the closed form bound in (8.10) can be used as it remains stable for MM.

Also note that the case of imperfect CSI is easily handled as [128] shows that imperfect CSI

simply scales the SNR for an MRC receiver. Hence, (8.9) and (8.10) can still be used for the imperfect CSI case with a suitable alteration to $\bar{\gamma}_c$.

8.4.3 Symbol Error Rate Calculation for Distributed Scenario

In principle, the SER for the distributed case can be calculated using the approach in [124] for QPSK modulation. However, in practice there will be numerical problems that occur for large systems. Each component of the SER expression in [124] requires the summation of $N_r(N_r-1)$ terms with oscillating signs and a huge range of magnitudes. For example, the simplest SER result in [124] is of the form

$$P_s = \sum_{i=1}^{N_r} \sum_{k \neq i}^{N_r} P_{s_{ik}}, \tag{8.11}$$

using the notation in [124]. Hence, there are $N_r(N_r-1)$ terms in the expression. Furthermore, each $P_{s_{ik}}$ is a function of

$$\xi_{ik} = \frac{P_{i1}^{N_r-2} \upsilon_{ik}^{N_r-3}}{\prod_{l \neq i,k}^{N_r} (\upsilon_{ik}\nu_{il} - \nu_{ik}\upsilon_{il})}, \tag{8.12}$$

again using the notation in [124]. The denominator of (8.12) is a function of the link gains and can be positive or negative, small or large. As a result, the terms in (8.11) oscillate and vary enormously in size. This expression is inherently unstable for large numbers of antennas. Therefore, we propose an approximation for the SER calculation. From (8.7), $\bar{\gamma}$ can be written as

$$\bar{\gamma} = \frac{\left(\mathbf{u}_1^H \tilde{\mathbf{P}}_1 \mathbf{u}_1\right)^2}{\mathbf{u}_1^H \tilde{\mathbf{P}}_1^{1/2} \tilde{\mathbf{Q}} \tilde{\mathbf{P}}_1^{1/2} \mathbf{u}_1}, \tag{8.13}$$

where $\tilde{\mathbf{Q}} = \left(\sum_{j=2}^{N_t} \tilde{\mathbf{P}}_j + \sigma^2 \mathbf{I}\right)$. Note that $\tilde{\mathbf{Q}}$ is a diagonal matrix with entries $\tilde{Q}_{11}, \ldots \tilde{Q}_{N_r N_r}$. Now define $\bar{q} = 1/N_r \sum_{i=1}^{N_r} \tilde{Q}_{ii}$ as the average diagonal element and write

$$\tilde{\mathbf{Q}} = \bar{q}\mathbf{I} + \tilde{\mathbf{E}}, \tag{8.14}$$

where $\tilde{\mathbf{E}}$ is a diagonal matrix with entries $\tilde{E}_{11}, \ldots \tilde{E}_{N_r N_r}$ and $\tilde{E}_{ii} = \tilde{Q}_{ii} - \bar{q}$. Thus,

$$\begin{aligned}
\frac{1}{\bar{\gamma}} &= \frac{\mathbf{u}_1^H \tilde{\mathbf{P}}_1^{1/2} \left(\bar{q}\mathbf{I} + \tilde{\mathbf{E}}\right) \tilde{\mathbf{P}}_1^{1/2} \mathbf{u}_1}{\left(\mathbf{u}_1^H \tilde{\mathbf{P}}_1 \mathbf{u}_1\right)^2}, \\
&= \frac{\bar{q}}{\left(\mathbf{u}_1^H \tilde{\mathbf{P}}_1 \mathbf{u}_1\right)} + \frac{\mathbf{u}_1^H \tilde{\mathbf{P}}_1^{1/2} \tilde{\mathbf{E}} \tilde{\mathbf{P}}_1^{1/2} \mathbf{u}_1}{\left(\mathbf{u}_1^H \tilde{\mathbf{P}}_1 \mathbf{u}_1\right)^2}, \\
&= \frac{\bar{q}}{\left(\mathbf{u}_1^H \tilde{\mathbf{P}}_1 \mathbf{u}_1\right)} \left(1 + \frac{\mathbf{u}_1^H \tilde{\mathbf{P}}_1^{1/2} \tilde{\mathbf{E}} \tilde{\mathbf{P}}_1^{1/2} \mathbf{u}_1}{\bar{q} \mathbf{u}_1^H \tilde{\mathbf{P}}_1 \mathbf{u}_1}\right). \qquad (8.15)
\end{aligned}$$

The second term in (8.15) is the complicating factor as it contains a ratio of quadratic forms. For MM systems, these quadratic forms involve the sum of a large number of squared terms (N_r). Dividing the numerator and denominator by N_r gives the quotient as a ratio of averages. These averages converge in probability to their mean values as $N_r \to \infty$ using the weak law of large numbers [129, page 71]. A sufficient condition required for this convergence is that the diagonal elements of $\tilde{\mathbf{P}}_1$ and $\tilde{\mathbf{E}}\tilde{\mathbf{P}}_1$ are bounded which must be satisfied by any real system. Hence, we propose the approximation

$$\bar{\gamma} \approx \frac{\mathbf{u}_1^H \tilde{\mathbf{P}}_1 \mathbf{u}_1}{\tilde{k}\bar{q}}, \qquad (8.16)$$

where

$$\tilde{k} = 1 + \frac{\mathrm{E}\left[\mathbf{u}_1^H \tilde{\mathbf{P}}_1^{1/2} \tilde{\mathbf{E}} \tilde{\mathbf{P}}_1^{1/2} \mathbf{u}_1\right]}{\bar{q}\mathrm{E}\left[\mathbf{u}_1^H \tilde{\mathbf{P}}_1 \mathbf{u}_1\right]} = 1 + \frac{\mathrm{Tr}(\tilde{\mathbf{P}}_1 \tilde{\mathbf{E}})}{\bar{q}\mathrm{Tr}(\tilde{\mathbf{P}}_1)}, \qquad (8.17)$$

and $\mathrm{Tr}(.)$ is the trace operator. Note that (8.16) is almost identical to the co-located form of $\bar{\gamma}$ (8.8) since (8.16) is a scaled quadratic form while (8.8) is a scaled chi-squared (a special case of a quadratic form). At first sight, this difference appears minor as $\mathbf{u}_1^H \tilde{\mathbf{P}}_1 \mathbf{u}_1$ is a simple linear combination of chi-squared variables. However, we demonstrate in the next section the numerical difficulty in obtaining the PDF of $\mathbf{u}_1^H \tilde{\mathbf{P}}_1 \mathbf{u}_1$. As a result, we employ a simple chi-

squared approximation to $\mathbf{u}_1^H\tilde{\mathbf{P}}_1\mathbf{u}_1$ defined by $\mathbf{u}_1^H\tilde{\mathbf{P}}_1\mathbf{u}_1 \approx \bar{p}_1\mathbf{u}_1^H\mathbf{u}_1 = \bar{p}_1\hat{t}$, where $\hat{t}$ is chi-squared with $2N_r$ DOF and $\bar{p}_1 = 1/N_r\sum_{i=1}^{N_r} P_{i1}$ is the average diagonal element of $\tilde{\mathbf{P}}_1$. This gives the final approximation

$$\bar{\gamma} \approx \frac{\bar{p}_1\hat{t}}{\tilde{k}\bar{q}}. \tag{8.18}$$

Not only does this approximation yield excellent SER results, it also expresses the performance metric for the distributed case in exactly the same form as the co-located version (8.8). Hence, distributed systems provide a simple shift in the SER curves relative to co-located performance as (8.18) is a scaled version of (8.8). Equating (8.18) and (8.8) gives the equivalent co-located parameters

$$P_1^{\text{eq}} = \bar{p}_1 \tag{8.19}$$

$$I_f^{\text{eq}} = \tilde{k}\bar{q} = \bar{q} + \text{Tr}(\tilde{\mathbf{P}}_1\tilde{\mathbf{E}})/\text{Tr}(\tilde{\mathbf{P}}_1). \tag{8.20}$$

Note that the equivalent link gain is simply the average of the distributed link gains (see (8.19)). Furthermore, from (8.20), the equivalent interference and noise is the average of the distributed interference and noise terms ($\bar{q}$) with a correction factor $\left(\text{Tr}(\tilde{\mathbf{P}}_1\tilde{\mathbf{E}})/\text{Tr}(\tilde{\mathbf{P}}_1)\right)$ that disappears in the co-located case. The simple approximation has the benefit of providing good SER results and an equivalent co-located system. However, much tighter approximations can be achieved using a gamma approximation [130] to $\bar{\gamma}$ in (8.16). This would give the correct mean and variance. However, since in MM the variance of (8.16) is small, the mean value dominates the results and this explains why (8.18) is so accurate in obtaining the SER. If the full distribution of $\bar{\gamma}$ is to be approximated closely, then the gamma approximation would be preferable.

8.5 Analysis of Ordering Methods

In this section, we derive the distribution of the column norms of the channel matrix, $\mathbf{H}$. This allows us to demonstrate that V-BLAST ordering based on long term powers is similar to the ordering based on instantaneous channel norms. Furthermore, the results motivate the approximation proposed in (8.18). We focus on evaluating the probability of disagreement between ordering based on C-V-BLAST (see (6.2)) and ordering based on P-V-BLAST (see (8.2)). Here, we consider two arbitrary UEs and evaluate whether the two ordering methods rank the UEs in the same order. The probability of disagreement depends on the powers of the UEs and will therefore vary across the UEs. The aim is to gain an indication of the similarity of the two ordering methods but the analysis also provides the PDF of $\bar{\gamma}$ in (8.16).

8.5.1 Co-located Scenario

Consider the co-located scenario and define the j^{th} column norm of $\mathbf{H}$ by

$$\sum_{i=1}^{N_r} |h_{ij}|^2 = \frac{P_j}{2} X_j, \tag{8.21}$$

where X_j has a standard chi-squared distribution with $2N_r$ DOF. Consider two columns of $\mathbf{H}$, i and j, where $P_i > P_j$. In this situation, the relative ordering of UEs i and j is different for the two ordering methods when $P_j X_j > P_i X_i$. The probability of disagreement is

$$\begin{aligned} P\left(P_j X_j > P_i X_i\right) &= P\left(\frac{X_j}{X_i} > \frac{P_i}{P_j}\right) && (8.22) \\ &= P\left(F > \frac{P_i}{P_j}\right) && (8.23) \\ &= 1 - I_q(N_r, N_r), && (8.24) \end{aligned}$$

where F is the ratio of two chi-squared variables and has an F distribution with $2N_r$ and $2N_r$ DOF [131, page 946]. Using the CDF of an F variable, (8.24) follows from (8.23) where $q = P_i/(P_i + P_j)$ and $I_q(.)$ is an incomplete beta function [131, page 263]. Note that the incomplete beta function in (8.24) can be written as a function of the binomial distribution such that [131, page 263]

$$\begin{aligned} I_q(N_r, N_r) &= \sum_{j=N_r}^{2N_r-1} \binom{2N_r-1}{j} q^j (1-q)^{2N_r-1-j} \\ &= P(X \geq N_r), \end{aligned} \tag{8.25}$$

where $X \sim \text{Binomial}(2N_r - 1, q)$. In the MM case, it is reasonable to use the normal approximation to the binomial distribution. This gives

$$\begin{aligned} P(X \geq N_r) &= P\left(\frac{X - (2N_r-1)q}{\sqrt{(2N_r-1)q(1-q)}} \geq \frac{N_r - (2N_r-1)q}{\sqrt{(2N_r-1)q(1-q)}}\right) \\ &\approx P\left(Z \geq \frac{Nr - (2N_r-1)q - 0.5}{\sqrt{(2N_r-1)q(1-q)}}\right) = Q(T), \end{aligned} \tag{8.26}$$

where $Z \sim \mathcal{N}(0, 1)$ and (8.26) is the standard normal approximation to a binomial tail probability using a continuity correction. In (8.26), $Q(.)$ is the Q-function and

$$T = \frac{N_r - (2N_r-1)q - 0.5}{\sqrt{(2N_r-1)q(1-q)}}. \tag{8.27}$$

Equation (8.27) gives a closed form link between a given probability of disagreement, defined by equating T to a percentile of Z, and two key parameters, N_r and q. For example, if the probability of disagreement is 5%, then $Q(T) = 95\%$ and T is the 5^{th} percentile of a standard Gaussian distribution which is -1.6449. Since $q = (1 + P_j/P_i)^{-1}$, (8.27) relates the probability of disagreement to array size (N_r) and the power differential (P_j/P_i). Solving (8.27) for the

required array size to give a probability of disagreement (controlled by T) for a given power differential gives

$$N_r = \frac{-T^2q^2 + T^2q + q^2 - q + 0.25}{2q^2 - 2q + 0.5}. \tag{8.28}$$

In other words, solving (8.27) for N_r allows us to identify the number of antennas required to give a probability of disagreement of $1 - Q(T)$ when the two UEs have a power differential of P_j/P_i. Further simplifications can be made by replacing $2N_r - 1$ in (8.27) by $2N_r$ and omitting the continuity correction. This is reasonable for large N_r and gives the simplified version of (8.28) as

$$N_r = \frac{2T^2 10^{\mathcal{Y}/10}}{(10^{\mathcal{Y}/10} - 1)^2}, \tag{8.29}$$

where $\mathcal{Y}$ is the power differential P_j/P_i, in dB. Results obtained from (8.28) and (8.29) are shown in Section 8.6.

8.5.2 Distributed Scenario

For ease of notation in the distributed case, we focus on the column norms of UEs 1 and 2 without loss of generality. Assume there are b_k antennas at BS k and using the notation $h_{ij} = \sqrt{P_j^{(k)}}U_{ij}$, where antenna i belongs to BS k, we obtain the column norm for UE 1 as

$$\begin{aligned} X &= P_1^{(1)} \sum_{r=1}^{b_1} |u_{r1}|^2 + \cdots + P_1^{(B)} \sum_{r=b_1+\cdots+b_{B-1}+1}^{b_1+\cdots+b_B} |u_{r1}|^2 \\ &= \frac{1}{2}\left(P_1^{(1)}\bar{X}_1 + P_1^{(2)}\bar{X}_2 + \cdots + P_1^{(B)}\bar{X}_B\right), \end{aligned} \tag{8.30}$$

where $\bar{X}_k \sim \chi^2_{2b_k}$. Similarly, the norm of column 2 is $Y = \sum_{k=1}^{B} \frac{P_2^{(k)}}{2}\bar{Y}_k$ and $\bar{Y}_k \sim \chi^2_{2b_k}$. If $\sum_{k=1}^{B} P_1^{(k)} > \sum_{k=1}^{B} P_2^{(k)}$, then the probability of disagreement between the two ordering

methods is $P(X < Y)$. First we compute the distribution of X and Y which are both linear combinations of chi-squared variables. There is considerable work on the distributions of such variables [130] but it is difficult to obtain a single general closed form solution from the PDF. Nevertheless, for any particular linear combination, the PDF can be derived using the basic approach outlined in [132]. Using the notation $\lambda_k = P_1^{(k)}/2$, the characteristic function (CF), $\phi_X(t)$, of $X = \sum_{r=1}^{B} \lambda_r \bar{X}_r$ is

$$\phi_X(t) = \prod_{r=1}^{B} (1 - 2jt\lambda_r)^{-b_r}. \tag{8.31}$$

By using partial fractions, we obtain

$$\phi_X(t) = \sum_{r=1}^{B} \sum_{s=1}^{b_r} \frac{A_{rs}}{(1 - 2jt\lambda_r)^s}, \tag{8.32}$$

where A_{rs} can be computed analytically using [133, page 66]. Note that the inverse transform of $(1 - 2jt\lambda_r)^{-s}$ is $\lambda_r^{-1} f_{2s}\left(x/\lambda_r\right)$, where $f_{2s}(.)$ is the PDF of a standard χ^2_{2s} variable. Hence, inverting (8.32) gives the PDF of X as

$$f_X(x) = \sum_{r=1}^{B} \sum_{s=1}^{b_r} A_{rs} \lambda_r^{-1} f_{2s}(x/\lambda_r). \tag{8.33}$$

For UE 2 we have,

$$f_Y(y) = \sum_{r=1}^{B} \sum_{s=1}^{b_r} B_{rs} \mu_r^{-1} f_{2s}(y/\mu_r), \tag{8.34}$$

where $\mu_r = P_2^{(r)}/2$ and the B_{rs} coefficients arise from the partial fraction expansion of $\phi_Y(t) = \prod_{r=1}^{B}(1-2jt\mu_r)^{-b_r}$. The probability of disagreement is given by

$$P(X < Y) \;=\; \int_0^\infty F_X(y) f_Y(y) dy, \tag{8.35}$$

where $F_X(.)$ is the CDF of X. Integrating (8.33) and substituting the resulting CDF into (8.35) gives

$$\begin{aligned} P(X < Y) &= \int_0^\infty \left(\sum_{r=1}^{B} \sum_{s=1}^{b_r} A_{rs} \lambda_r \lambda_r^{-1} F_{2s}(y/\lambda_r) \right) \times \left(\sum_{\bar{r}=1}^{B} \sum_{\bar{s}=1}^{b_r} B_{\bar{r}\bar{s}} \mu_{\bar{r}}^{-1} f_{2\bar{s}}(y/\mu_{\bar{r}}) \right) dy \\ &= \sum_{r=1}^{B} \sum_{s=1}^{b_r} \sum_{\bar{r}=1}^{B} \sum_{\bar{s}=1}^{b_r} A_{rs} B_{\bar{r}\bar{s}} \mu_{\bar{r}}^{-1} \times \int_0^\infty F_{2s}(y/\lambda_r) f_{2\bar{s}}(y/\mu_{\bar{r}}) dy. \end{aligned} \tag{8.36}$$

let $\mathcal{G}(r,s,\bar{r},\bar{s}) = \int_0^\infty F_{2s}(y/\lambda_r) f_{2\bar{s}}(y/\mu_{\bar{r}}) dy$. Then, by using the standard PDF [50, equation (2.32), page 13] and CDF of a chi squared distribution, we obtain

$$\mathcal{G}(r,s,\bar{r},\bar{s}) = \int_0^\infty \left(1 - \sum_{j=0}^{s-1} \frac{(y/\lambda_r)^j e^{-0.5y/\lambda_r}}{2^j j!} \right) \times \left(\frac{(y/\mu_{\bar{r}})^{\bar{s}-1} e^{-0.5y/\mu_{\bar{r}}}}{2^{\bar{s}}(\bar{s}-1)!} \right) dy.$$

Expanding (8.37) and using the result [133, page 358] $\int_0^\infty y^\alpha e^{-\beta y} dy = \alpha! \beta^{-(\alpha+1)}$ gives the result

$$\mathcal{G}(r,s,\bar{r},\bar{s}) = \mu_{\bar{r}} - \sum_{j=0}^{s-1} \binom{j+\bar{s}-1}{j} \frac{\lambda_r^{\bar{s}} \mu_{\bar{r}}^{j+1}}{(\lambda_r + \mu_{\bar{r}})^{j+\bar{s}}}. \tag{8.37}$$

Hence, the final result is

$$P(X > Y) = 1 - \sum_{r=1}^{B} \sum_{s=1}^{b_r} \sum_{\bar{r}=1}^{B} \sum_{\bar{s}=1}^{b_r} A_{rs} B_{\bar{r}\bar{s}} \mu_{\bar{r}}^{-1} \mathcal{G}(r,s,\bar{r},\bar{s}). \tag{8.38}$$

Numerically, the PDF in (8.33) and the probability of disagreement in (8.38) are awkward as they contain a large number of terms (N_r in (8.33) and N_r^2 in (8.38)) with oscillating signs. To see this, consider the special case of two BSs ($B = 2$) with b_1/b_2 antennas at BS1/BS2. Deriving A_{rs} and $B_{\bar{r}\bar{s}}$ using partial fractions [133, page 66] gives

$$A_{1s} = \frac{(-1)^{b_2}\binom{b_1+b_2-s-1}{b_1-s}\lambda_1^{b_2}\lambda_2^{b_1-s}}{(\lambda_2-\lambda_1)^{(b_2+b_1-s)}}, \tag{8.39}$$

$$A_{2s} = \frac{(-1)^{b_1}\binom{b_1+b_2-s-1}{b_2-s}\lambda_1^{b_2-s}\lambda_2^{b_1}}{(\lambda_1-\lambda_2)^{(b_2+b_1-s)}}, \tag{8.40}$$

$$B_{1s} = \frac{(-1)^{b_2}\binom{b_1+b_2-s-1}{b_1-s}\mu_1^{b_2}\mu_2^{b_1-s}}{(\mu_2-\mu_1)^{(b_2+b_1-s)}}, \tag{8.41}$$

$$B_{2s} = \frac{(-1)^{b_1}\binom{b_1+b_2-s-1}{b_2-s}\mu_1^{b_2-s}\mu_2^{b_1}}{(\mu_1-\mu_2)^{(b_2+b_1-s)}}. \tag{8.42}$$

Not only do the coefficients have oscillating sign but $\lambda_1 \approx \lambda_2$, $\mu_1 \approx \mu_2$ and large N_r all give rise to very large coefficients. Hence, (8.33) and (8.38) become unstable for MM. We have found that (8.33) and (8.38) are usually reliable for $N_r < 10$ with some attention given to the numerical handling of the components in the series. However, for $N_r \geq 10$ the expressions tend to be unstable.

As a result, in Section 8.4 we employed the approximation in (8.18) to avoid the problem in using (8.33). For the probability of disagreement, we approximate (8.38) by using gamma approximations for X and Y, which is a well established approximation to quadratic forms [130]. Using the method of moments, we approximate X and Y by $\mathrm{Gamma}(r_1, \theta_1)$ and $\mathrm{Gamma}(r_2, \theta_2)$ distributions where $r_i = \frac{\left(\sum_{r=1}^{B} b_r P_i^{(r)}\right)^2}{2\sum_{r=1}^{B} b_r P_i^{(r)2}}$ and $\theta_i = \frac{\sum_{r=1}^{B} b_r P_i^{(r)2}}{\sum_{r=1}^{B} b_r P_i^{(r)}}$ for $i = 1, 2$. Then, since the ratio of two independent gamma variables is generalized F [134, page 348], we

have

$$\begin{aligned} P(X > Y) &= P\left(\frac{X}{Y} > 1\right) \\ &\approx P\left(\frac{r_1\theta_1}{r_2\theta_2} F_{2r_1,2r_2} > 1\right) \\ &= P\left(F_{2r_1,2r_2} > \frac{r_2\theta_2}{r_1\theta_1}\right) \\ &= 1 - I_{\frac{\theta_2}{(\theta_1+\theta_2)}}(r_1, r_2). \end{aligned} \tag{8.43}$$

In (8.43) $F_{2r_1,2r_2}$ represents an F variable with $2r_1$ and $2r_2$ DOF. In summary, the density is numerically unstable and this motivated the approximation in Section 8.4. In addition, the probability of disagreement is obtained in (8.43), and is shown in Figure 8.7. Note that our analysis is applicable for traditional MIMO.

8.6 Results

All results in this section assume uniformly distributed UEs in a circular coverage area of radius 1 centered at the origin. The parameters used are: $N_r = 100$, $N_t = 10$, $\rho = 0$ dB, $\gamma = 3$, $\sigma_{SF} = 8$ dB, $A = 0.015$ and QPSK modulation. In order to prevent undesired high link gains in (2.10), the link distance is restricted by exclusion zone so that $d_{ij} > 0.01$. The value, $A = 0.015$, is chosen so that a linear ZF receiver has a reasonable median receive SNR of 7 dB in the co-located scenario with the given parameters. Three deployment scenarios, as shown in Figure 8.1, are considered. COL denotes the co-located case where all 100 antennas are at the center of the coverage area. 2BS denotes the case where the array has two locations with 50 antennas at $(-1/2, 0)$ and 50 antennas at $(1/2, 0)$. 4BS denotes the case of 4 locations with 25 antennas at each of the positions $(-1/2, -1/2)$, $(-1/2, 1/2)$, $(1/2, -1/2)$ and $(1/2, 1/2)$. We consider 2 and 4 BS locations as it is more likely that distributed arrays will be deployed at a handful of sites rather than being spread over the whole cell. Note that although the distributions

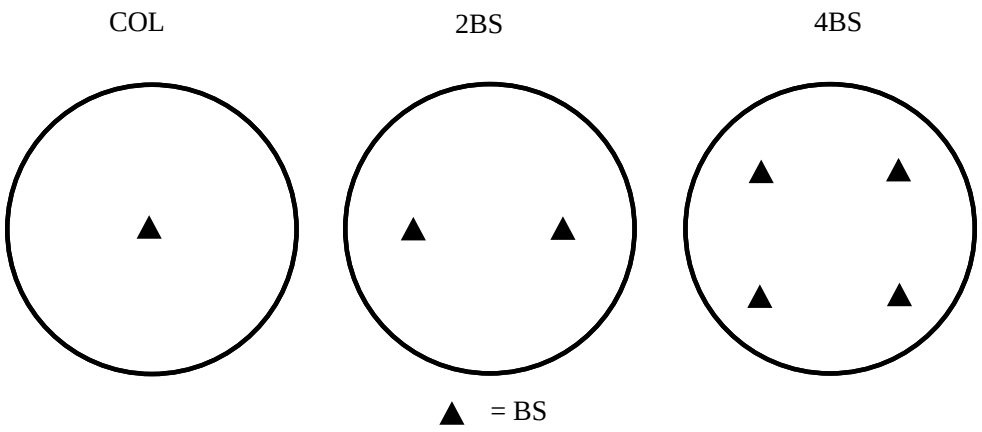

Figure 8.1: Three deployment scenarios.

of the BS coverage areas are the same, the coverage around each BS is not circular because of the defined cell boundary.

Figure 8.2 compares the simulated SER performance of P-V-BLAST, C-V-BLAST, a linear ZF receiver and a linear MRC receiver. Each point of the curve is averaged over both fast fading and random UE locations. Figure 8.2 supports the work in Chapter 6, which shows that the performance of the simple linear ZF receiver is very similar to C-V-BLAST while C-V-BLAST offers a complexity reduction. In addition, Figure 8.2 verifies the ordering analysis in Section 8.5 which indicated that P-V-BLAST and C-V-BLAST would have similar performance. Hence, C-V-BLAST can be further simplified to P-V-BLAST with virtually no performance loss and the assumptions behind the error rate analysis (based on P-V-BLAST) are supported. The poor performance of a linear MRC receiver shows the need for a V-BLAST structure. The linear MRC receiver also has a high error floor for the other scenarios but these results are not shown for clarity in Figure 8.2. Also shown in Figure 8.2 are the effects of deployment and system size. As N_r is reduced from 100 to 40 in the COL scenario performance drops but P-V-BLAST, C-V-BLAST and ZF remain very similar. As the array becomes more distributed, moving from COL to 2BS to 4BS, the performance increases as expected. Although a direct comparison is

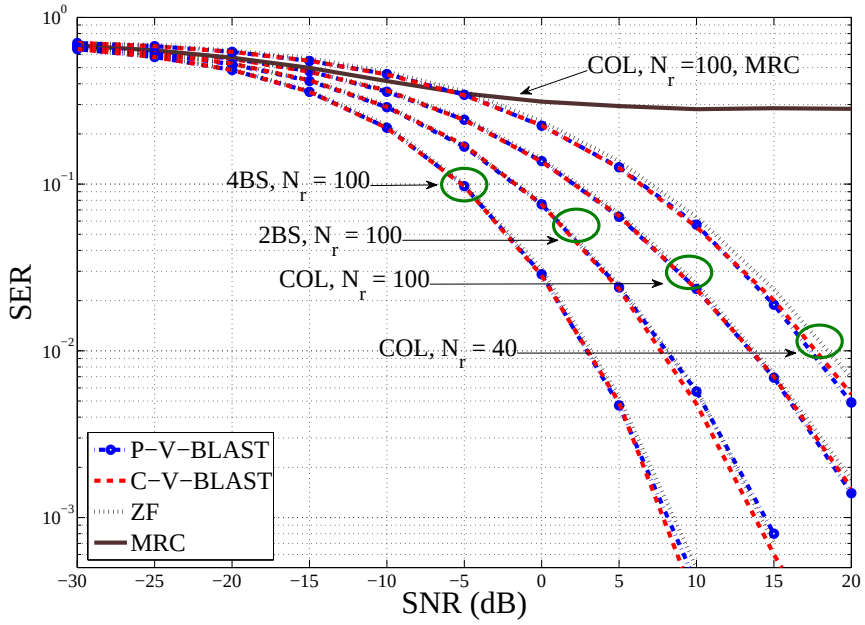

Figure 8.2: SER vs SNR for four different receivers, three deployment scenarios and $N_r \in \{40, 100\}$.

difficult as the channel power structures are inherently different, these results are averaged over many drops and the distributed gains are therefore seen on average over the entire cell.

Figure 8.3 evaluates the analytical error rate results for 3 random drops in the COL deployment. The simulated values of P_G are compared to two analytic approximations. The curve labeled Analysis (8.9) uses the P_G approximation in (8.4) with each $P(s_i)$ evaluated using numerical evaluation of (8.9). The curve labeled Analysis (8.10) uses (8.4) with the closed form result in (8.10) as an upper bound on $P(s_i)$. The very simple approximation shown in Analysis (8.10) is seen to be very effective, especially at higher SNR, and tends to provide a tight upper bound. Even more accurate results are possible using (8.9) but the benefits are limited and may not be worth the extra complexity of using a numerical integral for (8.9) or developing a numerically robust approach to the computation of (8.9). Note the massive variation between drops due to the lognormal shadowing and path loss differences.

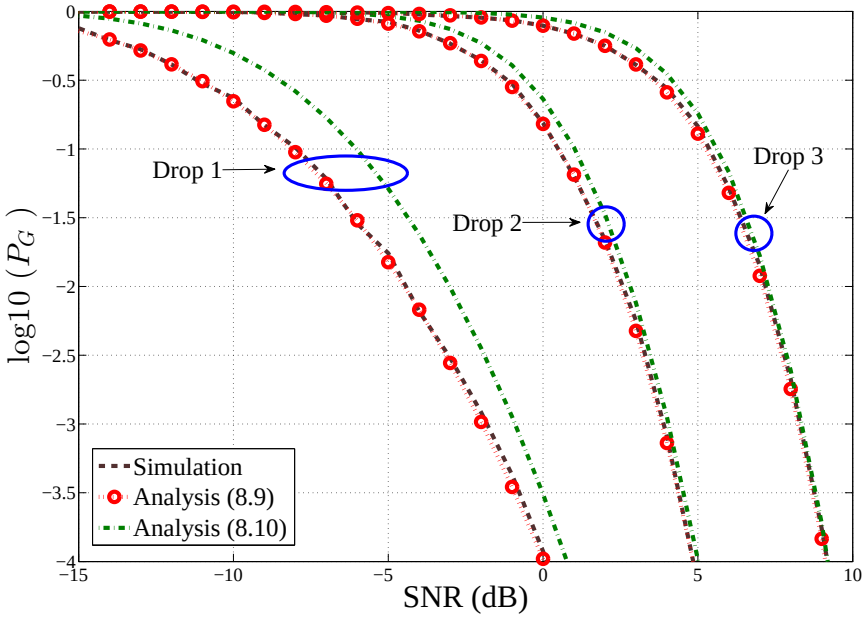

Figure 8.3: P-V-BLAST error performance (P_G) vs SNR showing simulated and analytical results for COL.

Figures 8.4 and 8.5 show the same type of results for the 4BS and 2BS deployments respectively. These results have an extra layer of approximation in that the approximate $\bar{\gamma}$ in (8.18) is used in (8.9) and (8.10) instead of the exact $\bar{\gamma}$ in (8.8) which is for the COL case. Nevertheless, Analysis (8.10) is still very accurate and Analysis (8.9) provides a tight upper bound. These results also validate the equivalence between co-located and distributed arrays derived in Section 8.5. As expected, the 4BS performance tends to be better 2BS which in turn is better than COL.

Figure 8.6 uses (8.28) and a numerical solution to (8.24) to find the required array size (N_r) to give a certain probability of disagreement (Prob.Dis.) at a given power differential. This is for the COL case. As shown, the approximate result in (8.28) is extremely accurate when compared to the exact result obtained by numerically solving (8.24). Furthermore, we observe the increasing demand on antenna numbers as the power differential decreases and the probability

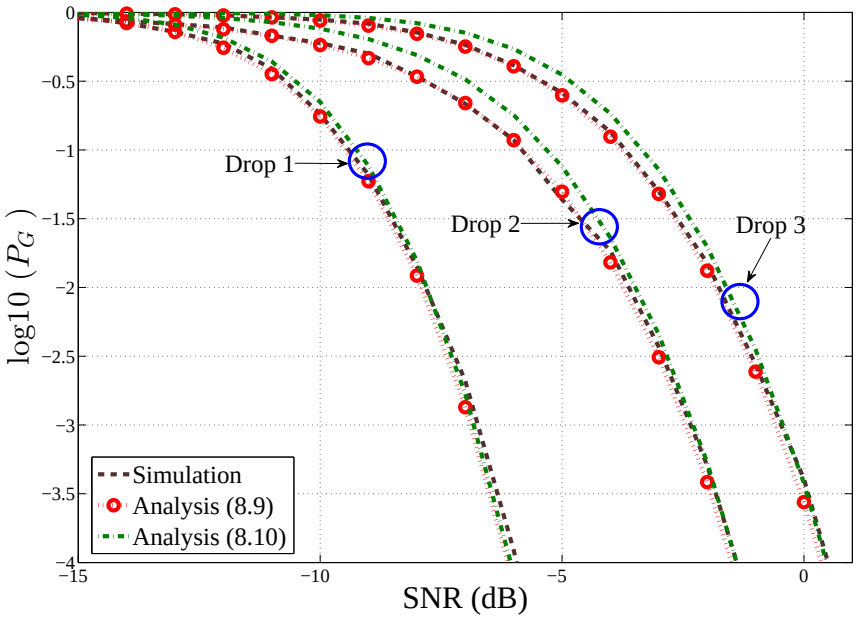

Figure 8.4: P-V-BLAST error performance (P_G) vs SNR showing simulated and analytical results for 4BS.

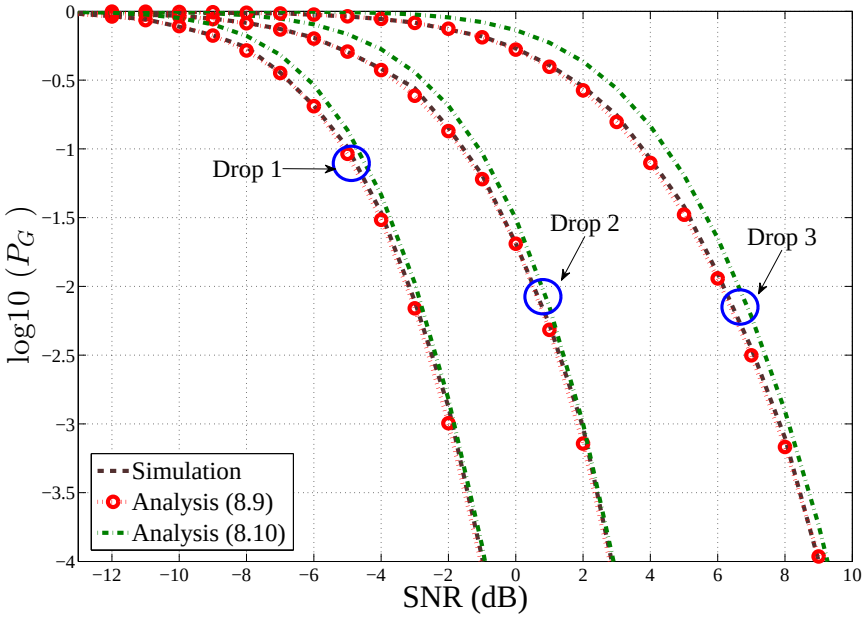

Figure 8.5: P-V-BLAST error performance (P_G) vs SNR showing simulated and analytical results for 2BS.

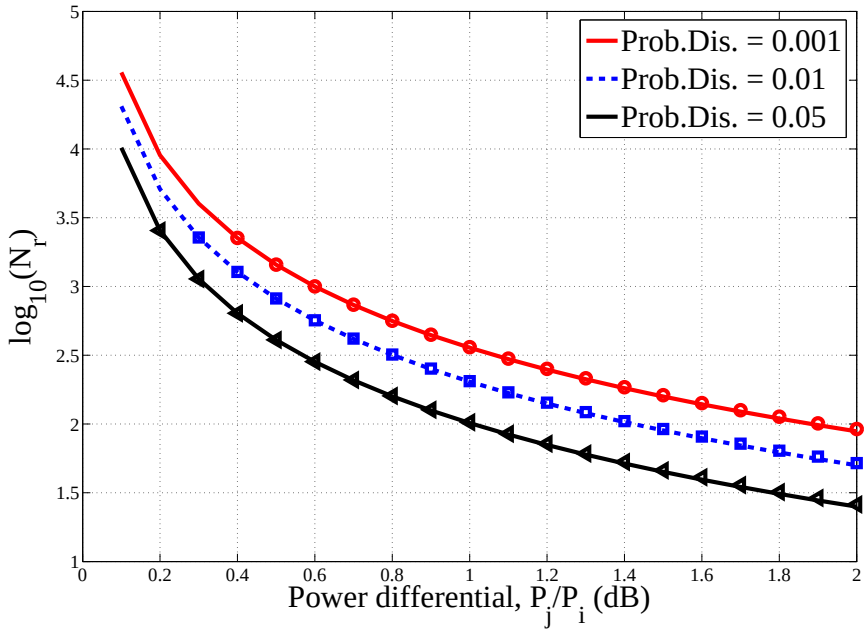

Figure 8.6: Required array size (N_r) to give a certain probability of disagreement at a given power differential (COL). Points represent N_r computed via (8.24) and lines use (8.28).

of disagreement decreases. For example, 100 antennas gives a 5% probability of disagreement at a 1 dB differential but a 0.1% probability at 2 dB.

Figure 8.7 uses (8.43) to approximate the probability of disagreement in the 2BS case. For 100,000 random drops, the probability of disagreement is computed using (8.43) and also by simulation. The CDF of the resulting absolute relative error is given, showing the accuracy of (8.43).

8.7 Summary

In this chapter, we have taken a proposed low-complexity V-BLAST receiver (C-V-BLAST) and further simplified the algorithm by replacing the channel norm ordering by a power based ordering giving P-V-BLAST. In both cases, ordering is performed once, before detection of

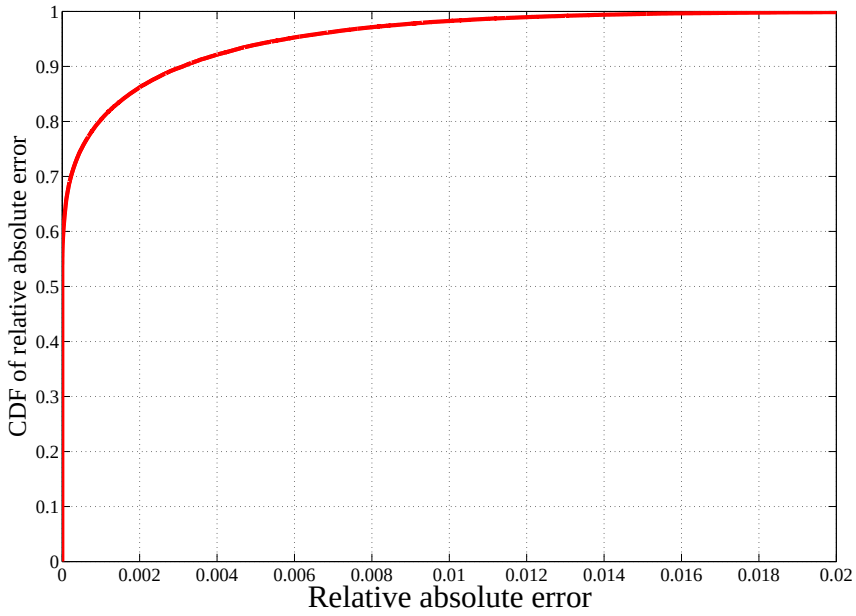

Figure 8.7: CDF of the relative absolute error between approximate and simulated probabilities of disagreement (2BS).

any UEs. The reduced complexity ordering is analyzed by evaluating the probability that the two ordering methods disagree (probability of disagreement) in both co-located and distributed antenna deployment scenarios. We demonstrate low probability of disagreement for MM and this not only supports the P-V-BLAST scheme but also leads to a convenient error rate analysis. In particular, we provide a simple, accurate, closed form approximation to the error rate of P-V-BLAST for both co-located and distributed scenarios. The analysis also provides two additional useful results. First, the SER of MRC in a distributed MM array is shown to have numerical problems and a simple, stable approximation is provided. Secondly, it is shown that a distributed array can be converted to an equivalent co-located system so the impact of link gain variation in the distributed case can be assessed. Furthermore, P-V-BLAST is shown to have potential benefits over C-V-BLAST in terms of enabling more rapid scheduling and link control functions.

Chapter IX

Conclusions and Future Work

9.1 Introduction

In the previous chapters, some contributions made in this thesis to the field of MM are presented. In this chapter, a summary of the main contributions presented in Chapters 3-8 is given in Section 9.2 and suggestions for future work are given in Section 9.3.

9.2 Conclusions

In Chapter 3, we investigated the interactions between deployment scenarios, ZF, MRC and propagation parameters. A mixture of analysis, simulation and physical interpretations were used to show that the improvements offered by distributed arrays are largely due to an averaging effect which is more prominent for the ZF case. This averaging improves the lower tail of the SINR CDF of the distributed case relative to the co-located case. We also show that imperfect CSI has a significant impact which is greater for distributed arrays than for co-located arrays and reduces the improvements offered by ZF. In addition, correlation does not play a role in degrading the performance in distributed arrays but strongly affects co-located deployments. As a result, a partially distributed ZF system is an ideal candidate if the cost and CSI requirements could be met, providing performance benefits and robustness to errors in CSI.

In Chapter 4, we have analytically justified a range of correlation models that have previ-

ously been used in the literature without verification. This analysis has also shown that correlation models must decay away from unity at zero separation with a power law behavior where the power is at most quadratic. Powers greater than two are invalid and so a quadratic roll-off is the slowest possible. Models such as Gaussian and Jakes which are quadratic near the origin are therefore extreme cases. This observation is closely tied to the differences between SQs and ULAs. We have shown that the capacity benefits of SQs are highly dependent on the correlation models. When the spatial correlation decays very slowly at the origin, then SQs offer substantial benefits in capacity. However, for more rapidly decaying correlations, the space savings offered by SQs are more important.

In Chapter 5, we have investigated V-BLAST with MRC and ZF in a MM system with imperfect CSI and channel correlation. We found that MRC V-BLAST performance can approach ZF V-BLAST, despite its lower complexity, for a range of imperfect CSI levels, different channel powers and different types of array, as long as the correlation is not too high. When the correlation level is increased, the performance of V-BLAST using either MRC or ZF is degraded and the gap between the two can become substantial. When the correlation is high, the ULA also offers large gains over the SQ if the same spacing is used. However, if the SQ is dimensioned using the closed form result derived, then MRC V-BLAST and ZF V-BLAST with SQ or ULA are shown to behave similarly.

In Chapter 6, we have investigated a variety of simple linear combiners and V-BLAST structures based on MRC and ZF. The key finding is that ZF performance can be reproduced using the C-V-BLAST approach with a much lower complexity in the most important scenario, where UEs are distributed and experience different link powers. This SER equivalence is found on a system-wide basis due to the fact that high SERs are dominated by low UE link powers. In this situation, we show that the SNR/SINR of the ZF/MRC receivers can become very similar.

In Chapter 7, we have also investigated the performance of C-V-BLAST in terms of through-

put in an AM system. Here, we show that the performance loss relative to ZF is small for perfect CSI and that C-V-BLAST can potentially provide both complexity reduction and performance improvement when the CSI is imperfect. In addition, gains due to PC are limited and so C-V-BLAST is a promising option, without the need for additional PC.

In Chapter 8, we have taken the proposed low-complexity V-BLAST receiver (C-V-BLAST) and further simplified the algorithm by replacing the channel norm ordering by a power based ordering giving P-V-BLAST. In both cases, ordering is performed once, before detection of any UEs. The reduced complexity ordering is analyzed by evaluating the probability that the two ordering methods disagree (probability of disagreement) in both co-located and distributed antenna deployment scenarios. We demonstrate low probability of disagreement for MM and this not only supports the P-V-BLAST scheme but also leads to a convenient error rate analysis. In particular, we provide a simple, accurate, closed form approximation to the error rate of P-V-BLAST for both co-located and distributed scenarios. The analysis also provides two additional useful results. First, the SER of MRC in a distributed MM array is shown to have numerical problems and a simple, stable approximation is provided. Secondly, it is shown that a distributed array can be converted to an equivalent co-located system so the impact of link gain variation in the distributed case can be assessed.

9.3 Future Work

In this section, some suggestions for future work are presented.

1. Optimal BS locations for distributed deployment.

    - In Chapter 3, we considered the scaling factor of the hexagonal cell, d_a, and explored the effect of spreading the antennas over increasing proportions of the cell. However, the relative locations of the BSs did not change. In DIST, we used a reg-

ular square grid, in 8BS we used equally spaced points on a circle and in 4BS we employed a rectangular grid. As shown in Figure 3.9, the largest percentage change in median SINR, for ZF with $b = 5$, is given by 72%, 42% and 29% for DIST, 8BS and 4BS, respectively. Hence, there are substantial gains to be made by BS placement. Future studies could consider optimizing the arrangement of arranged BSs or unequal numbers of antennas at BSs. We also investigated an intermediate deployment such as a massive array clustered at a few discrete locations, (BBS). We found that BBS can be more practical to implement and more robust when considering imperfect channel state information. Hence, a complete study could investigate the optimal number of BSs to deploy.

2. MM performance with low complexity V-BLAST and full V-BLAST receivers with channel imperfections including mutual coupling.

   - Correlation is an important factor when large numbers of antennas are deployed in a small physical volume. As shown in Chapters 3 and 5, we included correlation in the channel model using the idea of the one sided Kronecker model described in Section 2.6.4. In Chapter 3, we found that correlation does not play a major role in degrading the performance of distributed arrays but strongly affects co-located deployments (see Table 3.2 and Figure 3.6). This is because antennas in the COL scenario are deployed at one BS, but they are spaced out with large separations in the DIST scenario. In Chapter 5, we found that when increasing correlation levels, the performance of ZF V-BLAST and MRC V-BLAST are degraded and the gap between the two can become significant. For instance, in Chapter 5, when the correlation is high, the ULA offers large gains over the SQ if the same spacing is used (see Figure 5.7). However, if SQ was dimensioned using the closed form result

derived in Section 5.5.2, MRC V-BLAST and ZF V-BLAST with SQ or ULA were shown to behave similarly (see Figure 5.8). We showed that by equating median antenna spacings (see (5.17)) that a SQ needed to be increased in width from 9% of the ULA length (for equal inter-element spacing) to 57% in order to achieve similar performance. Correlation was also included in the analysis and simulations of C-V-BLAST, described in Chapter 6. All this work demonstrates that correlation can have an important impact on MM. Coupling is also associated with reduced antenna spacing and is modeled in a similar way to correlation via multiplication of the channel matrix by coupling matrices rather than correlation matrices. Hence, it is logical that coupling will also have an important effect on MM performance and it would be desirable to evaluate the lower complexity receivers in the presence of coupling to see if they are robust to such effects.

3. P-V-BLAST evaluation with real data or industrial channel models such as the WINNER Phase II Model [135].

    - In Chapter 7, we presented some results for C-V-BLAST using data obtained from a drive test of a suburban cell in an LTE network. Link gains were measured over a drive route covering the entire cell using equipment in the vehicle to measure the received signal strength at a mobile. Note that this test only provided link gains. In Chapter 8, we derived a simplified version of C-V-BLAST with an ordering scheme based on large scale fading information (P-V-BLAST). We also compared the results with the linear ZF receiver. We concluded that P-V-BLAST has potential benefits over C-V-BLAST in terms of enabling more rapid scheduling and link control functions. Hence, P-V-BLAST was shown to be a promising candidate for a MM receiver. However, only simple statistical channel models were used in this evaluation. Similarly, the only measured data used was link gain data rather than complete

channel measurements. By using complex industrial models, or channel data, we can assess whether the proposed receiver design (P-V-BLAST) is still effective in a variety of realistic channel conditions.

4. A low complexity precoding, using similar ideas to P-V-BLAST.

   - The purpose of a receiver is to extract the desired signal from the received signal. Linear receivers including ZF, MMSE and MRC, are relevant in MM due to their relatively low complexity. The simplest receiver among them is MRC. We considered an uplink model and focused on the receiver side in the MM system. By adopting MRC in a C-V-BLAST or P-V-BLAST structure, system performance is improved (see Figures 6.4-6.6 and Figure 8.2). Here, we were able to build on the simplest MRC receiver and make its performance similar to ZF. Precoding is a beamforming generalization which is used to assist in multiple transmission in multi-antenna wireless communications. An obvious extension of the receiver ideas to the downlink is to consider the simplest precoder, MF, and attempt to leverage this precoder in a downlink architecture which approximates the performance of ZF precoding without the complexity of a large inverse computation.

5. Analysis of P-V-BLAST with correlation, imperfect CSI, mutual coupling, noise inflation and error propagation.

   - The error analysis of P-V-BLAST in Chapter 8 did not include system imperfections such as correlation, imperfect CSI or mutual coupling. Also, the sequential detection effects of noise inflation and error propagation were avoided. A much more complete evaluation evaluation of P-V-BLAST is possible if the analysis could be extended to cover these situations. Mutual coupling in large arrays has been extensively researched (for example [136]). It would be interesting to apply the results

of previous studies on mutual coupling to the receiver structures discussed in this thesis. Note that correlation and imperfect CSI for a linear MRC receiver are included in Chapter 3. Hence, some of these extensions may well be feasible. Note that in Chapter 3, we provided some analysis with imperfect CSI and correlation for the linear ZF and MRC receivers. We found that our approximations work well for MRC. However, by including correlation in the ZF analysis, our approximations begin to lose accuracy especially in the COL scenario. Thus, improving the ZF approximations in the presence of correlation will be particularly beneficial.

6. More complex channel models can be used to investigate size and array shape for MM.

   - In Chapter 4 and Chapter 5, we considered the effects of array size and shape. Chapter 4 looked at ergodic capacity outage and Chapter 5 considered SER performance of linear receivers. The results demonstrated the potential for compact arrays to match performance of ULAs. However, this work was based on simple statistical models and ignored physical propagation effects such as angle spread and directions of arrival which are known to be important factors in array performance. Hence, a complete study could evaluate array performance using two or three dimensional scattering models.

Bibliography

[1] E. G. Larsson, F. Tufvesson, O. Edfors, and T. L. Marzetta, "Massive MIMO for next generation wireless systems," *IEEE Commun. Mag.*, vol. 52, no. 2, pp. 186–195, 2014.

[2] S. Haykin, *Communication Systems*. John Wiley & Sons, 2001.

[3] A. Haddad. (2013) UAE Telecom has Broadband Opportunities. [Online]. Available: http://english.nuqudy.com/Gulf/UAE_Poised_for_Rema-4629

[4] C. S. Jose. (2015) Cisco visual networking index (VNI) mobile forecast projects Nearly 10-fold global mobile data traffic growth over next five years. [Online]. Available: http://newsroom.cisco.com/release/1578507/Cisco-Visual-Networking-Index-VNI-Mobile-Forecast-ProjectsNearly\
-10-fold-Global-Mobile-Data-Traffic-Growth-Over-Next-Five-Years?utm_medium=rss

[5] F. Richter. (2014) Internet of Things to hit the mainstream by 2020. [Online]. Available: http://www.statista.com/chart/2936/internet-of-things-to-hit-the-mainstream-by-2020

[6] A. Chockalingam and B. S. Rajan, *Large MIMO Systems*. Cambridge University Press, 2014.

[7] F. Rusek, D. Persson, B. L. Kiong, E. Larsson, T. L. Marzetta, O. Edfors, and F. Tufvesson, "Scaling up MIMO: Opportunities and challenges with very large arrays," *IEEE Signal Process. Mag.*, vol. 30, no. 1, pp. 40–60, 2013.

[8] F. Boccardi, R. W. Heath, A. Lozano, T. L. Marzetta, and P. Popovski, "Five disruptive technology directions for 5G," *IEEE Commun. Mag.*, vol. 52, no. 2, pp. 74–80, 2014.

[9] P.-S. Kildal and K. Rosengren, "Correlation and capacity of MIMO systems and mutual coupling, radiation efficiency, and diversity gain of their antennas: Simulations and measurements in a reverberation chamber," *IEEE Commun. Mag.*, vol. 42, no. 12, pp. 104–112, 2004.

[10] R. Irmer, H. Droste, P. Marsch, M. Grieger, G. Fettweis, S. Brueck, H. Mayer, L. Thiele, and V. Jungnickel, "Coordinated multipoint: Concepts, performance, and field trial results," *IEEE Commun. Mag.*, vol. 49, no. 2, pp. 102–111, 2011.

[11] Mobile Europe. (2014) Massive MIMO tech in the spotlight as ZTE announces trial, Huawei unveils prototype. [Online]. Available: http://www.mobileeurope.co.uk/Press-Wire/massive-mimo-tech-in-the-spotlight-as-zte-announces-trial-huawei-unveils-protoype

[12] ——. (2015) Samsung, SK Telecom to demo 3D beamforming to boost mm wave tech. [Online]. Available: http://www.mobileeurope.co.uk/Press-Wire/samsung-sk-telecom-to-demo-3d-beamforming-to-boost-millimetre-wave-tech

[13] E. Dahlman, S. Parkvall, J. Skold, and P. Beming, *3G Evolution: HSPA and LTE for Mobile Broadband*. Academic Press, 2010.

[14] K. Hosseini, J. Hoydis, S. T. Brink, and M. Debbah, "Massive MIMO and small cells: How to densify heterogeneous networks," in *Proc. 2013 IEEE Int. Conf. on Commun. (ICC)*, pp. 5442–5447.

[15] T. L. Marzetta, "Noncooperative cellular wireless with unlimited numbers of base station antennas," *IEEE Trans. Wireless Commun.*, vol. 9, no. 11, pp. 3590–3600, 2010.

[16] B. Vucetic and J. Yuan, *Space-Time Coding*. John Wiley & Sons, 2003.

[17] D. Tse and P. Viswanath, *Fundamentals of Wireless Communication*. Cambridge University Press, 2005.

[18] C. Oestges and B. Clerckx, *MIMO Wireless Communications: From Real-World Propagation to Space-Time Code Design*. Academic Press, 2010.

[19] A. B. Gershman, N. D. Sidiropoulos, and J. Wiley, *Space-Time Processing for MIMO Communications*. Wiley Online Library, 2005.

[20] E. Biglieri, R. Calderbank, A. Constantinides, A. Goldsmith, A. Paulraj, and H. V. Poor, *MIMO Wireless Communications*. Cambridge University Press, 2007.

[21] L. Bai and J. Choi, *Low Complexity MIMO Detection*. Springer Science & Business Media, 2012.

[22] S. Verdu, *Multiuser Detection*. Cambridge University Press, 1998.

[23] R. Heath, S. Peters, Y. Wang, and J. Zhang, "A current perspective on distributed antenna systems for the downlink of cellular systems," *IEEE Commun. Mag.*, vol. 51, no. 4, pp. 161–167, 2013.

[24] H. Q. Ngo, E. G. Larsson, and T. L. Marzetta, "Uplink power efficiency of multiuser MIMO with very large antenna arrays," in *Proc. 2011 IEEE Conf. on Commun., Control and Computing (Allerton)*, pp. 1272–1279.

[25] L. Lu, G. Li, A. Swindlehurst, A. Ashikhmin, and R. Zhang, "An overview of massive MIMO: Benefits and challenges," *IEEE Selected Topics in Signal Process.*, vol. 8, no. 5, pp. 742 –758, 2014.

[26] J. Hoydis, S. T. Brink, and M. Debbah, "Massive MIMO: How many antennas do we need?" in *Proc. 2011 IEEE Conf. on Commun., Control and Computing (Allerton)*, pp. 545–550.

[27] E. Björnson, J. Hoydis, M. Kountouriss, and M. Debbah, "Hardware impairments in large-scale MISO systems: Energy efficiency, estimation, and capacity limits," in *Proc. 2013 Int. Conf. on Digital Signal Process. (DSP)*.

[28] R. Rogalin, O. Y. Bursalioglu, H. C. Papadopoulos, G. C. Caire, and A. F. Molisch, "Hardware-impairment compensation for enabling distributed large-scale MIMO," in *Proc. 2013 IEEE Workshop on Inf. Theory and Applicat. (ITA)*, pp. 1–10.

[29] H. Q. Ngo, T. L. Marzetta, and E. G. Larsson, "Analysis of the pilot contamination effect in very large multicell multiuser MIMO systems for physical channel models," in *Proc. 2011 IEEE Conf. on Acoust. Speech and Signal Process. (ICASSP)*, pp. 3464–3467.

[30] Y. Nam, B. L. Ng, K. Sayana, Y. Li, J. Zhang, Y. Kim, and J. Lee, "Full-dimension MIMO (FD-MIMO) for next generation cellular technology," vol. 51, no. 6, pp. 172–179, 2013.

[31] K. Zheng, S. Ou, and X. Yin, "Massive MIMO channel models: A survey," *Int. J. Antennas and Propagation*, vol. 2014, 2014.

[32] J. Li, X. Su, J. Zeng, Y. Zhao, S. Yu, L. Xiao, and X. Xu, "Codebook design for uniform rectangular arrays of massive antennas," in *Proc. 2013 IEEE Conf. on Veh. Technol. (VTC)*, pp. 1–5.

[33] Y. Zhu, L. Liu, A. Wang, K. Sayana, and J. C. Zhang, "DoA estimation and capacity analysis for 2D active massive MIMO systems," in *Proc. 2013 IEEE Int. Conf. on Commun. (ICC)*, pp. 4630–4634.

[34] X. Su, J. Zeng, J. Li, L. Rong, L. Liu, X. Xu, and J. Wang, "Limited feedback precoding for massive MIMO," *Int. J. Antennas and Propagation*, vol. 2013, 2013.

[35] A. L. Swindlehurst, E. Ayanoglu, P. Heydari, and F. Capolino, "Millimeter-wave massive MIMO: The next wireless revolution?" *IEEE Commun. Mag.*, vol. 52, no. 9, pp. 56–62, 2014.

[36] W. Liu, S. Han, C. Yang, and C. Sun, "Massive MIMO or small cell network: Who is more energy efficient?" in *Proc. 2013 IEEE Workshop. on Wireless Commun. and Networking (WCNCW)*, pp. 24–29.

[37] E. Björnson, M. Kountouriss, and M. Debbah, "Massive MIMO and small cells: Improving energy efficiency by optimal soft-cell coordination," in *Proc. 2013 IEEE Conf. on Telecommun. (ICT)*, pp. 1–5.

[38] H. Suzuki, R. Kendall, K. Anderson, A. Grancea, D. Humphrey, J. Pathikulangara, K. Bengston, J. Matthews, and C. Russell, "Highly spectrally efficient Ngara rural wireless broadband access demonstrator," in *Proc. 2012 IEEE Conf. on Commun. Inform. Technol. (ISCIT)*, pp. 914–919.

[39] K. Koivunen, "Characterisation of MIMO propagation channel in multi-link scenarios," Master's thesis, Helsinki University of Technology, Finland.

[40] C. Shepard, H. Yu, N. Anand, E. Li, T. Marzetta, R.Yang, and L. Zhong, "Argos: Prac-

tical many-antenna base stations," in *Proc. 2012 ACM Conf. on Mobile Computing and Networking*, pp. 53–64.

[41] T. Datta, N. Srinidhi, A. Chockalingam, and B. S. Rajan, "A hybrid RTS-BP algorithm for improved detection of large-MIMO M-QAM signals," in *Proc. 2011 IEEE Conf. on Nat. Commun. (NCC)*, pp. 1–5.

[42] J. Chen and X. Yu, "Worst-case optimized V-BLAST receiver design for imperfect MIMO channels," in *Proc. 2006 IEEE Conf. on Military Commun. (MILCOM)*, pp. 1–6.

[43] T. Q. Duong, H. Trang, E. Hong, and S. Y. Lee, "Performance evaluation of the V-BLAST system under correlated fading channels," in *Proc. 2005 IEEE. Conf. on Advanced Industrial Telecommun.*, pp. 220–225.

[44] S. Loyka and F. Gagnon, "V-BLAST without optimal ordering: Analytical performance evaluation for Rayleigh fading channels," *IEEE Trans. Commun.*, vol. 54, no. 6, pp. 1109–1120, 2006.

[45] N. B. Sinha, R. Bera, and M. Mitra, "MIMO detection algorithms for high data rate wireless transmission," *IEEE Comput. and Eng.*, vol. 1, no. 1, pp. 91–98, 2010.

[46] E. Dahlman, S. Parkvall, and J. Skold, *4G: LTE/LTE-Advanced for Mobile Broadband*. Academic Press, 2013.

[47] T. S. Rappaport, *Wireless Communications: Principles and Practice*. Prentice Hall PTR, 1996.

[48] S. K. Das, *Mobile Handset Design*. John Wiley & Sons, 2013.

[49] A. Goldsmith, *Wireless Communications*. Cambridge University Press, 2005.

[50] M. K. Simon, *Probability Distributions Involving Gaussian Random Variables*. Springer, 2006.

[51] C. Oestges, "Validity of the Kronecker model for MIMO correlated channels," in *Proc. 2006 IEEE Conf. on Veh. Technol. (VTC)*, vol. 6, pp. 2818–2822.

[52] X. Liu and M. E. Bialkowski, "Effect of antenna mutual coupling on MIMO channel estimation and capacity," *Int. J. Antennas and Propagation*, vol. 2010, 2010.

[53] A. Skupch, D. Seethaler, and F. Hlawatsch, "Free probability based capacity calculation for MIMO channels with transmit or receive correlation," in *Proc. 2005 IEEE Conf. on Wireless Networks, Commun. and Mobile Computing*, vol. 2, pp. 1041–1046.

[54] H. Gao, P. J. Smith, and M. V. Clark, "Theoretical reliability of MMSE linear diversity combining in Rayleigh-fading additive interference channels," *IEEE Trans. Commun.*, vol. 46, no. 5, pp. 666–672, 1998.

[55] P. Smith, P. Dmochowski, M. Chiani, and A. Giorgetti, "On the number of independent channels in multi-antenna systems," *IEEE Trans. Wireless Commun.*, vol. 13, no. 1, pp. 75–85, 2014.

[56] W. C. Jakes, *Microwave Mobile Communications*. Wiley-IEEE Press, 1974.

[57] A. Lozano, A. M. Tulino, and S. Verdú, "High-SNR power offset in multiantenna communication," *IEEE Trans. Inform. Theory*, vol. 51, no. 12, pp. 4134–4151, 2005.

[58] S. L. Loyka, "Channel capacity of MIMO architecture using the exponential correlation matrix," *Commun. Lett.*, vol. 5, no. 9, pp. 369–371, 2001.

[59] C. Wang, E. K. Au, R. D. Murch, and V. K. Lau, "Closed-form outage probability and BER of MIMO zero-forcing receiver in the presence of imperfect CSI," in *Proc. 2006 IEEE Workshop on Signal Process. Advances in Wireless Commun. (SPAWC)*, pp. 1–5.

[60] G. L. Stuber, *Principles of Mobile Communication*. Springer, 2011.

[61] V. K. Nguyen and J. S. Evans, "Multiuser transmit beamforming via regularized channel inversion: A large system analysis," in *Proc. 2008 IEEE Conf. on Global Telecommun. (GLOBECOM)*, pp. 1–4.

[62] H. Prabhu, J. Rodrigues, O. Edfors, and F. Rusek, "Approximative matrix inverse computations for very-large MIMO and applications to linear pre-coding systems," in *Proc. 2013 IEEE Conf. on Wireless Commun. and Networking (WCNC)*, pp. 2710–2715.

[63] P. W. Wolniansky, G. J. Foschini, G. Golden, and R. A. Valenzuela, "V-BLAST: An architecture for realizing very high data rates over the rich-scattering wireless channel," in *Proc. 1998 IEEE Symp. on Signals, Syst., and Electron. (ISSSE)*, pp. 295–300.

[64] P. Li, D. Paul, R. Narasimhan, and J. Cioffi, "On the distribution of SINR for the MMSE MIMO receiver and performance analysis," *IEEE Trans. Inform. Theory*, vol. 52, no. 1, pp. 271–286, 2006.

[65] H. Q. Ngo, M. Matthaiou, and E. G. Larsson, "Performance analysis of large scale MU-MIMO with optimal linear receivers," in *Proc. 2012 IEEE Workshop on Swedish Commun. Technol. (Swe-CTW)*, pp. 59–64.

[66] G. D. Golden, C. J. Foschini, R. A. Valenzuela, and P. W. Wolniansky, "Detection algorithm and initial laboratory results using V-BLAST space-time communication architecture," *IET Electron. Lett.*, vol. 35, no. 1, pp. 14–16, 1999.

[67] J. Proakis, *Digital Communications*. McGraw-Hill, 2000.

[68] J. Hoydis, M. Kobayashi, and M. Debbah, "Asymptotic performance of linear receivers in network MIMO," in *Proc. 2010 IEEE Conf. on Signals, Syst. and Comput. (ASILOMAR)*, pp. 942–948.

[69] S. Khattak, *Base Station Cooperation Strategies for Multi-user Detection in Interference Limited Cellular Systems*. Jörg Vogt Verlag, 2008.

[70] V. Kostina and S. Loyka, "On optimum power allocation for the V-BLAST," *IEEE Trans. Wireless Commun.*, vol. 56, no. 6, pp. 999–1012, 2008.

[71] A. Gjendemsjo, D. Gesbert, G. E. Oien, and S. G. Kiani, "Optimal power allocation and scheduling for two-cell capacity maximization," in *Proc. 2006 IEEE Symp. on Modeling and Optimization in Mobile, Ad Hoc and Wireless Networks*.

[72] Q. Gao, X. Zhang, and J. Li, "Power control of V-BLAST system with per-antenna power constraints," *IEEE Commun. Lett.*, vol. 11, no. 11, pp. 833–835, 2007.

[73] C. Wei, L. Qiu, and J. Zhu, "A power control method based on post-detection SINR balancing in cellular V-BLAST systems," in *Proc. 2006 IEEE Symp. on Spread Spectrum Techniques and Applicat.*, pp. 263–267.

[74] A. Gjendemsjo, G. E. Oien, and P. Orten, "Optimal discrete-level power control for adaptive coded modulation schemes with capacity-approaching component codes," in *Proc. 2006 IEEE Int. Conf. on Commun. (ICC)*, vol. 11, pp. 5047–5052.

[75] A. Gjendemsjø, G. E. Øien, H. Holm, M. Alouini, D. Gesbert, K. J. Hole, and P. Or-

tenl, "Rate and power allocation for discrete-rate link adaptation," *EURASIP J. Wireless Commun. and Networking*, vol. 2008, p. 16, 2008.

[76] E. Altman, K. Avrachenkov, G. Miller, and B. J. Prabhu, "Uplink dynamic discrete power control in cellular networks," *IEEE Trans. Autom. Control*, vol. 54, pp. 2328–2340.

[77] Y. Xing and R. Chandramouli, "Stochastic learning solution for distributed discrete power control game in wireless data networks," *IEEE Trans. AMC Networking*, vol. 16, no. 4, pp. 932–944, 2008.

[78] K. Chawla and X. Qiu, "Throughput performance of adaptive modulation in cellular systems," in *Proc. 1998 IEEE Int. Conf. on Universal Personal Commun. (ICUPC)*, vol. 2, pp. 945–950.

[79] G. Gritsch and H. Weinrichter, "Adaptive subspace modulation in spatially correlated MIMO systems," in *Proc. 2002 IEEE Conf. on Personal, Indoor and Mobile Radio Commun. (PIMRC)*, vol. 4, pp. 1772–1776.

[80] H. Zhu, Z. Lei, and F. P. Chin, "On effects of power reallocation and ordering in V-BLAST systems with adaptive modulation and antenna selection," in *Proc. 2004 IEEE Conf. on Spread Spectrum Techniques and Applicat. (ISSSTA)*, vol. 1, pp. 374–378.

[81] J. Hoydis and M. Debbah, "Green networks: Small cells or massive MIMO?" in *Methodological Foundations on Green Radio, Telecom Paristech, 2012*.

[82] A. Liu and V. K. N. Lau, "Joint power and antenna selection optimization for energy-efficient large distributed MIMO networks," in *Proc. 2012 IEEE Conf. on Commun. Systems (ICCS)*, pp. 230–234.

[83] K. T. Truong and R. W. Heath, "The viability of distributed antennas for massive MIMO systems," in *Proc. 2013 IEEE Conf. on Signals, Syst. and Comput. (ASILOMAR)*, pp. 1318–1323.

[84] Z. Liu and L. Dai, "A comparative study of downlink MIMO cellular networks with co-located and distributed base-station antennas," *IEEE Trans. Wireless Commun.*, vol. 13, no. 11, pp. 6259 – 6274, 2014.

[85] H. Dai, "Distributed versus co-located MIMO systems with correlated fading and shadowing," in *Proc. 2006 IEEE Conf. on Acoust. Speech and Signal Process. (ICASSP)*, vol. 4, pp. 561–564.

[86] M. V. Clark, T. W. III, L. J. Greenstein, A. Rustako, V. Erceg, and E. Roman, "Distributed versus centralized antenna arrays in broadband wireless networks," in *Proc. 2001 IEEE Conf. on Veh. Technol. (VTC)*, vol. 1, pp. 33–37.

[87] S. Schwarz, R. W. Heath, and M. Rupp, "Single-user MIMO versus multi-user MIMO in distributed antenna systems with limited feedback," *Springer EURASIP J. Advances in Signal Process.*, vol. 2013, no. 1, pp. 1–20.

[88] J. Hoydis, S. T. Brink, and M. Debbah, "Massive MIMO in the UL/DL of cellular networks: How many antennas do we need?" *IEEE J. Sel. Areas Commun.*, vol. 31, no. 2, pp. 160–171, 2013.

[89] M. Gudmundson, "Correlation model for shadow fading in mobile radio systems," *IET Electron. Lett.*, vol. 27, no. 23, pp. 2145–2146, 1991.

[90] J. Weitzen and T. J. Lowe, "Measurement of angular and distance correlation properties

of log-normal shadowing at 1900 MHz and its application to design of PCS systems," *IEEE Trans. Veh. Technol.*, vol. 51, no. 2, pp. 265–273, 2002.

[91] K. Kopsa, G. Matz, H. Artés, and F. Hlawatsch, "Bit error rate estimation for a joint detection receiver in the downlink of UMTS/TDD," in *Proc. 2003 IEEE Conf. on IST Mobile and Wireless Commun.*, pp. 256–260.

[92] D. A. Basnayaka, P. J. Smith, and P. A. Martin, "Performance analysis of macrodiversity MIMO systems with MMSE and ZF receivers in flat Rayleigh fading," *IEEE Trans. Wireless Commun.*, vol. 12, no. 5, pp. 2240–2251, 2013.

[93] O. Lieberman, "A Laplace approximation to the moments of a ratio of quadratic forms," *Biometrika*, vol. 81, no. 4, pp. 681–690, 1994.

[94] M. F. Hanif, M. Shafi, P. J. S. P., and Dmochowski, "Interference and deployment issues for cognitive radio systems in shadowing environments," in *Proc. 2009 IEEE Conf. on Commun. (ICC)*, 2009, pp. 1–6.

[95] D. N. C. Tse and S. V. Hanly, "Linear multiuser receivers: Effective interference, effective bandwidth and user capacity," *IEEE Trans. Inform. Theory*, vol. 45, no. 2, pp. 641–657, 1999.

[96] J. Nam, J. Ahn, A. Adhikary, and G. Caire, "Joint spatial division and multiplexing: Realizing massive MIMO gains with limited channel state information," in *Proc. 2012 IEEE Conf. on Inform. Sciences and Systems (CISS)*, pp. 1–6.

[97] C. E. Rasmussen and C. K. I. Williams, "Gaussian processes for machine learning," *The MIT Press*, 2006.

[98] G. Samorodnitsky and M. S. Taqqu, *Stable non-Gaussian random processes: stochastic models with infinite variance*. CRC Press, 1994, vol. 1.

[99] M. Kiessling and J. Speidel, "Mutual information of MIMO channels in correlated Rayleigh fading environments-a general solution," in *Proc. 2004 IEEE Int. Conf. on Commun. (ICC)*, vol. 2, pp. 814–818.

[100] G. Alfano, A. M. Tulino, A. Lozano, and S. Verdú, "Capacity of MIMO channels with one-sided correlation," in *Proc. 2004 IEEE Conf. on Spread Spectrum Techniques and Applicat. (ISSSTA)*, pp. 515–519.

[101] D. B. Smith and T. D. Abhayapala, "Maximal ratio combining performance analysis in spatially correlated Rayleigh fading channels with imperfect channel knowledge," in *Proc. 2005 IEEE Asia-Pacific Conf. on Commun.*, pp. 549–553.

[102] C. Siriteanu, Y. Miyanaga, S. D. Blostein, S. Kuriki, and X. Shi, "MIMO zero-forcing detection analysis for correlated and estimated Rician fading," *IEEE Trans. Veh. Technol.*, vol. 61, no. 7, pp. 3087–3099, 2012.

[103] M. Vehkapera, K. Takeuchi, R. Muller, and T. Tanaka, "Analysis of large MIMO DS-CDMA systems with imperfect CSI and spatial correlation," in *Proc. 2010 Conf. IEEE Int.l Symp. on Inform. Theory (ISIT)*, pp. 2098–2102.

[104] R. Narasimhan, "Error propagation analysis of V-BLAST with channel-estimation errors," *IEEE Trans. Commun.*, vol. 53, no. 1, pp. 27–31, 2005.

[105] J. Huang and S. Signell, "Impact of channel estimation error on performance of adaptive MIMO systems," in *Proc. 2008 IEEE. Conf. on Acoust. Speech and Signal Process. (ICASSP)*, pp. 2865–2868.

[106] J. Chen, X. Yu, and C. J. Kuo, "V-BLAST receiver for MIMO relay networks with imperfect CSI," in *Proc. 2007 IEEE Conf. on Global Telecommun. (GLOBECOM)*, 2007, pp. 571–575.

[107] H. Q. Ngo, E. G. Larsson, and T. Marzetta, "Energy and spectral efficiency of very large multiuser MIMO systems," *IEEE Trans. Commun.*, vol. 61, no. 4, pp. 1436–1449, 2013.

[108] A. Papoulis, *Probability, Random Variables, and Stochastic Processes*. 3rd Ed., McGraw-Hill, 1991.

[109] R. Hunger, *Floating point operations in matrix-vector calculus*. Technical report V1.3, Munich University of Technology, 2007.

[110] N. I. Miridakis and D. D. Vergados, "Performance analysis of the ordered V-BLAST approach over Nakagami-m fading channels," *IEEE Wireless Commun. Lett.*, vol. 2, no. 1, pp. 18–21, 2013.

[111] Y. Jiang, M. K. Varanasi, and J. Li, "Performance analysis of ZF and MMSE equalizers for MIMO systems: An in-depth study of the high SNR regime," *IEEE Trans. Inform. Theory*, vol. 57, no. 4, pp. 2008–2026, 2011.

[112] T. W. Anderson, *An Introduction to Multivariate Statistical Analysis*. Wiley New York, 1958, vol. 2.

[113] X. Feng, S. Zhu, and L. W, "Adaptive bit and power allocation algorithm in V-BLAST system," in *Proc. 2004 IEEE Conf. on Personal, Indoor and Mobile Radio Commun. (PIMRC)*, vol. 1, pp. 489–492.

[114] J. Choi, "Massive MIMO with joint power control," *IEEE Wireless Commun. Lett.*, vol. 3, no. 4, pp. 329–332, 2014.

[115] Y. Guo, G. Fodor, and G. Ascheid, "Uplink power control with MMSE receiver in multi-cell MU-massive-MIMO systems," in *Proc. 2014 IEEE Int. Conf. on Commun. (ICC)*, pp. 5184–5190.

[116] H. A. David and H. N. Nagaraja, *Order Statistics*. Wiley Online Library, 1970.

[117] S. Loyka and F. Gagnon, "On BER analysis of the BLAST without optimal ordering over Rayleigh fading channel," in *Proc. 2004 IEEE conference on Veh. Technol. (VTC)*, vol. 2, pp. 1473–1477.

[118] ——, "On outage and error rate analysis of the ordered V-BLAST," *IEEE Trans. Wireless Commun.*, vol. 7, no. 10, pp. 3679–3685, 2008.

[119] W. Peng, F. Adachi, S. Ma, J. Wang, and T. Ng, "Effects of channel estimation errors on V-BLAST detection," in *Proc. 2008 IEEE Conf. on Global Telecommun. (GLOBECOM)*, pp. 1–5.

[120] S. Loyka and F. Gagnon, "Analytical BER analysis of the V-BLAST in a Rayleigh fading channel," in *Proc. 2006 IEEE Conf. on Wireless Commun. and Networking (WCNC)*, pp. 827–832.

[121] ——, "Performance analysis of the V-BLAST algorithm: An analytical approach," *IEEE Trans. Wireless Commun.*, vol. 3, no. 4, pp. 1326–1337, 2004.

[122] B. Bandemer and S. Visuri, "Capacity-based uplink scheduling using long-term channel knowledge," in *Proc. 2007 IEEE Int. Conf. on Commun. (ICC)*, pp. 785–790.

[123] P. J. Smith and D. A. Basnayaka, "Multiuser scheduling for radio resource allocation," May 17 2013, US Patent App. 13/896,969.

[124] D. A. Basnayaka, P. J. Smith, and P. A. Martin, "The effect of macrodiversity on the performance of maximal ratio combining in flat Rayleigh fading," *IEEE Trans. Commun.*, vol. 61, no. 4, pp. 1384–1392, 2013.

[125] A. A. Basri and T. J. Lim, "Exact average bit-error probability for maximal ratio combining with multiple cochannel interferers and Rayleigh fading," in *Proc. 2007 IEEE Int. Conf. on Commun. (ICC)*, pp. 1102–1107.

[126] J. Lu, T. Tjhung, and C. C. Chai, "Error probability performance of L-branch diversity of MQAM in Rayleigh fading," *IEEE Trans. Commun.*, vol. 46, no. 2, pp. 179–181, 1998.

[127] S. Chennakeshu and J. B. Anderson, "Error rates for Rayleigh fading multichannel reception of MPSK signals," *IEEE Trans. Commun.*, vol. 43, no. 2, pp. 338–346, 1995.

[128] M. Castaneda, A. Mezghani, and J. A. Nossek, "Optimal resource allocation in the downlink/uplink of single-user MISO/SIMO FDD systems with limited feedback," in *Proc. 2009 IEEE Workshop on Signal Process. Advances in Wireless Commun. (SPAWC)*, pp. 354–358.

[129] P.Billingsley, *Probability and Measure*. John Wiley & Sons, 1979.

[130] R. W. Heath, T. Wu, Y. H. Kwon, and A. C. Soong, "Multiuser MIMO in distributed antenna systems," in *Proc. 2010 IEEE Conf. on Signals, Syst. and Comput. (ASILOMAR)*, pp. 1202–1206.

[131] M. Abramowitz and I. A. Stegun, *Handbook of Mathematical Functions With Formulas, Graphs, and Mathematical Tables*. 10th Ed., U.S. Government Printing Office, 1972.

[132] N. L. Johnson and S. Kotz, *Continuous Univariate Distributions - 2*. 1st Ed., John Wiley & Sons, 1970.

[133] I. S. Gradshteyn and I. M. Ryzhik, *Table of Integrals, Series, and Products*. 5th Ed., Academic Press, 1994.

[134] N. L. Johnson and S. Kotz, *Continuous Univariate Distributions - 2*. 2nd Ed., John Wiley & Sons, 1995.

[135] Winner. (2006) WINNER Phase II Model. [Online]. Available: http://www.ist-winner.org/phase_2_model.html

[136] C. Masouros, M. Sellathurai, and T. Ratnarajah, "Large-scale MIMO transmitters in fixed physical spaces: The effect of transmit correlation and mutual coupling," *IEEE Trans. Commun.*, vol. 61, no. 7, pp. 2794–2804, 2013.